DYNAMICAL AND ELECTRONIC PROPERTIES OF INCOMMENSURATE AND FULLERENE CRYSTALS

P.H.M. VAN LOOSDRECHT

DYNAMICAL AND ELECTRONIC PROPERTIES OF INCOMMENSURATE AND FULLERENE CRYSTALS

P.H.M. VAN LOOSDRECHT

DYNAMICAL AND ELECTRONIC PROPERTIES OF INCOMMENSURATE AND FULLERENE CRYSTALS

EEN WETENSCHAPPELIJKE PROEVE OP HET GEBIED VAN
DE NATUURWETENSCHAPPEN

PROEFSCHRIFT

TER VERKRIJGING VAN DE GRAAD VAN DOCTOR AAN
DE KATHOLIEKE UNIVERSITEIT NIJMEGEN,
VOLGENS BESLUIT VAN HET COLLEGE VAN DECANEN
IN HET OPENBAAR TE VERDEDIGEN
OP MAANDAG 29 MAART 1993,
DES NAMIDDAGS OM 3.30 UUR PRECIES

DOOR

PAULUS HUBERTUS MARIA VAN LOOSDRECHT

GEBOREN OP 26 OKTOBER 1963
TE WAALWIJK

PROMOTORES: PROF.DR. A.G.M. JANNER
PROF.DR. H. VAN KEMPEN
COPROMOTOR: DR. G. MEIJER

Over de randen van mijn handen
tasten mijn handen
naar mijn andere handen
onophoudelijk.

Paul van Ostaijen.

MANUSCRIPT COMMITTEE: DR. T. JANSSEN
DR. H. MEEKES

CIP-DATA KONINKLIJKE BIBLIOTHEEK, DEN HAAG

Loosdrecht, Paulus Hubertus Maria van

Dynamical and Electronic Properties of Incommensurate and Fullerene Crystals / Paulus Hubertus Maria van Loosdrecht - [S.l. : s.n.] (Nijmegen: Quickprint). - Ill.
Thesis Nijmegen. - With ref. - With summary in Dutch.
ISBN 90-9005863-X
Subject headings: incommensurate crystals / fullerenes / optical spectroscopy.

FOREWORD

This thesis comprises the work I have been doing during my PhD studies in the groups Theoretical Solid State Physics I of Prof.Dr. A.G.M. Janner and Experimental Solid State Physics 2 of Prof.Dr. H. van Kempen at the University of Nijmegen. It describes experiments on the structural, dynamical and electronical properties of crystalline solids. From these studies insight is gained into many physical and chemical properties of crystals, such as structural symmetry properties, the vibrational and electronic excitation spectrum, the chemical composition, order and disorder in solids, and interactions between excitations.

This thesis consists of two parts. The first part is dedicated to the properties of incommensurate crystals, a class of materials which lack the usual lattice periodicity but nevertheless exhibit a perfect long range order. It is shown for instance (chapter 1) that the incommensurability can have a strong influence on the vibrational excitation spectrum, revealed by the observation of additional inelastic optical scattering processes in Raman scattering experiments. Thermometry experiments (chapter 5) show that incommensurate materials are interesting not only from a fundamental, but also from a technological point of view.

The second part of this thesis describes spectroscopic studies on the solid state properties of fullerenes, the recently discovered third allotrope of carbon. It includes studies of the orientational ordering (chapter 6), the interaction of the vibrational spectrum with electronic excitations (chapter 8), and of the lattice dynamics (chapter 9) in these molecular crystals.

Doing physics is not a one-man-show and I have benefitted from many stimulating collaborations during my PhD studies. I want to take the opportunity here to express my gratitude to all people from the Theoretical Solid State Physics I group, the Experimental Solid State Physics 2 group, the Solid State Chemistry group, the Nijmegen High Field Magnet Laboratory, the State University of Uzhgorod, and last but not least the Molecule and Laser Physics group, who were in one way or another involved in the work presented here. In particular I want to thank Jan van Bentum and Gerard Meijer for the stimulating collaboration and their enthousiastic support. I thank also the State University of Uzhgorod for the kind hospitality given to me during my stay in Uzhgorod.

Apart from crossing scientific barriers, a PhD student often has to cross psychological ones as well. Again, I did not do all the crossing by myself. I like to thank all those colleagues and friends who have given me the right push at the right time to overcome these barriers. I also want to thank all friends and colleagues who have been a constant pleasant reminder that there is more than physics to the world. You made life as a PhD student a joyous and exciting period for me.

Finally, I wish to thank Karen for sticking with her often absent or frustrated companion in life. Without You life would be not nearly half as much fun.

Nijmegen, January 1993 *Paul van Loosdrecht*

CONTENTS

PART I

INCOMMENSURATE CRYSTALS

INTRODUCTION

One of the most important concepts in conventional solid state physics is the notion of lattice periodicity, *i.e.* a periodic distribution of matter in space.[1] A faceted morphology, sharp peaks in diffraction patterns, the formation of energy branches for electrons and phonons, all of these are a direct consequence of this microscopic regularity of crystalline matter. Yet, three dimensional (3D) lattice translational invariance is not a necessary prerequisite for these properties. In fact many solids exist, in nearly any class of materials, which lack the 3D periodicity but nevertheless exhibit sharp diffraction peaks, well developed crystal faces, and so on, *i.e.* they do possess a long range regularity. Examples are found in dehydrated soda, quartz, thiourea, chromium, TTF-TCNQ, the Bi based high T_c superconductors, and AlMnFe quasicrystals. The diffraction patterns of these so-called quasi-periodic systems can not, however, be indexed by the usual three integers, and notions like Bloch waves and space groups seem to be no longer valid. Furthermore, new excitations can occur in these systems such as the phason and amplitudon modes in incommensurate crystals.

A first step towards a natural description of these materials was made by P.M. de Wolff[2] who introduced a four-dimensional space group to describe the diffraction pattern of incommensurately modulated γ-Na_2CO_3. Later, this approach was generalised to arbitrary finite dimensions by A. Janner and T. Janssen.[3] In their "superspace" formalism, Janner and Janssen describe a 3D quasi-periodic system by considering it as an intersection of a $(3+d)$-dimensional periodic structure, where d is the minimum number of additional integers needed to describe the diffraction pattern of the 3D structure. The restored periodicity in $(3+d)$-dimensions allows for a simple generalisation of many of the concepts formally used to understand 3D periodic systems. The approach, which is well established by now, has proved to be very convenient in understanding the physical properties of quasi-periodic crystals (QPC's). The introduction of $(3+d)$-dimensional space groups enables, for instance, for the classification of QPC's, the understanding of their diffraction patterns and morphology, and the prediction of selection rules in scattering experiments.[4] One of the most appealing examples of the success of the superspace approach is the simple description it gives for the morphology of the mineral ore calaverite[5], in contrast to the complex description which arises when conventional methods are used.

The work presented in the first part of this thesis concerns the structural, dynamical, and electronic properties of incommensurate materials. These are studied using optical spectroscopic techniques and dielectric measurements.

Calaverite is an incommensurately modulated semimetal with a relatively large modulation amplitude. Raman spectroscopic experiments on calaverite reveal a large influence of the incommensurability on the inelastic light scattering properties of the phonon system (chapter 1). The electronic properties of calaverite are studied using infrared spectroscopy. A comparison with theoretical calculations shows the possible existence of minigaps near the Fermi-surface, induced by the incommensurability (chapter 2).

The ionic solid solution $[N(CH_3)_4]_2ZnCl_{4-x}Br_x$ is a member of the well known A_2BX_4 family of incommensurate dielectrics. The effects on the vibrational properties of the substitution of Cl by Br in this compound are discussed, and it is shown that from the Raman experiments one can easily obtain a good estimate for the composition of the crystals. In this case the influence of the incommensurability is strongly masked by the presence of orientational disorder in the system (chapter 3).

The vibrational properties of the ferroelectric semiconductor $Sn_2P_2Se_6$ are studied using Raman spectroscopy. A strong interaction is found between the lattice modes and the central peak observed in the spectra. It is proposed that the central peak arises from scattering due to the dynamics of polar clusters or domain walls, which form a soliton structure in the incommensurate phase (chapter 4). Incommensurate materials are not only interesting from a fundamental, but also from a technological point of view. The strong temperature dependence of the dielectric constant found for the solid solution $(Pb_{0.45}Sn_{0.55})_2P_2Se_6$ in the incommensurate phase makes this material a most promising candidate for applications in sensors for low temperature thermometry in high magnetic fields (chapter 5).

REFERENCES

1 R.J. Haüy, *"Essai d'une théorie sur la structure des cristaux"*, Paris (1784).

2 P.M. de Wolff, Acta Cryst. A **28**, s111, (1972).

3 A. Janner and T. Janssen, Phys. Rev. B **15**, 643 (1977).

4 T. Janssen, J. Phys. C: Solid State Physics **12**, 5381 (1979).

5 B. Dam, A. Janner, and J.D.H. Donnay, Phys. Rev. Lett. **55**, 2301 (1985).

CHAPTER 1

RAMAN STUDY OF INCOMMENSURATELY MODULATED CALAVERITE[1]

P.H.M. van Loosdrecht, P.J.M. van Bentum, and K. Balzuweit

*Research Institute of Materials, University of Nijmegen, Toernooiveld,
NL-6525 ED Nijmegen, The Netherlands.*

ABSTRACT.

Raman spectra of incommensurately modulated $AuTe_2$ are presented. The large number of observed Raman active modes indicates a strong influence of the incommensurability on the dynamical properties. The resulting spectra are discussed in terms of the selection rules derived using the superspace symmetry of $AuTe_2$.

---

[1] Previously published in *Ferroelectrics* **125**, 517 (1992).

1.1 INTRODUCTION

The incommensurate modulation in the mineral calaverite ($Au_{1-p}Ag_pTe_2$, $p < 0.15$) has a strong influence on its structural properties. This is illustrated by the occurrence of a large number of satellite faces (hklm,m≠0), with a high morphological importance[1], and by the results of electron[2] and X-ray[3] diffraction studies. Because of these large structural effects in $Au_{1-p}Ag_pTe_2$ one expects also a large influence of the incommensurate modulation on other physical properties.

In a study of the optical properties of $Au_{1-p}Ag_pTe_2$ Dijkstra *et al.*[4] observed an optical rotation of linearly polarised light upon reflection. Although this is not surprising for a metallic biaxial system, they argued that it is possible that part of this optical rotation is due to the incommensurate modulation, as was also observed in several other incommensurate materials with (super)space inversion symmetry.[5, 6, 7]

In the present paper we report on a Raman study of the lattice dynamical properties of pure calaverite ($AuTe_2$). Because in an incommensurately modulated structure wavevectors with $\mathbf{k} = \pm l\mathbf{q}$ (l integer) are equivalent to $\mathbf{k} = 0$, additional scattering processes from phonons with $\mathbf{k} = \pm l\mathbf{q}$ are allowed in optical spectroscopies.

1.2 CRYSTAL STRUCTURE

The average room temperature structure of calaverite has space group C2/m with a = 7.19 Å, b = 4.40 Å, c = 5.07 Å and monoclinic angle $\beta = 90.04°$.[8] Van Tendeloo *et al.*[2] studied pure $AuTe_2$ by means of electron diffraction and HREM and showed that the structure of calaverite is incommensurately modulated. In an X-ray study Schutte and de Boer[3] solved the structure of calaverite containing 10% Ag substituted for Au. They found a nearly temperature independent incommensurately modulated structure with superspace group $P^{C2/m}_{\bar{1}s}(\alpha,0,\gamma)$, modulation wavevector $\mathbf{q} = -0.408\mathbf{a}^* + 0.448\mathbf{c}^*$, and the modulation amplitude primarily along the **b** direction. The modulation amplitude in calaverite is rather large, especially for the Te atoms (up to 0.4 Å). The modulation wave is non-sinusoidal, i.e. higher harmonics of **q** play an important role. Both papers reported observations of at least up to third order satellites.

1.3 SELECTION RULES

The average structure of calaverite has three atoms per primitive cell, leading to nine phonon branches. The nine $\mathbf{k} = 0$ modes of the average structure are obtained in the usual way to give three Raman active modes ($2A_g \oplus B_g$), three infrared active modes ($A_u \oplus 2B_u$) and three acoustic modes ($A_u \oplus 2B_u$). Hence, for the average structure one expects to observe in Raman scattering only one mode in B_g geometry and two modes in A_g geometry.

The above considerations hold for a non-modulated structure. In a modulated structure optical scattering processes are allowed not only from phonons with $\mathbf{k} = 0$, but also from those with $\mathbf{k} = \pm l\mathbf{q}$(both modulo a reciprocal lattice vector of the average structure).[9] Using the superspace group method outlined by Currat and Janssen[10], one can determine the optical activity of the modes with $\mathbf{k} = \pm l\mathbf{q}$. The results of this analysis are shown in Tables 1.1 and 1.2.

Table 1.1 : Correlations of the modes with $\mathbf{k} = \pm l\mathbf{q}$ *to the* $\mathbf{k}=0$ *modes. Each irreducible representation correlates to a pair consisting of a gerade and an ungerade symmetry.*

l odd	$l = 0$	l even
$A_u \oplus B_g$	$\leftarrow A_g \rightarrow$	$A_g \oplus B_u$
$A_g \oplus B_u$	$\leftarrow B_g \rightarrow$	$A_u \oplus B_g$
$A_g \oplus B_u$	$\leftarrow A_u \rightarrow$	$A_u \oplus B_g$
$A_u \oplus B_g$	$\leftarrow B_u \rightarrow$	$A_g \oplus B_u$

Table 1.2 : Activity of the vibrational modes in calaverite for l=0, l=0, 1 and for l=0, 1, 2. The Table can easily be extended to higher order in l using Table 1.1.

C_{2h}	$l = 0$	$l = 0, \pm 1$	$l = 0, \pm 1, \pm 2$	activity
A_g	2	5	11	(a,a), (b,b), (c,c), (a,c)
B_g	1	7	10	(a,b),(b,c)
A_u	1	7	10	b
B_u	2	5	11	a,c

Table 1.1 shows that the symmetry of the modes with $\mathbf{k} = \pm l\mathbf{q}$ depends on the parity of l, and that for each l one has a pair consisting of a gerade and an ungerade mode. This has three important consequences.

- Phonons belonging to a branch which has an infrared active $\mathbf{k} = 0$ mode of either symmetry become Raman active and vice versa.
- Phonons belonging to a branch with A_g (A_u) symmetry for $\mathbf{k} = 0$ become active in B_g (B_u) symmetry and vice versa.
- Acoustic phonons (inactive at $\mathbf{k} = 0$) become active in both Raman and infrared spectra.

In Table 1.2, the numbers of optical active modes in different geometries are tabulated for $l = 0$, $l = 0$, 1 and $l = 0$, 1, 2. For a purely sinusoidal modulation one expects only the zeroth and first order (l = 0, 1) phonons to be active in optical scattering processes.[11] In calaverite higher harmonics can not be neglected, and one therefore expects to observe also Raman and infrared active modes for $\mathbf{k} = \pm l\mathbf{q}$ ($l > 1$).

1.4 EXPERIMENTAL

The crystals used in our experiments were grown using the Kyropoulos technique with a magnetic pulling system.[12] The large, nicely faceted crystals were oriented using both Laue backscattering photographs and their extremely rich morphology. In this way the principal crystal axes are easily found, as well as the angles (α, β, γ), and thus the (hklm) assignment of the crystal faces.

A SEM microprobe analysis of the purity of our samples, limited by the accuracy of our experimental set up (1 %), showed that the impurity level at the surface of our samples was below 1 %.

The experiments have been performed on crystal faces (h0lm) parallel with the b-axis, allowing for measurements in both A_g (($\perp\mathbf{b}$,$\perp\mathbf{b}$) or (//$\mathbf{b}$,//$\mathbf{b}$)) and B_g (($\perp\mathbf{b}$,//$\mathbf{b}$)) geometry. The crystals were mounted in a cryostat (temperature stabilisation better than 1 K), and spectra have been recorded at $T = 50$ K using a DILOR XY spectrometer in retro-reflection geometry with the 514.5 nm line of an Ar^+-laser as excitation source (power < 10 mW, focused to ~ 1000 μm^2).

1.5 RESULTS AND DISCUSSION

We have studied several samples, all yielding essentially the same results. The data presented here were all taken from the same sample ($AuTe_2$-5-3). The spectra were obtained from experiments on a highly reflecting ($20\bar{1}2$) satellite face, which is parallel to the **b**-axis and makes an angle of 7°05' with the **a** axis.

In Figure 1.1 typical Raman spectra (35 - 190 cm^{-1}) are shown, recorded at $T = 50$ K in $z(xx)\bar{z}$, $z(yy)\bar{z}$ (A_g symmetry) and $z(xy)\bar{z}$ (B_g symmetry) geometry, where x//**b**, y ~ //**a**, and z ~ //**c**. The spectra are analyzed using Lorentzian lineshapes. One should bear in mind however that the lineshapes are not necessarily Lorentzian because of possible near degeneracies of the active modes with $\mathbf{k} = \pm l\mathbf{q}$, for instance in the case of a relatively flat phonon dispersion. In our case however we obtained reasonable fits of the spectra using this lineshape. In the A_g spectra an increasing 'background' is observed in the low frequency region, caused by Rayleigh scattering, which has been subtracted before analyzing the data. The results of the fits are tabulated in Table 1.3.

At least 11 modes are observed in A_g, and at least 10 in B_g symmetry. This indicates a large effect of the incommensurate modulation on the lattice dynamics of calaverite. Above

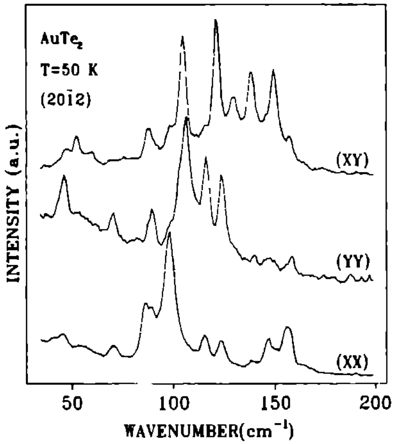

Figure 1.1 : Polarised Raman spectra at T=50 K of calaverite in **(xx)**,**(yy)** *and* **(xy)** *geometry, showing a large number of peaks induced by the incommensurability.*

80 cm^{-1}, 6 relatively strong modes are observed in the B_g and A_g(xx) spectra, together with some smaller peaks and shoulders. One can speculate that these peaks are directly related to the 6 optical phonon branches of the average structure. In the A_g(yy) spectrum only 4 relatively strong modes are observed above 80 cm^{-1}. We assume that the modes below $\sim$ 70 cm^{-1} are resulting from the acoustic branches of the average structure. At 72 cm^{-1} there is a peak in the A_g spectra, which has a rather position-dependent intensity. This could indicate that this mode is induced by impurities on the surface. Some peaks are observed in both symmetries. We do not believe that this is due to experimental conditions, but rather is caused by accidental (almost) degeneracies of the numerous modes. Another striking observation is the difference in the A_g spectra. For instance the peak at 109 cm^{-1} in the (yy) spectrum is not observed in (xx) geometry. Instead a peak is observed at 101 cm^{-1}, which in turn is only weakly observed in (yy) geometry. Hence, for these modes there is a large difference in first order polarisabilities. By comparing this kind of geometry dependence with the atomic displacements of the phonon modes, one can in principle make assignments to the observed peaks. At present, we can only speculate on the assignments of the observed modes, and more experimental and theoretical results are needed to make any definite conclusions concerning the assignments.

Table 1.3 : Frequencies (ω_0), widths ($\delta\omega$, full width at half the maximum) and intensities (I) of the observed peaks in the Raman spectra in $A_g(xx)$, $A_g(yy)$ and $B_g(xy)$ geometry. The intensities given are relative to the strongest peaks in the spectra.

$A_g(xx)$			$A_g(yy)$			$B_g(xy)$		
ω_0	$\delta\omega$	I	ω_0	$\delta\omega$	I	ω_0	$\delta\omega$	I
172	6	5.8						
162	6	28.7	163	5	11.4	162	3	12.1
			155	4	0.6	154	6	100
152	6	18.4	151	5	6.7			
143	2	1.3	144	2	2.3	142	6	89.0
			134	8	7.6	133	7	66.7
128	4	11.7	127	4	32.0	125	4	98.7
119	5	13.3	119	5	45.4	118	7	24.9
			109	7	100	108	4	94.2
			106	2	4.0			
101	7	100	101	2	2.3	101	5	24.8
92	5	17.6	92	3	14.6	91	5	29.1
88	3	15.6						
73	3	3.3	72	3	8.0			
						61	5	9.5
57	6	4.0	57	8	7.1			
						54	4	16.5
47	5	7.6	47	4	18.6	48	8	22.8
42	4	2.1						

1.6 CONCLUDING REMARKS

We have shown that the incommensurability in calaverite has a huge effect on the lattice dynamics. In comparison with for instance Rb_2ZnBr_4[13], $AuTe_2$ exhibits a large number of Raman active modes. Most of the modes in the spectra are resolved as a narrow peak. In Na_2CO_3[14], which has a structure comparable to $AuTe_2$, the additional modes are not resolved. The fact that in our spectra these modes are resolved is caused by the relative large modulation wavevector in $AuTe_2$. A difficulty arises in interpreting the spectra due to the large relative intensities of the $\mathbf{k} = \pm l\mathbf{q}$ modes. The strongest peaks observed in the Raman spectra are believed to result from scattering processes with $\mathbf{k} = \pm l\mathbf{q}$ phonons for $l = 0$, 1 or 2. Phonons with higher l are observed as weaker peaks and shoulders in the spectra. The relative small peak width, and the reasonable fits of the spectra to Lorentzian shaped peaks indicate a small electron-phonon coupling in $AuTe_2$.

We are far from a complete understanding of the Raman scattering in calaverite. More insight can can be gained from a study of the temperature and angle dependencies, as well as of the optical activity in far-infrared experiments. It would also be interesting to perform inelastic neutron scattering experiments, in order to reveal more of the phonon band structure.

ACKNOWLEDGEMENTS Valuable discussions with Prof.Dr. A. Janner are gratefully appreciated, as well as the critical reading of the manuscript. One of the authors, K. Balzuweit, wishes to thank the Conselho Nacional de Pesquisa (CNPq, Brazil) for financial support (Project 200644/88.2). Part of this work was financed by the Stichting Fundamenteel Onderzoek der Materie (FOM, Dutch Foundation of Fundamental Research of Matter).

REFERENCES

1 B. Dam, A. Janner, and J.D.H. Donnay, Phys. Rev. Letters **55**, 2301 (1985).

2 G. van Tendeloo, P. Gregoriadas, and S. Amelinckx, J. Solid State Chem. **50**, 321 (1983).

3 W.J. Schutte and J.L. de Boer, Acta Cryst. B **44**, 486 (1988).

4 E. Dijkstra, M. Kremers, and M.A.C. Deviller, Z. Phys. B: Condensed Matter **76**, 487 (1989).

5 K. Saito, T. Kawabe, and J. Kobayashi, Ferroelectrics **75**, 153 (1987).

6 H. Meekes and A. Janner, Phys. Rev. B **38**, 8075 (1988).

7 E. Dijkstra, J. Phys.: Condensed Matter **3**, 141 (1991).

8 G. Tunell and L. Pauling, Acta Cryst. **5**, 375 (1952).

9 T. Janssen, J. Phys. C: Solid State Phys. **12**, 5381 (1979).

10 R. Currat and T. Janssen, Solid State Phys. **41**, 201 (1987).

11 C. de Lange and T. Janssen, J. Phys. C: Solid State Phys. **14**, 5269 (1981).

12 K. Balzuweit, H. Meekes, and P. Bennema, J. Phys. D: Applied Physics **24**, 203 (1991).

13 Th. Rasing, P. Wyder, A. Janner, and T. Janssen, Phys. Rev. B **25**, 7504 (1982).

14 H. Meekes, Th. Rasing, P. Wyder, A. Janner, and T. Janssen, Phys. Rev. B **34**, 4240 (1986).

OPTICAL PROPERTIES OF INCOMMENSURATELY MODULATED CALAVERITE[1]

P.H.M. van Loosdrecht, A.M. Gerrits, K. Balzuweit,
and P.J.M. van Bentum.

High Field Magnet Laboratory and Research Institute of Materials, University of Nijmegen, Toernooiveld, NL-6525 ED Nijmegen, The Netherlands.

ABSTRACT.

The optical reflection spectrum of incommensurately modulated calaverite is presented. Using a Kramers Kronig analysis the dielectric function is derived from the reflection spectrum. The results for the imaginary part of the dielectric function are qualitatively discussed in terms of absorption by phonon-, free electron- and interband scattering. The phonon contribution clearly shows the influence of the incommensurability by the activity of phonons with $\mathbf{k}\neq0$. The free electron scattering can be understood in terms of a simple Drude model. The interband scattering is found at a lower frequency than predicted from electronic band structure calculations.

---

[1] Submitted to *Journal of Physics: Condensed Matter*.

2.1 INTRODUCTION

Natural calaverite ($Au_{1-p}Ag_pTe_2$, $p < 0.15$) is a mineral ore which belongs to the class of displacively modulated incommensurate materials. As has been shown recently, the relatively large amplitude of the modulation wave in this material has a strong influence on its physical properties. Dam *et al.*[1] have shown that the complex morphology is easily understood if one fully accounts for the incommensurability of $Au_{1-p}Ag_pTe_2$. In Raman experiments it was found that scattering processes involving $\mathbf{k} = \pm l\mathbf{q}$ ($l = 1,2$), activated due to the incommensurate modulation, are important in the understanding of the vibrational spectra of $AuTe_2$.[2] Optical experiments by Dijkstra *et al.*[3] indicate that calaverite is optically active, despite the fact that calaverite is centro-symmetric. It was argued that the optical activity might be due to the incommensurability of $Au_{1-p}Ag_pTe_2$.

In the incommensurate phase the structural symmetry of calaverite is given by the superspace group $PC2/m(\alpha,0,\gamma)\bar{1}s$, with the modulation wavevector $\mathbf{q} = -0.408\mathbf{a}^* + 0.448\mathbf{c}^*$.[4] The cell parameters of the average structure are a = 7.19 Å, b = 4.40 Å, c = 5.07 Å, and $\beta = 90.04°$.[5] At ambient pressure calaverite does not exhibit any structural phase transition as a function of temperature. The modulation wavevector is approximately temperature independent below 400K.[4] At higher temperature the modulation wavevector becomes slightly temperature dependent.[6] Pressure dependent X-ray experiments[7] have shown that at ~ 25 kbar ($T = 300$ K) a phase transition occurs to a commensurate cubic structure. This simple cubic structure is also found in crystals which are produced by a temperature quenching method.[8] It has been shown that these quenched cubic crystals are superconducting with a transition temperature of $T = 2.5$ K. The fact that cubic calaverite becomes superconducting might give an explanation of the superconductivity observed in incommensurate calaverite in pointcontact experiments. Meekes *et al.*[9] observed that $AuTe_2$-$AuTe_2$ pointcontacts become superconducting below $T = 2.3$ K and that Ag-$AuTe_2$ pointcontacts exhibit characteristics reminiscent of Andreev reflection, even though bulk incommensurate calaverite is not a superconductor. It seems very well possible that the pressure needed to produce the pointcontact locally induces a phase transformation to the cubic phase leading to the observed superconducting properties.

The presence of a modulation wave in a conductor leads to the formation of small additional gaps in the electronic band structure, besides the usual gaps induced by the lattice periodicity. In an incommensurately modulated conductor there is an infinitely large number of these gaps, formed whenever $\mathbf{k} = \pm l\mathbf{q} + \mathbf{K}$ ($l = 1,2,\ldots$)[10], where $\mathbf{q}$ is the modulation wavevector, and $\mathbf{K}$ a reciprocal lattice vector. The magnitude of these gaps is expected to decrease strongly upon increasing l. This leads to a distribution of small gaps, with the largest gaps formed for $\mathbf{k} = \pm\mathbf{q}$. Infrared experiments in chromium have shown the existence of at least the first order gap, with a magnitude of 125 meV.[11] In addition, the zero bias anomaly in pointcontact experiments on Cr shows the existence of this gap, with a reported value of 110 meV.[12]

The interest of the present paper concerns both the vibrational and the electronic properties of incommensurately modulated calaverite. These properties are probed using reflection spectroscopy over a wide frequency range in order to be able to derive the frequency dependence of the complex dielectric constant. One of the aims is to extract the electronic interband contribution to the optical spectra in order to investigate the possible existence of minigaps near the Fermi-surface induced by the incommensurate modulation. The results are compared to existing experimental and theoretical literature data.

2.2 EXPERIMENTAL

The crystals used in the experiments have been grown using the Kyropoulos technique with a magnetic pulling system as described elsewhere.[13] A SEM microprobe analysis of the purity of our samples, limited by the accuracy of our experimental set up (1 %), showed that the impurity level at the surface of our samples was below 1 %.

The reflection experiments have been performed on the natural surfaces of the obtained crystals. For the infrared measurements the samples were mounted in a dynamic flow cryostat using polyethylene windows in the far-infrared region and KRS5 and ZnSe windows in the mid infrared region. A gold mirror has been used as a reference material. The spectra are recorded using a BRUKER IFS 113V FT-IR spectrometer. A KBr beamsplitter and mylar beamsplitters of various thicknesses have been employed to cover the complete infrared region. The experiments in the ultraviolet are performed at room temperature using a CARY spectrometer with an aluminium mirror as a reference.

2.3 DATA ANALYSIS

The complex dielectric function can in general not be derived directly from a measurement of the reflection. Only if the reflection is known over the complete frequency range, one can calculate the dielectric response using the relations between the reflection and the phase derived from the Kramers-Kronig (KK) relations. The reflection spectrum of calaverite has been measured over a wide frequency range (see Tab. 2.1); there are only three regions missing in the data: 1) the low frequency part below 20 cm^{-1}, 2) the near-infrared part between 5500 cm^{-1} and 14000 cm^{-1}, and 3) the part above 47000 cm^{-1}. For the low frequency part one can assume the widely used Hagen-Rubens relation for the frequency dependence of the reflection given by $R = 1 - a\sqrt{\omega}$ to extrapolate the data to zero frequency. Since one expects no structure in the near-infrared region, one can interpolate the region between 5500 and 14000 cm^{-1} using a smooth curve. A suitable function to interpolate

Table 2.1 : Overview of the measured and inter-/extrapolated regions of the reflection of calaverite recorded using the given reference materials at temperature T and angle of incidence θ_i. Also listed are the most relevant excitations which contribute in the given regions as well as the inter-/extrapolation methods used.

Region (cm^{-1})	T (K)	θ_i	Excitations	Reference, Extrapolation
0-20				$1 - a\sqrt{\omega}$
20-650	20	45	Phonons	Gold
650-5500	20	45	Free electrons	Gold
5500-14000				$a(1 - b\omega^2)$
14000-47000	300	0	Bound electrons	Aluminium
47000-10^6				$a\omega/(\omega^2 + b^2)^2$

this region is $R = a(1 - b\omega^2)$. The high frequency part can be extrapolated using a suitable function which tends to zero for high enough frequencies. For this a function is used of the form $a\omega/(\omega^2 + b^2)^2$, with the derivative matched to the high frequency part of the available data. The neglect of any additional structure in this region, for instance due to atomic transitions, will not lead to changes in the positions of spectral features in the calculated optical spectra, but will merely lead to an error in the absolute intensities, which are not of particular interest here.

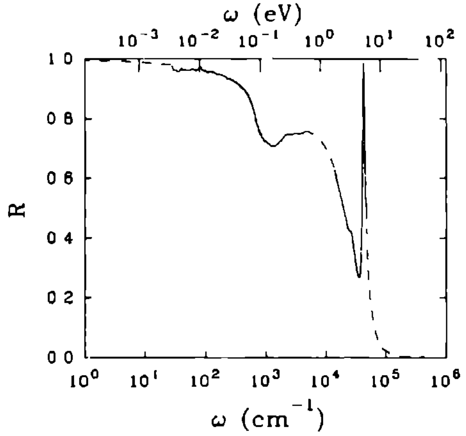

Figure 2.1 : Frequency dependence of the reflection of calaverite. The solid and dashed lines show the measured data and the inter- and extrapolated data, respectively (see text).

Figure 2.1 shows the measured (11,200 points, solid lines) and extrapolated parts (6500 points, dashed lines) of the reflection as a function of frequency. The reflection shows a metallic behaviour with some phonon structure at low frequency, and a dip due to interband transitions just above 0.1 eV. The sharp peak at 5.2 eV in the spectrum probably is due to transitions from the Au^{5d} states in calaverite. These transitions have also been observed in XPS experiments at 5 eV.[14] The wiggles in the spectrum around 0.1 eV are caused by interference effects in the spectrometer.

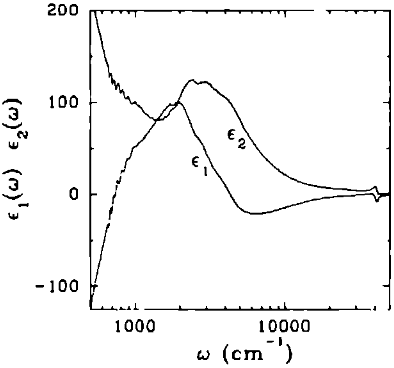

Figure 2.2 : Real ϵ_1 and imaginary ϵ_2 part of the dielectric function of calaverite calculated using a KK analysis from the reflection data shown in Fig. 2.1.

The dielectric function calculated using a KK analysis are shown in Fig. 2.2. The various vibrational and electronic excitations contributing to the dispersion of the dielectric function will be discussed in the next paragraphs.

2.4 ABSORPTION BY PHONONS

The average structure of calaverite has three atoms per primitive cell. Although there are nine phonon modes in this structure, the selection rules predict only three of them to be infrared active.[2] Due to the incommensurate modulation one expects, however, that not only phonons with momentum $\mathbf{k} = 0$ are active, but also those with $\mathbf{k} = \pm l\mathbf{q}$ ($l = 1,2,\ldots$) in optical scattering experiments.[15] This has already been confirmed in Raman experiments where 18 additional modulation induced modes have been observed.[2] In principle all phonons with $\mathbf{k} = \pm l\mathbf{q}$ ($l = 1\ldots\infty$) contribute to the optical scattering. However, their activity strongly depends on the number of harmonics which are needed to adequately describe the structure. It is usually sufficient to take only those phonons into account with low values of l. In the case of calaverite the selection rules predict that in addition to the three phonons for $l = 0$ an additional 9 modes are expected for each value of l taken into account (see Tab. 1.2).[2] The Raman experiments showed that phonons with $l = 1, 2$ contribute to the optical scattering. If the same holds for infrared absorption one expects 21 active modes in the spectra.

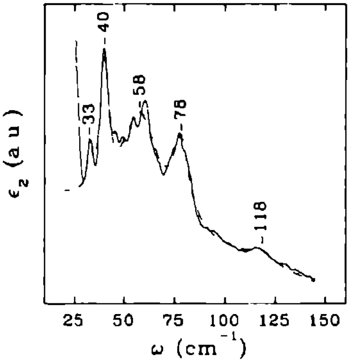

Figure 2.3 : Low frequency part of the imaginary part of the dielectric function showing activity of several phonons (solid line). The dashed line is a fit of Lorentzian shaped peaks to the data (see text) whose peak frequencies are indicated at the markers.

Phonon scattering contributes to the reflection spectrum of calaverite in the region below 150 cm^{-1}. The imaginary part of the dielectric function derived from the reflection spectrum showing the phonon structure is shown in Fig. 2.3 (solid line). The fact that more than three phonons are observed clearly demonstrates the influence of the incommensurability in the optical spectrum. At least five reproducible modes are observed. The phonon contribution to ϵ_2 can be described using the Lorentz model for absorption by a harmonic oscillator. The spectral dependence of the absorption within this model is given by:

$$\epsilon_2 = \sum_j \frac{S_j \gamma_j \omega}{(\omega_{0j}^2 - \omega^2)^2 + \gamma_j^2 \omega^2} \approx \sum_j \frac{S_j \gamma_j / (4\omega_{0j})}{(\omega_{0j} - \omega)^2 + (\gamma_j/2)^2} \quad \text{for } \gamma_j \ll \omega_{0j} \;, \tag{2.1}$$

where S_j is the oscillator strength, ω_{0j} the resonance frequency, and γ_j the linewidth. The dashed line in Fig 2.3 represents a fit of 5 Lorentzians to the data. A linear background was assumed in the fitting procedure to account for the absorption due to other processes. The resonance frequencies of the fitted Lorentzians are 33, 40, 58, 78, and 118 cm^{-1}, respectively. There seems to be more structure in the data and the peaks at 58 and

78 cm^{-1} may be split into more components. This additional structure does not reproduce very well and has therefore been neglected.

Since there are more phonons active than expected for the average structure of $AuTe_2$, one can conclude that the incommensurability has a strong effect on the vibrational absorption spectrum of $AuTe_2$. The selection rules for the incommensurate structure predict the activity of 12 (l = 0,1) or 21 (l = 0,1,2) phonon modes. In Raman scattering it has been possible to observe most of these modes.[2] Clearly the infrared spectrum shows only part of the predicted modes. In the low frequency region this is probably due to the broad linewidth of the observed bands in the infrared spectrum, leaving many of the expected modes unresolved. One expects from the Raman data to observe modes above 120 cm^{-1}. The infrared spectrum, however, does not show any reproducible structure in this region. The precise origin of this difference is at present not known, but it may be related to a decreasing skin depth upon increasing frequency, leading to a decreasing sensitivity to phonon structure.

2.5 ABSORPTION BY ELECTRONS

The most important electronic processes which contribute to the dispersion of the dielectric function are absorptions due to interband, and due to intraband transitions. It is often convenient to distinguish between these two processes in discussing the electronic scattering. Therefore this section starts with a discussion of the contribution of intraband transitions to the imaginary part of the dielectric constant. In the second part of this section the contribution of the interband transitions are discussed.

2.5.1 INTRABAND PROCESSES

Fig. 2.4 (solid line) shows the imaginary part of the dielectric function as obtained from the KK analysis. The steep increase of ϵ_2 towards low frequencies is due to the intraband processes. The frequency dependence of the dielectric function in a metal can be understood in terms of the Drude free electron model. Within this model the dielectric function is given by:

$$\epsilon_1(\omega) = \epsilon_\infty \left(1 - \frac{\omega_p^2 \tau^2/\epsilon_\infty}{1+\omega^2\tau^2}\right) , \qquad (2.2)$$

$$\epsilon_2(\omega) = \frac{\omega_p^2 \tau}{\omega(1+\omega^2\tau^2)} , \qquad (2.3)$$

where ϵ_∞ is the high frequency limit of the dielectric constant if the interband transitions are neglected, τ the electronic intraband scattering time, and ω_p the plasma frequency.

Before discussing the data in terms of the Drude behaviour it is interesting to first consider the low frequency limit of the Drude behaviour, *i.e.* the DC conductivity $\sigma(0)$.

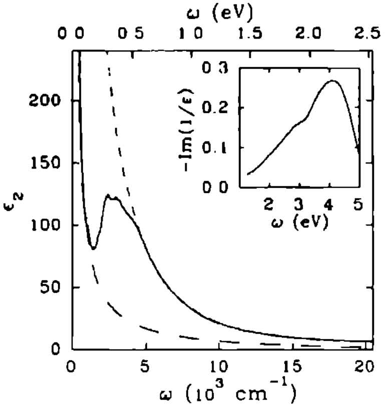

Figure 2.4 : Imaginary part of the dielectric function (solid line). The long dashed line give the Drude behaviour as derived from the plasmon peak in the loss function shown in the inset. The short dashed line gives a Drude-like fit to the tail of the interband transitions.

This can be estimated from an extrapolation of the real part of the optical conductivity $\sigma(\omega) = \omega\epsilon_2/4\pi$ to zero frequency, yielding $\sigma(0) \approx 1\ (\mu\Omega m)^{-1}$. This is in relatively good agreement with the value of 2 $(\mu\Omega m)^{-1}$ at $T = 20$ K determined from resistance measurements, giving confidence in the results of the KK analysis.

Dijkstra *et al.*[3] measured, using ellipsometry, the dielectric function of calaverite for 1.5 eV $< \hbar\omega <$ 5 eV. The present data agrees with their results to within 5 %, giving confidence in the results of the KK analysis. The ellipsometry data were interpreted in terms of a Drude model, with the Drude parameters given in Tab. 2.2. It is obvious from the present data, however, that interband scattering rather than free electron scattering gives the largest contribution to ϵ_2 for energies above 1.5 eV. The characteristic Drude-like free electron contribution is found to be prominent at much lower enegy ($\hbar\omega <$ 0.2 eV). Since free electron scattering is important in a small energy range only it is difficult to

Table 2.2 : Comparison of the plasma frequency and scattering time derived here with the results of Ref. 3. ϵ_∞ gives the high energy limit of the dielectric constant. $d\epsilon_2$ gives the "background" assumed in Ref. 3.

	ω_p (eV)	τ (10^{-16} s)	ϵ_∞	$d\epsilon_2$
Drude	4.8	3.2	1.03	
Ref. 3	7.5	4.0		3.00

fit the data directly to a Drude behaviour. One can, however, obtain a good estimate of the parameters of the Drude behaviour from the energy dependence of the loss function, defined as -Im($1/\epsilon$), which is shown in the inset of Fig. 2.4. This function peaks at the position ω_c where ϵ_1 is zero, and has a full width of $\Delta\omega = 1/\tau$.[16] Within the Drude model the frequency ω_c is related to the plasma frequency through $\omega_p^2 = \epsilon_\infty(\omega_c^2 + 1/\tau^2)$. Thus from a determination of the peak width and peak frequency of the loss function, one can in combination with the high frequency limit of the dielectric constant obtain a good estimate of the characteristic parameters of the free electron scattering ω_p and τ. The dashed curve in Fig. 2.4 (long dashes) gives the Drude behaviour calculated from the values obtained in this way (see Tab. 2.2). From the agreement with the data one can conclude that the free electron contribution can be approximated by a Drude behaviour having a plasma frequency $\hbar\omega_p = 4.8$ eV and a characteristic scattering time $\tau = 3.2 \cdot 10^{-16}$ s. The electron density estimated from the plasma frequency $\omega_p = \sqrt{ne^2/m^*\epsilon_0}$, substituting the free electron mass m_0 for the effective mass m^*, is $n \approx 2 \cdot 10^{28}$ m^{-3}, a value typical for metals.

2.5.2 INTERBAND PROCESSES

The contribution from interband processes to ϵ_2 can be found by subtraction of the Drude behaviour from the data presented in Fig. 2.2. As shown in Fig. 2.5 (curve marked exp.). The interband contribution peaks at 0.4 eV having a peak width of 0.5 eV. Krutzen[17]

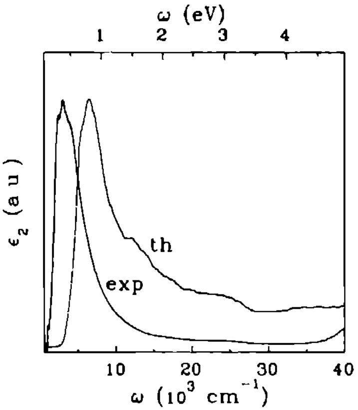

Figure 2.5 : Contribution of the interband transitions to ϵ_2 obtained after subtraction of the Drude contribution (exp.). The curve marked th. shows the results for ϵ_2 as calculated in Ref. 18.

has performed electronic band structure calculations for commensurate approximants of $AuTe_2$. From these results the interband part of ϵ_2 has been calculated[18], assuming equal matrix elements for all interband transitions. For comparison these results are also shown in Fig. 2.5 (curve marked th.). The predicted interband contribution peaks at 0.8 eV and has a bandwidth of 0.65 eV. These theoretical results overestimate the experimentally found values by a factor of 1.3 to 2. There can be several reasons for this discrepancy. It might be due to the partial neglect of the incommensurability in the electronic structure calculations for calaverite, *i.e.* due to the neglect of the possible existence of minigaps at the Fermi-surface, leading to an overestimate of the onset of the interband transitions. In that case, one would also expect to observe structure in the low energy tail of the interband contribution, which is evidently not the case. The agreement of the structure observed near the peak in both the experimental and theoretical spectra suggests that the discrepancy can be resolved by shifting the theoretical spectrum towards lower energy, *i.e.* the theoretical Fermi-energy has to be shifted. The theoretical overestimate of the peak width and the magnitude of the high energy tail then results from a neglect of the energy dependence of the transition matrix elements. This leads to the conclusion that the matrix elements in general decrease upon increasing energy.

It seems surprising that Dijkstra *et al.*[3] could fit their data with a Drude-like behaviour. Also for the present data it is possible to fit the high energy tail of the interband contribution with a Drude-like behaviour, giving a "scattering time" $\tau = 8.1 \cdot 10^{-16}$ s^{-1} and a "plasma frequency" of 7.8 eV (see Fig. 2.4, dashed curve (short dashes)). This Drude-like high energy behaviour of the interband contribution may be due to the very rich, and relatively dense band structure of calaverite.[17] For this kind of band structure one expects that for high enough energy, where the details of the band structure are no longer important and there are many final states, the contribution of interband processes to the optical spectrum shows a spectral dependence more or less similar to that expected for free electron processes.[19] It should be noted, however, that ω_p and τ are parameters which strongly depend on the details of the band structure, and are not simply related to a real scattering time or electron density.

2.6 CONCLUDING REMARKS

The data presented here show a good agreement with the ellipsometry data of Dijkstra *et al.*[3]. From this, and the good agreement found with the DC conductivity, one can conclude that KK analysis yields sensible results. However, the used data set contains some inconsistencies which leads to errors in the derived optical spectra. In particular, the data below 0.7 eV have been measured at 45° incidence, a rather arbitrary interpolation function has been used for the 0.7–1.7 eV region, and the UV data have been measured at room temperature. One can expect, however, that these deficits primarily lead to an error in the absolute values, and do not strongly affect the spectral dependence of the dielectric function.

Calaverite is usually considered to be a semimetal. The results here show that synthetic pure $AuTe_2$ is a conductor with a DC conductivity and a Drude scattering time typical for semimetals. The electron density $n \approx 2{\cdot}10^{28}$ m^{-3} of pure $AuTe_2$, estimated from derived from the low frequency Drude behaviour, is typical for a metal. For an incommensurately modulated conductor the combination of a semimetallic conductivity with a metallic density may be not so surprising. If the modulation induces Fermi-surface nesting for wavevectors $\mathbf{k} = \pm l\mathbf{q}$, leading to a distribution of minigaps at or near the Fermi-surface, one can expect that the inelastic scattering time of the conduction electrons strongly decreases, resulting in a decreased conductivity. However, since the electron density estimate depends crucially on the effective electron mass m^* in calaverite this can not be concluded from the present data alone. It seems therefore interesting to determine the effective mass for calaverite, for instance from magneto-conduction experiments.

One expects that the existence of a contribution of minigaps also leads to a contribution to the interband scattering, with an absorption edge at the largest gap induced for $\mathbf{k} = \pm\mathbf{q}$. If this gap indeed exists in calaverite its magnitude is smaller than 60 meV, since no structure is observed in the low energy tail of the interband contribution shown in Fig. 2.5 above this energy. For a definitive conclusion a careful analysis of the low energy part of the spectrum is needed. The present data do not allow for this, and moreover do not extend to low enough energies.

To summarise, the incommensurate modulation of $AuTe_2$ is reflected in the optical absorption spectrum by the activity of additional phonons with wavevector $\mathbf{k} = \pm l\mathbf{q}$ ($l \neq 0$). The free electron scattering in this semimetal can qualitatively be described with a Drude model ($\omega_p = 4.8$ eV, $\tau = 3.2{\cdot}10^{-16}$ s). The Drude parameters derived in Ref. 3 describe the tail of the interband scattering, which main contribution to the optical spectra is centered around 0.4 eV. The combination of semimetallic conductivity with a metallic electron density gives an indication for a modulation induced Fermi-surface nesting in calaverite, though additional experimental research is needed for a definitive conclusion. The interband contribution to the optical spectrum sets an upper limit for the energy gaps of 60 meV.

ACKNOWLEDGEMENTS The authors wish to thank Dr. W. König from the MPI Stuttgart for performing the reflection experiments in the UV part of the spectrum. We also thank Dr. A. Wittlin for providing the program for the Kramers Kronig analysis. One of the authors (KB) wishes to thank the Conselho Nacional de Pesquisa (CNPq, Brazil) for financial support (Project 200644/88.2). Part of this work was financed by the Stichting

Fundamenteel Onderzoek der Materie (FOM, Dutch Foundation of Fundamental Research of Matter).

REFERENCES

1 B. Dam, A. Janner, J.D.H. Donnay, Phys. Rev. Lett. **55**, 2301 (1985).

2 P.H.M. van Loosdrecht, P.J.M. van Bentum, and K. Balzuweit, Ferroelectrics **125**, 517 (1992), and chapter 1 of this thesis.

3 E. Dijkstra, M. Kremers, and M.A.C. Devillers, Z. Phys. B: Condensed Matter **76**, 487 (1989).

4 W.J. Schutte and J.L. de Boer, Acta Cryst. **B 44**, 486 (1988)

5 G. Tunell and L. Pauling, Acta Cryst. **5**, 375 (1952).

6 K. Balzuweit, A. Hovestad, H. Meekes, and J.L. de Boer, submitted to J. Cryst. Growth.

7 K. Reithmayer, W. Steurer, H. Schulz, and J.L. de Boer, Proceedings of the XV^{th} CUIC, Bordeaux-France (1990).

8 C.C. Tsuei and L.R. Newkirk, Phys. Rev. **183**, 619 (1969).

9 H. Meekes, P.H.M. van Loosdrecht, M. Kremers, Unpublished.

10 C. de Lange and T. Janssen, Phys. Rev. B **28**, 195 (1983).

11 A.S. Barker and J.A. Ditzenberger, Phys. Rev. B **1**, 4378 (1970).

12 H. Meekes, Phys. Rev. B **38**, 5924 (1988).

13 K. Balzuweit, H. Meekes, and P. Bennema, J. Phys. D: Applied Physics **24**, 203 (1991).

14 A. van Triest, W. Folkerts, and C. Haas, J. Phys.: Condensed Matter **2**, 8733 (1990).

15 T. Janssen, J. Phys. C: Solid State Phys. **12**, 5381 (1979).

16 H. Raether, *Excitations of Plasmons and Interband Transitions by Electrons*, (Springer Verlag, Berlin 1990).

17 B.C.H. Krutzen and J.E. Inglesfield, J. Phys.: Condensed Matter **2**, 4829 (1990).

18 B.C.H. Krutzen, M. Kremers, Ferroelectrics **105**, 559 (1990).

19 H. Ehrenreich and H.R. Philipp, Phys. Rev. **128**, 1622 (1962).

A RAMAN AND FIR SPECTROSCOPIC STUDY OF THE SOLID SOLUTION $[N(CH_3)_4]_2ZnCl_{4-x}Br_x$[1]

P.H.M. van Loosdrecht[a,b], A. Janner[b].

[a] *Research Institute of Materials, University of Nijmegen, Toernooiveld, NL-6525 ED Nijmegen, The Netherlands.*
[b] *Institute of Theoretical Physics, University of Nijmegen, Toernooiveld, NL-6525 ED Nijmegen, The Netherlands.*

ABSTRACT.

Polarised Raman and far-infrared spectra (10-350 cm^{-1}) of the $[N(CH_3)_4]_2ZnCl_{4-x}Br_x$ solid solution are presented for several compositions ($x = 0$, 1, 2, 2.9 and 4) in the high (300 K) and low (60 K) temperature phases of the crystals. Apart from the internal modes of the $ZnCl_4^{2-}$ and $ZnBr_4^{2-}$ ions, several new active internal modes are found in the spectra, originating from the mixed $[ZnCl_{4-n}Br_n]^{2-}$ ions ($n = 1$, 2, 3 and 4). The spectra are in fair agreement with a simple 'free' ion model for the vibrational modes of the $[ZnCl_{4-n}Br_n]^{2-}$ ions. From the intensities of the tetrahedral ν_1 modes, the relative concentrations of the various $[ZnCl_{4-n}Br_n]^{2-}$ ions in the crystals are estimated. Using these relative concentrations the value of x in the crystals is calculated, and found to be in good agreement with the stoichiometries of the crystal growth solutions. A pronounced low frequency mode is observed in the spectra which scales with the average moment of inertia of the $[ZnCl_{4-n}Br_n]^{2-}$ ions, and is therefore assigned to a librational mode of these ions.

---

[1] Previously published in *Journal of Physics: Condensed Matter* **3**, 8113 (1991).

3.1 INTRODUCTION

The solid solution $[N(CH_3)_4]_2ZnCl_{4-x}Br_x$ belongs to the A_2BX_4 family of dielectrics, having in general an orthorhombic ($\beta - K_2SeO_4$) high temperature phase. At lower temperature, different sequences of modulated phases are found for the members of this family, among which an incommensurate one is often found. The many common structural features among the members leads to the assumption that the modulation in this family has a common origin.[1, 2] In fact, for many members the phases (both commensurate and incommensurate) can be described to a very good approximation as different three-dimensional intersections of a four-dimensional structure, with a single superspace group symmetry (the prototype symmetry group).

A few years ago, E. Colla *et al.*[3] determined the x-T phase diagram of the solid solution $[N(CH_3)_4]_2ZnCl_{4-x}Br_x$ (tetramethylammonium-tetra(chloro,bromo)zincate, hereafter denoted by TZCB). They found a rich variety of phases and phase transitions. The phase transitions in this system result mainly from modulated rotations $(\theta_x, 0, \theta_z)$ and translations $(0, t_y, 0)$ of the $N(CH_3)_4^+$ and of the $[ZnCl_{4-n}Br_n]^{2-}$ (hereafter denoted by ZCB_n^{2-}) tetrahedra. At high temperature ($T > 293$ K) the phase has space group symmetry Pnma for all compositions. At lower temperature the pure chloride compound exhibits phase transitions[5] to respectively an incommensurate phase, an orthorhombic, two monoclinic and finally an orthorhombic phase again. The pure bromide compound, however, only exhibits one phase transition to a monoclinic low temperature phase[6, 7] The modulated incommensurate phase present in the $x = 0$ compound disappears at $x \approx 3$. Near $x \approx 3$, the wavevector of the modulation continuously changes from an incommensurate to a commensurate value. Indeed, this is very exceptional, as usually one observes a discontinuous jump of the order of 10^{-2} to the rational value in the modulation parameter. The continuity of the modulation parameter is interesting in view of a possible additional electromagnetic propagation mode in incommensurate structures with a nearly commensurate modulation, as predicted by van Beest.[8]

The purpose of the present paper is to obtain a better insight into the basic vibrational properties of TZCB. In order to study these properties we have performed Raman and far-infrared (FIR) spectroscopic experiments on several solid solutions in their high and low temperature phases. An extensive Raman investigation of the pure Cl compound has already been performed by Meekes *et al.*[9]. We have concentrated our attention to the region of ZCB_n^{2-} vibrational modes, not only because of their relation to the phase transitions in this material, but also in order to obtain a better understanding of the distribution of Cl and Br in this system. The Cl,Br distribution is expected to influence both the selection rules and the intensities in Raman and FIR experiments, as will be shown in sections 3.3 and 3.4.

This paper is organised as follows. In section 3.2 the experiments are described and the resulting spectra are presented. The activity of the internal ZCB_n^{2-} modes is discussed in terms of the free tetrahedral ion symmetry modes in section 3.3. In section 3.4 the spectra presented in section 3.2 are discussed. Finally, in section 3.5 some conclusions are given.

3.2 EXPERIMENTAL

The crystals used in the experiments are grown from a seed in an aqueous solution of a stoichiometric mixture of $[N(CH_3)_4]Y$ and ZnY_2 ($Y = Cl,Br$) by a slow convection method.[10] In this way, optically transparent crystals (~ 1 cm^3) were obtained from a solution with a known bromide concentration (x). The actual Br concentration is expected to be somewhat higher than this value. The crystals are oriented using their rich morphology.[11, 12] The unit cell dimensions for a crystal with $x = 2.9$ are determined by X-ray diffraction to be $a = 12.49$ Å, $b = 9.24$ Å and $c = 15.90$ Å, which is consistent with the results of Arend *et al.*[10].

For the polarised Raman experiments, the crystals are cut and polished to platelets (dimension $\sim 2 \times 3$mm^2, 0.5-1 mm thick). The platelets are mounted in an OXFORD cryostat (temperature stabilisation better than 1 K). The Raman spectra are recorded in a standard way (90° geometry) using the 514.5 nm line of an Ar$^+$-laser (unfocussed, power < 250 mW) as excitation source.

The TZCB crystals have a strong absorption in the FIR region, making it very difficult to measure the absorption directly on single crystals. In order to be able to obtain FIR absorption spectra, we have therefore powdered the crystals and embedded them in a polyethylene platelet (~ 0.35 mm thick). In this way, samples are obtained with a known low molar concentration of the crystal (~ 5 %). The unpolarised FIR transmission spectra were measured at room temperature using a BRUKER IFS 113V spectrometer.

3.2.1 FIR EXPERIMENTS

FIR transmission spectra of the powdered samples embedded in a polyethylene matrix were measured relative to the transmission of pure polyethylene. Some typical spectra at room temperature for $x = 0,1,2.9$ and 4 are shown in Figure 3.1. As x increases some modes shift in frequency and new modes appear in the spectra, although the modes of the mixed tetrahedra are not resolved in this case. The structure at 456 cm^{-1}, present in all spectra is due to the tetrahedral ν_4 symmetry modes of the $N(CH_3)_4^+$ ions.[13] The ν_3 and ν_4 modes of $ZnCl_4^{2-}$ and $ZnBr_4^{2-}$ are clearly visible as broad absorption lines in the spectra.

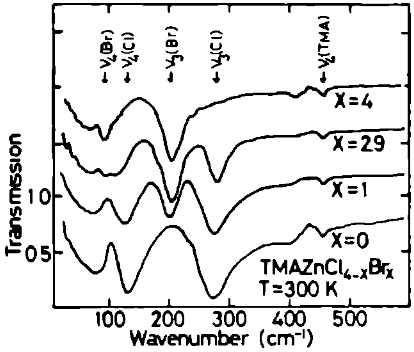

Figure 3.1 : Room temperature FIR transmission spectra of powdered TZCB *crystals (x=0, 1, 2.9 and 4) embedded in a polyethylene matrix. A pure polyethylene sample has been taken as a reference.*

3.2.2 RAMAN EXPERIMENTS

Polarised Raman spectra are measured for x = 0, 1, 2, 2.9 and 4 in the high and low temperature phases. As already mentioned, we focused on the frequency range of the internal ZCB_n^{2-} modes $\nu_1, \ldots, \nu_4$ (10-350 cm^{-1}).[14] There are two regions of interest in the spectra. The first one (10-150 cm^{-1}) contains the external modes and the ν_2 and ν_4 internal ZCB_n^{2-} modes, whereas the second one (150-350 cm^{-1}) contains the ν_1 and ν_3 internal modes of the ZCB_n^{2-} tetrahedra. The internal modes of the $N(CH_3)_4^+$ ions lie at higher frequencies.[13] The results of the Raman experiments can be found in Figure 3.2.a (T = 300 K) and b ($T \approx 60$ K). Raman spectra of different crystals are generally difficult to compare quantitatively due to the variations of for instance the optical quality of the samples. In order to get a better quantitative comparison of the spectra, we have therefore normalised the spectra of the crystals with a different composition in Figure 3.2.a and b with respect to the integrated intensity of the 150-350 cm^{-1} region in A_g geometry of the same crystal, thereby assuming that the scattering efficiency of the ZCB_n^{2-} tetrahedra is approximately the same for all n.

In the monoclinic low temperature phases, domains differing in monoclinic angle, and a rotation of the indicatrix around the unique axis are observed under a polarisation microscope. Due to the rotation of the indicatrix, light polarised along one of the two non-unique axes becomes elliptical, resulting in a mixing of the scattering polarisations.

In the spectra of the mixed crystals new modes appear, due to the mixed character of the ZCB_n^{2-} anions. Also some modes shift in frequency as function of the composition

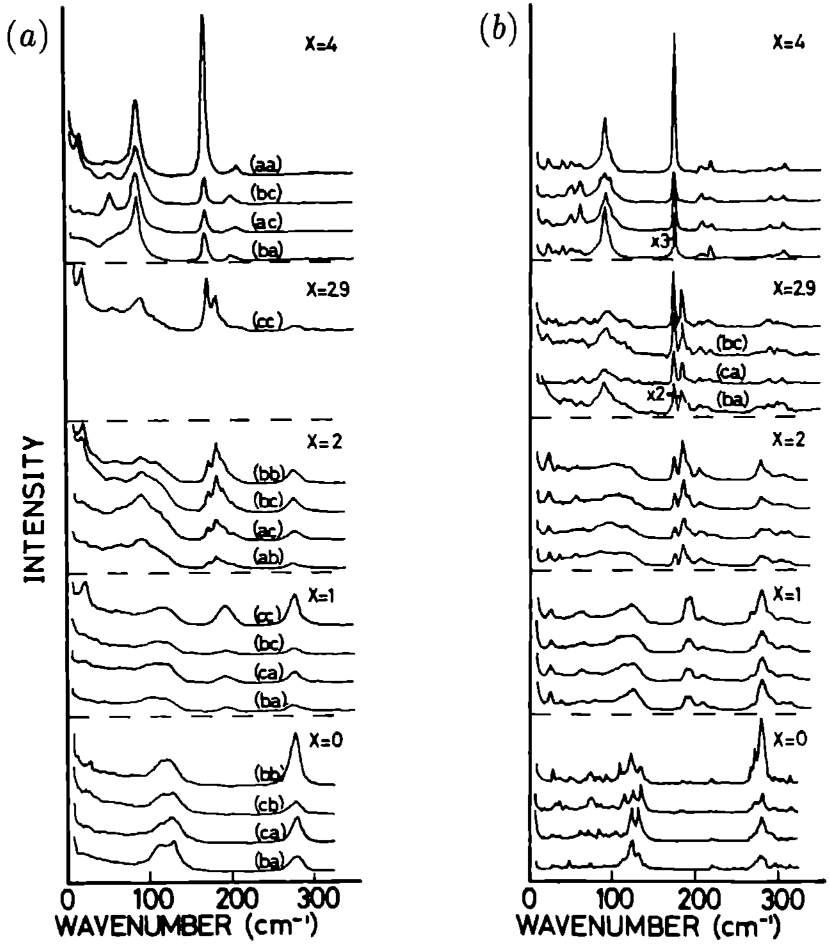

Figure 3.2 : a) Polarised Raman spectra at $T=300$ K of the solid solution TZCB *for $x=0,1,2,2.9$ and 4. Clearly new modes appear in the spectra of the mixed crystals, resulting from the internal modes of the mixed* ZCB_n^{2-} *ions. The scattering geometry is indicated for each curve ((**a**,**b**) means incoming polarisation along **a**, polarisation of the scattered light along **b**). The corresponding irreducible representations of the point group can be found in Table 3.2.*
b) Polarised Raman spectra at $T \approx 60$ K of the solid solution TZCB *for $x=0,1,2,2.9$ and 4. The scattering geometries are the same as in a). The corresponding irreducible representations can be found in Table 3.3.*

and/or the temperature. This is illustrated by the measurement of the lattice mode at ~ 24 cm^{-1} for several temperatures (Figure 3.3.a) and by the comparison of the frequency of this mode for different mixing ratios (Figure 3.4).

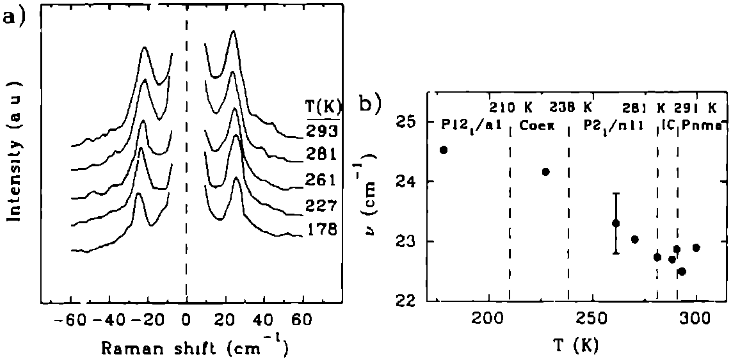

Figure 3.3 : a) Stokes and anti-Stokes A_g Raman spectra of the ~ 24 cm^{-1} mode and the quasi-elastic scattering in TZCB *for x=1 at various temperatures.*
b) Temperature dependence of the ~ 24 cm^{-1} mode in an x=1 crystal. The mode is insensitive to the phase transition to the incommensurate phase. A hardening of this mode is observed below the phase transition to the monoclinic $P2_1/n11$ phase.

3.3 RAMAN AND IR ACTIVITY OF THE $[ZnCl_{4-n}Br_n]^{2-}$ MODES

Before we turn to the actual activity of the ZCB_n^{2-} modes, we will first make some remarks on the structure of the TZCB crystals. At room temperature the structure of TZCB is isomorphic for all x. The space group is Pnma (Z = 4). The unit cell dimensions change continuously from a = 12.268 Å, b = 8.946 Å and c = 15.515 Å for x = 0 to a = 12.681 Å, b = 8.238 Å and c = 16.025 Å for x = 4.[10] The structure is built up from more or less rigid $N(CH_3)_4^+$ and ZCB_n^{2-}tetrahedra positioned at $(x,\frac{1}{4},z)$ with site symmetry C_s in the pure crystals. On lowering the temperature, the TZCB crystals undergo several structural phase transitions, resulting mainly in rotations $(\theta_x, 0, \theta_z)$ and translations $(0, t_y, 0)$ of the tetrahedra. Due to the rotations, the site symmetry of the tetrahedra changes from C_s to C_1 (the mirror plane m_y is lost). The low temperature phases have been determined for the x = 0[5], x = 2.2[4] and x = 4[7] compounds. The space groups of the x = 0 and x = 4 compounds are respectively orthorhombic $P2_12_12_1$ (Z = 12, T < 161 K) and monoclinic $P112_1/a$ (Z = 4, T < 287 K). For the mixed crystals we assume that the low temperature structures are those found in the phase diagram by Colla *et al.*[3], that is $P12_1/a1$ (Z = 8,

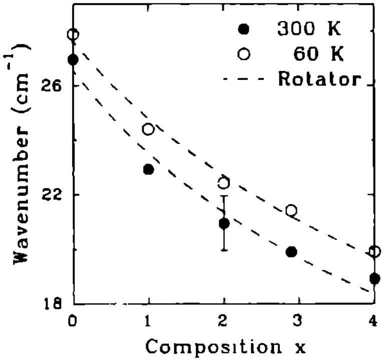

Figure 3.4 : Composition dependence of the ~ 24 cm^{-1} mode at T=300 K (dots) and at T=60 K (open circles). The mode scales with the average mass of the outer atoms of the heavy ZCB_n^{2-} tetrahedra. This is shown by the dashed lines which are fits of the data for a chain of classical harmonic rotators, with frequency $\nu^2 \sim I^{-1}$ (I: moment of inertia).

$T < 210$ K) for x = 1 and x = 2 crystals, and $P112_1/a$ ($Z = 4$, $T < 273$ K) for x = 2.9 crystals.

3.3.1 FREE ION APPROXIMATION

Since we consider the structure as being built up from rigid tetrahedra, we can discriminate between the internal tetrahedra modes and the external vibration modes (including the vibrational and librational modes of the rigid tetrahedra). The validity of this assumption will be considered later, when we discuss the experimental results. We only consider phonons with wavevector $\mathbf{k} = 0$.

Here we restrict ourselves to a discussion of the internal ZCB_n^{2-} modes. We first consider the 'free' ZCB_n^{2-} anions, neglecting the crystal field and the coupling between the ions. The point group of the ZCB_n^{2-} anions depends on the value of n. For n = 0 and n = 4 ions the point group is T_d, for n = 1 and n = 3 ions C_{3v} and for the n = 2 ions C_{2v}. In Figure 3.5 the correlation diagram of the vibrational modes for these various point groups is given. Since C_{2v} is not a subgroup of C_{3v}, the correlations can not be determined by a direct subduction. Instead, the correlation is found by a projection of the C_{3v} modes onto the C_{2v} modes.

Figure 3.5 shows that the degenerate modes in the pure ions split up in the mixed cases. One can gain some more insight in this splitting by considering a simple valence-bond model for the ions, which we briefly discuss now. In this model we consider the change of

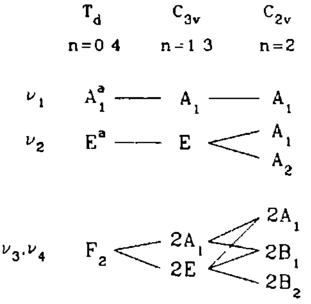

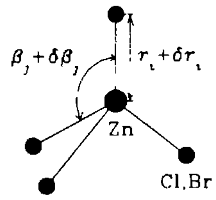

Figure 3.5 : (left) Correlation diagram of the symmetry modes of the free ZCB$_n^{2-}$ *tetrahedra in different compositions* (T_d: *n=0 or 4*, C_{3v}: *n=1 or 3 and* C_{2v}: *n=2). All modes are both Raman and infrared active, except for the modes marked with a which are only Raman active.*

Figure 3.6 : (right) Zn-Y stretching (δr_i) *and Y-Zn-Y bending* ($\delta\beta_j$) *coordinates in a tetrahedral* ZnY_4 *ion, where Y stands for Cl, Br.*

mass upon substituting a Cl atom by a Br atom. The valence-bond potential is taken to be

$$V = \sum_{i=1}^{4} \lambda_i (\delta r_i)^2 + \sum_{j=1}^{6} \mu_j (\delta\beta_j)^2, \tag{3.1}$$

where δr_j and $\delta\beta_j$ are respectively the Zn-Y stretching and Y-Zn-Y bending coordinates (see Figure 3.6). The force constants λ_i, μ_j are determined from the ν_1 and ν_2 ZCB$_n^{2-}$ mode frequencies in the pure compounds using (for T_d symmetry)

$$\begin{aligned} \nu_1^2 &= \lambda/m \quad (\mathrm{Zn-Cl, Zn-Br\ \ stretching}) \\ \nu_2^2 &= \mu/3m \quad (\mathrm{Cl-Zn-Cl, Br-Zn-Br\ \ bending}), \end{aligned} \tag{3.2}$$

with m the mass of either a Cl, or a Br atom. For the Cl-Zn-Br bending force constant a linear interpolation between the two pure cases is used. The resulting force constants are shown in Table 3.1. The model uses only two (T_d symmetry) or four (C_{2v} and C_{3v} symmetry) independent force constants, whereas the actual problem has more (4 for T_d, 6 for C_{3v} and 9 for C_{2v} symmetry). This leads for instance to a higher frequency for the ν_3 modes of the ions. Despite the restrictions of the model, we think that it gives a clear qualitative picture of the vibrational properties of the heavy tetrahedra. The frequencies of the symmetry modes of the various ions are determined by solving the dynamical matrix of the model. The results of this calculation are shown in Figure 3.7. Three groups of modes are found for the tetrahedra, based on the symmetry modes $\nu_1, \ldots, \nu_4$ of the pure

Table 3.1 : Force constants used in the valence-bond model, calculated from the frequencies of the ν_1 and ν_2 modes in the pure compounds.

Zn-Cl stretching	(ν_1=278cm^{-1})	λ=160 N/m
Zn-Br stretching	(ν_1=170cm^{-1})	λ=136 N/m
Cl-Zn-Cl bending	(ν_2=116cm^{-1})	μ=9 N/m
Br-Zn-Br bending	(ν_2=56cm^{-1})	μ=5 N/m
Cl-Zn-Br bending		μ=7 N/m

ions. The ν_3 group at 310-390 cm^{-1}, the ν_1 group at 180-280 cm^{-1} and the ν_2,ν_4 group at 80-130 cm^{-1}. In all groups, the frequency generally decreases as n is increased, which is expected because of the higher mass of the Br atoms. The splitting of the modes expected from group theory is clearly observed in the model (Figure 3.7). The ν_3 modes seem to give the best opportunity to measure it because of the relatively large splitting of these modes, whereas the ν_2 and ν_4 modes are probably too closely spaced. If TZCB is a true solid solution, then all the different anions ZCB_n^{2-} will in general be present in the crystals, and all the modes presented in Figure 3.7 are expected to be observable as internal modes in Raman and FIR experiments. We return to this model in the next section, where the results of the Raman and FIR experiments are discussed.

3.3.2 TETRAHEDRAL MODES IN THE CRYSTALS

We now turn to the activity of the internal ZCB_n^{2-} modes in the crystals. In Table 3.2 the activity of these modes in the high temperature Pnma phase are given. This Table is based on the site symmetry C_s for the ZCB_n^{2-} ions. In the mixed crystals however, this mirror symmetry may be lost. This is in particular the case when the two atoms which are outside the mirror plane m_y are of a different kind. In that case the site symmetry is C_1, and the modes will be active in all geometries (in both Raman and FIR experiments). If the substitution of Cl by Br is totally disordered, the site symmetry will also be C_1.

The above differences in site symmetry, and thus in selection rules, gives a means to determine whether there is some kind of ordering, leaving the mirror m_y intact. This is for instance the case if the substitution of Cl by Br preferably takes place on the Y site of the tetrahedra with the smallest thermal motions[4, 15], with Zn-Y in the mirror plane, and the bond along **a**.

At low temperatures the site symmetry of the tetrahedra is always C_1, leading to an activity of all modes in all geometries. Detectable in the spectra is however the number of different frequencies of a given mode, due to the presence of a different number of tetrahedra in the primitive cell of the compounds, and the mixed character of the tetrahedra. The activity of the ZCB_n^{2-} modes are given in Table 3.3.a for x = 0, in Table 3.3.b for x = 1

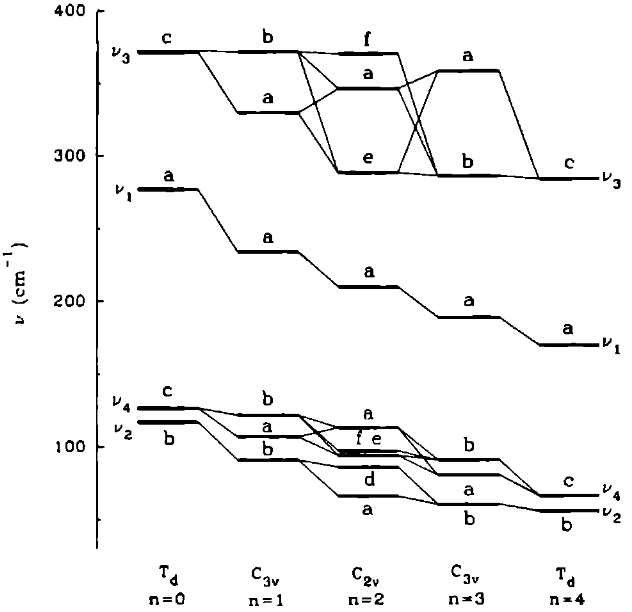

Figure 3.7 : Vibrational energy levels calculated from a valence bond potential model for the various ZCB_n^{2-} *anions. The force constants used, and the characteristic features of this model are discussed in section 3.3. The lettering a-f refers to the irreducible representations of the relevant point groups for the various levels with* a:A_1; b:E; c:F_2; d:A_2; e:B_1; and f:B_2.

and x = 2, and in Table 3.3.c for the x = 2.9 and x = 4 compounds.

3.4 INTERPRETATION OF THE SPECTRA

In the first part of this section the FIR and Raman spectra presented in section 3.2 are discussed in terms of the internal modes of the ZCB_n^{2-} ions. A discussion of the external modes will be given in the second part of this section.

3.4.1 INTERNAL $[ZnCl_{4-n}Br_n]^{2-}$ MODES

FIR spectra Three broad absorption bands are observed in the FIR spectra of the pure compounds, of which two are assigned to the ν_3 and ν_4 internal ZCB_n^{2-} modes (see Figure 3.1). For the pure Cl compound the absorption maxima of these modes are found at approximately $\nu_3 = 275$ cm^{-1} and $\nu_4 = 130$ cm^{-1}, for the Br compound the frequencies

Table 3.2 : Raman and infrared activity of the internal ZCB$_n^{2-}$ *modes in the high temperature Pnma phase of the* TZCB *crystals. The site symmetry of the ions is* C_s.

Pnma (Z=4)	site symmetry C_s			
D_{2h}	ν_1	ν_2	$\nu_3+\nu_4$	activity
A_g	1	1	4	(a,a),(b,b),(c,c)
B_{1g}	0	1	2	(b,c)
B_{2g}	1	1	4	(a,c)
B_{3g}	0	1	2	(a,b)
A_u	0	1	2	-
B_{1u}	1	1	4	a
B_{2u}	0	1	2	b
B_{3u}	1	1	4	c

are respectively 200 cm^{-1} and 90 cm^{-1}.

The low frequency absorption band in the spectra is assigned to the external vibrational modes. Due to the weak coupling to the lattice of the internal modes, the tetrahedral symmetry of the ions is almost conserved. Hence, the ν_1 and ν_2 modes are expected to be only weakly absorbing in FIR experiments. In the pure compounds, the ν_2 modes are not observed. In the Cl compound this results from the (almost) degeneracy of these modes with the ν_4 modes, whereas in the Br compound the ν_2 modes coincide with the external modes.

The frequencies of the fully symmetric ν_1 modes nearly coincide with those of the ν_3 modes, and are not observed in the spectra. The spectra of the mixed crystals show absorption bands at the ν_3 frequencies for both pure compounds. These bands result from the ν_3 modes of the pure ions, as well as from the ions with a mixed character. This can be concluded from the valence-bond model (Figure 3.7) and the relative strong intensity of the 200 cm^{-1} band in the x = 1, and the 278 cm^{-1} band in the x = 2.9 spectra.

The ν_4 absorption band shifts toward lower frequency as x increases, consistent with the valence-bond model. In the spectrum of the x = 2.9 compound two absorption dips are observed at 92 cm^{-1} and 109 cm^{-1}. The structure at 92 cm^{-1} is mainly due to the ν_3 modes of the ZnBr$_4^{2-}$ ions. As will be shown later on, the ions with a mixed character present in the x = 2.9 crystals are mainly the ZnClBr$_3^{2-}$ ions. We therefore assign the structure at 109 cm^{-1} to the ν_3 internal modes of the ZnClBr$_3^{2-}$ ions.

Raman spectra of the pure compounds Before we turn to the spectra of the mixed crystals, we will first examine the spectra of the pure compounds, starting with the x = 4 compound. In the high temperature Raman A_g spectrum (Figure3.2.a, upper curve), the four internal modes of the ZnBr$_4^{2-}$ anions are all clearly observed as more or less sharp

Table 3.3 : Raman and infrared activity of the internal ZCB$_n^{2-}$ *modes in the low temperature phases of the various* TZCB *crystals. The site symmetry is* C_1 *in all cases. a)* $x=0$ *crystals, space group* $P2_12_12_1$ *(Z=12). b)* $x=4$ *and* $x=2.9$ *crystals, space-group* $P112_1/a$ *(Z=4). c)* $x=1$ *and* $x=2$ *crystals, space-group* $P12_1/a1$ *(Z=8).*

a. $P2_12_12_1$ (Z=12) site symmetry C_1				
D_2	ν_1	ν_2	$\nu_3+\nu_4$	activity
A	3	6	18	(a,a),(b,b),(c,c)
B_1	3	6	18	a,(b,c)
B_2	3	6	18	b,(a,c)
B_3	3	6	18	c,(a,b)
b. $P112_1/a$ (Z=4) site symmetry C_1				
C_{2h}	ν_1	ν_2	$\nu_3+\nu_4$	activity
A_g	1	2	6	(a,a),(b,b), (c,c),(a,b)
B_g	1	2	6	(a,c),(b,c)
A_u	1	2	6	c
B_u	1	2	6	a,b
c. $P12_1/a1$ (Z=8) site symmetry C_1				
C_{2h}	ν_1	ν_2	$\nu_3+\nu_4$	activity
A_g	2	4	12	(a,a),(b,b), (c,c),(a,c)
B_g	2	4	12	(a,b),(b,c)
A_u	2	4	12	b
B_u	2	4	12	a,c

peaks in the spectrum. In Table 3.4 we have compared the frequencies of these modes with the frequencies measured for the anions in an aqueous solution.[14] Since there are only slight differences between these two, we can conclude that the effect of the crystal field on the intra-molecular forces in ZCB$_n^{2-}$ are fairly small. This can also be concluded from the small FWHM (full width at half maximum) of the modes, which indicates only a small splitting of the modes due to the crystal field. In the x = 4 Raman B_{1g}, B_{2g} and B_{3g} spectra at 300 K (Figure 3.2.a) we again observe all the internal ZnBr$_4^{2-}$ modes. For the ν_2, ν_3 and ν_4 modes this is expected from the selection rules (Table 3.2). The ν_1 mode, however, should be inactive in B_{1g} and B_{3g} symmetry. The fact that in these cases also a non-zero intensity is found is probably due to the large degree of rotational freedom[4] of the ZnBr$_4^{2-}$ tetrahedra around the a- and c-axis, effectively lowering the site symmetry from C_s to C_1.

In the x = 4 low temperature spectra (Figure 3.2.b), all modes are active in all geometries, consistent with the selection rules (Table 3.3.c). A single ν_1 mode is observed in all geometries and the six different ν_3 and ν_4 modes are better resolved. It is not clear whether the ν_2 modes (2 in each geometry) are resolved due to the coincidence with the external modes.

Table 3.4 : Comparison of the frequencies of the internal $ZnBr_4^{2-}$ *and* $ZnCl_4^{2-}$ *modes measured by Raman spectroscopy for the crystals with the corresponding frequencies for the ions in an aqueous solution*[14].

	ν_1	ν_2	ν_3	ν_4
$ZnCl_4^{2-}/H_2O$	275	79	306	104
$[N(CH_3)_4]_2ZnCl_4$	278	116	275*	127
$ZnBr_4^{2-}/H_2O$	172	66	208	88
$[N(CH_3)_4]_2ZnBr_4$	170	56	210	88

* From the FIR data.

For the x = 0 compound there are some degeneracies which blur the above picture a bit. The ν_2 and ν_4 modes are strongly overlapping and the ν_1 modes are (almost) degenerate with the ν_3 modes. The latter can be concluded from a comparison of ν_1 modes in the Raman spectra (Figure 3.2.a and b, lower curves) with the ν_3 modes in the FIR spectrum (Figure 3.4, lower curve). The comparison of the observed frequencies of the $ZnCl_4^{2-}$ internal modes with those of the ions in an aqueous solution[14] in Table 3.4 shows that in this case the differences are rather large, indicating a non-negligible effect of the crystal field on the intra-molecular forces. This makes the subdivision into external and internal modes in this compound questionable.

In the high temperature Raman spectra (Figure 3.2.a) again a non-zero intensity is found in the ν_1 region in all geometries. Indeed, part of the intensity in the B_{1g} and B_{3g} spectra can be explained by the activity of the ν_3 mode, as proposed by Meekes *et al.*[9]. The large intensity in these geometries indicates, however, that it is also partly due to the activity of the ν_1 modes, again resulting from the large thermal factors of the $ZnCl_4^{2-}$ anions.

In the x = 0 low temperature spectra (Figure 3.2.b) the different modes are as expected active in all geometries. The ν_1 mode is split up into several peaks, reflecting the larger number of formula units in the unit cell in this case (see also Table 3.3.a). It is not clear whether part of the structure in the ν_1 region results from the (weak) activity of the ν_3 modes.

Raman spectra of the mixed compounds We now turn to the spectra of the mixed crystals. In the Raman spectra (Figure 3.2.a and b) additional peaks appear in the spectra, which are not observed in the spectra of the pure compounds. This is clearest in the region of ν_1, ν_3 modes (150-350 cm^{-1}). These extra modes are due to the presence of mixed $[ZnCl_{4-n}Br_n]^{2-}$ ions in the crystals, indicating that the compounds are true solid solutions, and not just a mixture of the two pure crystals. The peaks in the ν_1, ν_3 region of the A_g Raman spectra at T = 300 K (Figure 3.1.a) are fitted to Lorentzian shaped modes. The results of these fits can be found in Table 3.5. The additional modes observed in the ν_1, ν_3 region are assigned to the ν_1 modes (neglecting the ν_3 modes, which generally have a low intensity) of respectively the $ZnCl_3Br^{2-}$ ion (183 cm^{-1}), the $ZnCl_2Br_2^{2-}$ ion (191 cm^{-1}) and the $ZnClBr_3^{2-}$ ion (202 cm^{-1}), based on the qualitative model presented earlier and the results obtained by Delwaulle[16] for the mixed anions in an aqueous solution. The FWHM of these ν_1 modes increases as the number of Cl atoms in the ion increases (see Figure 3.8), indicating that the ions become more sensitive to the crystal field. This is possibly connected to the large number of phases found for low x values (the anharmonicity of the potential increases as x decreases).

Table 3.5 : Frequencies and relative intensities resulting from fits of the ν_1 modes in the A_g Raman spectra at T=300 K to Lorentzian shaped peaks.

x=0		x=1		x=2		x=2.9		x=4	
ν (cm^{-1})	I_0	ν (cm^{-1})	I_0	ν (cm^{-1})	I_0	ν (cm^{-1})	I_0	ν (cm^{-1})	I_0
				173	13.1	171	43.0	170	93.4
		184	9.7	183	33.0	182	35.9		
		192	28.1	191	17.8	192	4.0		
		202	7.6	202	7.4	205	6.4	210	6.6
278	100	276	54.6	276	28.7	280	10.6		

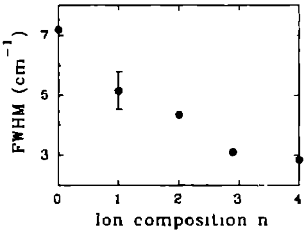

Figure 3.8 : Ion composition (n) dependence for the ZCB_n^{2-} ions of the FWHM of the ν_1 modes in the Raman A_g high temperature spectra as determined from the Lorentz fits presented in Table 3.5.

Using the intensities listed in Table 3.5, an estimate can be made of the relative concentrations $\rho_n(x)$ of the various ZCB_n^{2-} anions in the different TZCB crystals, which in turn can be used to estimate the value of x. In order to do this, we assume that the intensity of the peaks is only proportional to the concentration of scatterers in the crystal, and therefore one has an equal scattering efficiency for the various ZCB$_n^{2-}$ anions. A problem arises for the $ZnCl_3Br^{2-}$ ion, because the ν_1 mode of this ion is (almost) degenerate with the ν_3 modes of the $ZnBr_4^{2-}$ ion. The influence of the ν_3 modes can be estimated using the intensity ratio $I_o(\nu_3)/I_o(\nu_1)$ of $ZnBr_4^{2-}$ in the spectra of the x = 4 compound and the intensity $I_o(\nu_1)$ of $ZnBr_4^{2-}$ in the spectra of the mixed crystals. The estimated values of $\rho_n(x)$ are listed in Table 3.6. This Table shows that the $ZnCl_3Br^{2-}$ anion is only present in very low concentrations in the mixed crystals. From the Raman results of Benhmida *et al.*[17] we conclude that the concentration of this ion is only appreciable for very low values of x. It seems that there is a preference to form either the pure anions or mixed ions with a number of Br atoms larger than one. Table 3.6 also shows the calculated values x_{calc} of the composition of the crystals. These values lie within 10 % of those of the growth solutions, which is a fair agreement in view of the method used to obtain x_{calc}.

Table 3.6 : Relative concentrations $\rho_n(x)$ of the various configurations of the mixed tetrahedra in crystals with different composition (x), calculated from the fitted intensities presented in Table 3.4. From these concentrations the crystal composition x_{calc} has been calculated.

	x				
n	0	1	2	2.9	4
0	100	54.7	28.9	11.0	0
1	0	7.5	6.6	3.5	0
2	0	28.1	18.0	4.1	0
3	0	9.7	33.3	37.0	0
4	0	0	13.2	44.4	100
x_{calc}	0	0.93	1.95	3.00	4

Until now we have been mainly discussing the ν_1 modes of the mixed ions in the Raman high temperature A_g spectra. The other modes of the mixed ions are not directly observed in the Raman spectra. For the ν_3 modes this is due to the nearly degeneracy with the ν_1 modes of the tetrahedra. In the FIR spectra we observed two bands in the ν_1,ν_3 region, mainly originating from the ν_3 modes. In our model (Figure 3.7) the ν_3 frequencies are generally too high. Qualitatively, however, the model predicts for the mixed crystals two groups of ν_3 modes, approximately at the ν_3 frequencies of the pure ions, as is also observed in the FIR spectra.

The ν_2 and ν_4 modes generally overlap with each other, and with the external modes in both the Raman and FIR spectra. In the mixed crystals the ν_2 and ν_4 structure is broadened due to the splitting of the modes, and it shifts towards lower frequency as x increases (see also Figure 3.7).

Using the polarised Raman spectra and the selection rules of the ν_1 modes in the Pnma phase of the mixed crystals, one can in principle determine whether the site symmetry of the ions is C_s or C_1, and thus obtain some insight in a possible ordering of the substitution of Cl by Br (see section 3.3). Unfortunately, the large thermal factors of the ions already effectively lower the site symmetry to C_1 in the pure compounds, as it follows from the ν_1 presence in the B_{1g} and B_{3g} spectra. Therefore the site symmetry of the ions in the mixed crystals is also expected to be C_1, regardless of any ordering in the substitution.

3.4.2 EXTERNAL MODES

In the high temperature FIR and Raman spectra the external modes are observed as broad structures at low frequencies. The only resolved peak is found at $\sim 24\ \mathrm{cm}^{-1}$ in the Raman spectra (see Figures 3.2.a and 3.3). The composition dependence of this mode (see Figure 3.4) suggests that it is a librational mode of the ZCB_n^{2-} ions. This is shown by the dashed curves in Figure 3.4, which give the $\mathbf{k} = 0$ frequency dependence of a chain of harmonically coupled rotators with the same moments of inertia as an average ZCB_n^{2-} ion in the corresponding crystal. On the other hand, the pure librational modes of the crystals in the Pnma phase are expected to be only Raman active in either A_g and B_{2g} or B_{1g} and B_{3g} geometry, whereas Figure 3.2.a shows that this mode is mainly active in A_g and B_{1g} geometry. Figure 3.3 shows the temperature dependence of this mode in a $x = 1$ compound. The mode is insensitive to the phase transition to the incommensurate phase at $T_i \approx 291$ K, which is mainly a modulated rotation of the heavy tetrahedra around the **b**-axis. After the transition to the monoclinic $P2_1/n11$ phase at $T_m = 282$ K a hardening of the mode is observed.

Another interesting feature in the high temperature Raman spectra is the broadening of the Rayleigh wings observed predominantly in the A_g and B_{1g} spectra. The temperature dependence in Figure 3.3.a shows that this broadening decreases as the temperature decreases. Indeed, in the low temperature spectra (Figure 3.2.b) this broadening has disappeared. This broadening possibly results from quasi-elastic scattering from the $N(CH_3)_4^+$ ions due to the large rotational freedom of these ions at higher temperatures.[18, 19] At low temperatures this freedom freezes out.[20]

3.5 CONCLUSIONS

We have presented polarised Raman spectra and FIR transmission spectra of the solid solution $[N(CH_3)_4]_2ZnCl_{4-x}Br_x$ for $x = 0, 1, 2, 2.9$ and 4 at $T \approx 60$ K and $T \approx 300$ K. In the spectra new modes appear, which are not present in the spectra of the pure Cl and Br crystals. These modes are assigned to the internal modes of the ZCB_n^{2-} ions, in agreement with a simple valence-bond model. The thermal motions of the heavy tetrahedra effectively lower the site symmetry in the high temperature phase from C_s to C_1. It is therefore not possible to determine from the selection rules whether there are preferred ion sites for the substitution of Cl by Br. The appearance of all the ν_1 mixed ion modes in the spectra indicate, however, that there are no preferred sites for the substitution.

The most interesting features in the spectra for further investigations are the $\sim 24\ \mathrm{cm}^{-1}$ mode of the ZCB_n^{2-} ions, which given its temperature dependence (hardening in the lock-in phase) could be coupled to a "soft mode" which is responsible for the incommensurate phase transition. It should be noted, however, that experimentally no soft mode behaviour has been observed so far, possibly due to a strong broadening of this mode resulting from couplings to other excitations in the crystal. Another interesting feature is the broadening of the Rayleigh wing, possibly caused by quasi-elastic light scattering from the $\mathrm{N(CH_3)_4^+}$ ions. This broadening is expected to change discontinuously at the various phase transitions of the crystals. From the temperature and composition dependence of these modes one can gain some more insight in the mechanisms of the phase transitions in this system.

ACKNOWLEDGEMENTS We would like to express our thanks to Dr. H. Meekes and Dr. Th. Rasing for valuable discussions on the subject, and Prof.Dr. H. van Kempen for his support. This work is part of the research program of the Stichting voor Fundamenteel Onderzoek der Materie (FOM).

REFERENCES

1 T. Janssen, Ferroelectrics **66**, 203 (1986).

2 G. Godefroy, Phase Trans. **14**, 139 (1989).

3 E. Colla, P. Muralt, H. Arend, R. Perret, R. Godefroy, and C. Dumas, Sol. St. Comm. **52**, 1033 (1984).

4 E. Colla, *PhD thesis*, ETH Zürich, Switzerland (1987).

5 S. Sawada, Y. Shiroishi, A. Yamamoto, M. Takashige, and M. Matsuo, Phys. Lett. **67A**, 56 (1978).

6 K. Gesi, J. Phys. Soc. Jpn. **51**, 203 (1982).

7 P. Trouelan, J. Lefebvre, and P. Derollez, Acta Cryst. C **41**, 846 (1985).

8 B.W.H. van Beest, Phys. Rev. B **33**, 960 (1986).

9 H. Meekes, A. Janner, and T. Janssen Z. Phys. B **71**, 273 (1988).

10 H. Arend, R. Perret, H. Wüest, and P. Kerkoc, J. Cryst. Growth **74**, 321 (1986)

11 B. Dam and A. Janner, Acta Cryst. B **42**, 69 (1986).

12 L.J.P. Vogels, M.A. Verheijen, and P. Bennema, J. Cryst. Growth **110**, 604 (1991).

13 J.T. Edsall, J. Chem. Phys. **5**, 225 (1937).

14 D.F.C. Morris, E.L. Short, and D.N. Waters, J. Inorg. Nucl. Chem. **25**, 975 (1963).

15 E. Colla, V. Gramlich, and W. Petter, Acta Cryst. C **43**, 1070 (1987).

16 M.-L. Delwaulle, Bull. Soc. Chem. Fr., 1294 (1955).

17 M. Benhmida, R. Machet, J.-C. Jules, and B. Janot, Phase Trans. **9**, 111 (1987).

18 L. Pauling, Phys. Rev. **36**, 430 (1930).

19 J. Frenkel, Acta Phys. Chem. **3**, 23 (1935).

20 R. Blinc, M. Burger, J. Slak, and F. Milia, Phys. Stat. Sol. **a56**, K65 (1979).

CHAPTER 4

RAMAN STUDY OF THE FERROELECTRIC SEMICONDUCTOR $SN_2P_2SE_6$[1]

P.H.M. van Loosdrecht[a], M.M. Maior[a,b], S.B. Molnar[b],
Yu.M. Vysochanskii[b], P.J.M. van Bentum[a], and H. van Kempen[a].

[a] *Research Institute of Materials, University of Nijmegen, Toernooiveld,
NL-6525 ED Nijmegen, The Netherlands.*
[b] *Institute of Physics and Chemistry of Solid State, Uzhgorod State University,
29400 Uzhgorod, Ukraine.*

ABSTRACT.

The Raman spectrum of $Sn_2P_2Se_6$ is found to be in good agreement with the selection rules in the para- and ferroelectric phases. The incommensurability has only a minor influence on the phonon scattering in $Sn_2P_2Se_6$. A broad central peak is found in the ferroelectric phase, which intensity reaches a maximum near the lock-in phase transition. Line shape distortions of some of the phonon modes indicate a Fano type of coupling to the excitations causing the central peak.

---

[1] Submitted to *Physical Review B*.

4.1 INTRODUCTION

The $Sn_2P_2Se_6$ compound is a member of the isomorpic $(Pb_xSn_{1-x})_2P_2(S_ySe_{1-y})_6$ family of ferroelectric semiconductors. The (x,y,T)-phase diagram of this monoclinic family exhibits a ferroelectric ($x < 0.4$) and a paraelectric phase, with for $y < 0.72$ an intermediate incommensurate phase.[1] At room temperature the pure $Sn_2P_2Se_6$ compound is in a paraelectric phase with centro-symmetric space group $P2_1/c$ ($Z = 2$). At $T_i = 221$ K a second order phase transition occurs to a displacively modulated incommensurate phase with the average structure of the high temperature phase and modulation wavevector $\mathbf{q} \approx 0.85\mathbf{a}^* + 0.75\mathbf{c}*$. At $T_l = 193$ K there is a first order lock-in transition to a proper ferroelectric phase with space group P_c ($Z = 2$).[2] The incommensurate phase is absent in the pure $Sn_2P_2S_6$ compound which has only a single second order phase transition from the paraelectric to the ferroelectric phase. This phase transition is induced by the condensation of a soft mode of B_u symmetry in the high temperature phase and of A' symmetry in the low temperature phase.[3] Due to phonon-phonon coupling the frequency of the soft mode in $Sn_2P_2S_6$ does not vanish at T_c. Apart from this phonon-phonon coupling Slivka *et al.*[3] observed a coupling of the soft mode to the observed broad central peak in their Raman spectra. This is not unusual since many ferroelectrics show a strong coupling between the phonon system and dielectric fluctuations near the ferroelectric phase transition.[4, 5, 6] One can expect that in $Sn_2P_2Se_6$ similar coupling effects exist.

In the present paper we report the first Raman spectroscopic study of the dynamical properties of $Sn_2P_2Se_6$ in the paraelectric, incommensurate, and ferroelectric phases. In addition results are reported on the temperature dependence of the low frequency part of the Raman spectrum in the ferroelectric phase. Lineshape distortions of some of the phonons strongly indicate a Fano[7] type of coupling to the excitations causing the broad central peak observed in the spectra.

4.2 EXPERIMENTAL

Nicely faceted $Sn_2P_2Se_6$ single crystals are obtained using a sublimation growth technique. The crystals used in the experiments are oriented on the basis of their morphology and by X-ray diffraction, and are mounted on the cold finger of a flow cryostat (stabilised to ±0.1 K, absolute error ±2 K). Polarised Raman experiments are performed in a backscattering geometry on natural crystal faces using a DILOR XY multichannel spectrometer (spectral slit width 1.5 cm^{-1}) with a Ti:Sapphire-laser (740 nm, 200 mW/cm^2) as excitation source. The photon energy of the excitation used has the advantage that it is below the bandgap energy of $Sn_2P_2Se_6$, preventing excessive heating due to strong absorption as observed under 514 nm excitation. Polarised Raman spectra (5-2000 cm^{-1}) are recorded in $\mathbf{a}(\mathbf{b},\mathbf{b})\bar{\mathbf{a}}$

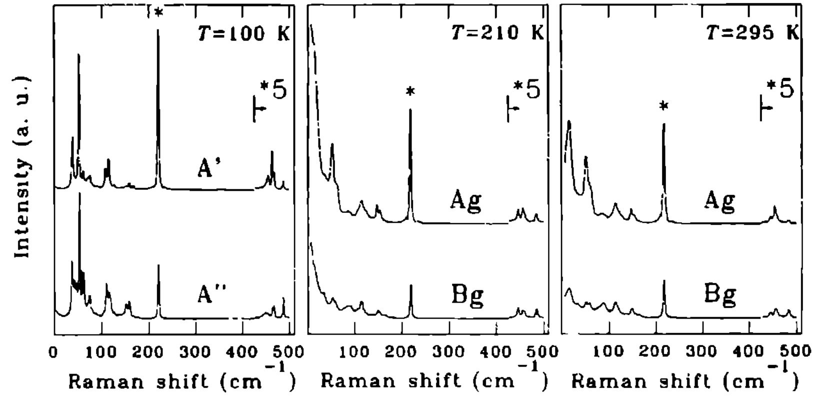

Figure 4.1 : Polarised Raman spectra of $Sn_2P_2Se_6$ *in* **a(b,b)a** *(A' and* A_g*) and* **a(b,c)a** *(A'' and* B_g*) geometries for the ferroelectric (T=100 K), incommensurate (T=210 K) and paraelectric (T=295 K) phases. The P-P vibrations denoted by * in the* **a(b,b)a** *spectra are scaled down by a factor of two. Above 425* cm^{-1} *the spectra are scaled up by a factor of five.*

and **a(b,c)ā** geometries, corresponding to A_g (A') and B_g (A'') symmetry in the paraelectric (ferroelectric) phase, respectively. Fig. 4.1 shows the polarised Raman spectra recorded in the paraelectric (T = 295 K), incommensurate (T = 210 K), and ferroelectric phases (T = 100 K) for 5 cm^{-1} $< \omega <$ 500 cm^{-1}. The frequencies of the peaks observed in the spectra are listed in Tab. 4.1. No structure is found above 500 cm^{-1}. A large number of modes is observed at all temperatures, reflecting both the low symmetry of the crystals as well as the large number of atoms (20) in the primitive cell of the structure. The total number of observed modes is given in the last row of Tab. 4.1.

4.3 DYNAMICAL PROPERTIES OF $SN_2P_2SE_6$

The Raman spectra of Fig. 4.1 show three regions of interest. The first region below 200 cm^{-1} contains the external modes and the internal Se-P-Se bending modes of the structural $(PSe_3)^{2-}$ units. Since the Se-P-Se bending modes overlap with the external modes one can expect some mixing of these modes. Therefore a distinction between external and internal modes is somewhat questionable here. The two other regions are found around 220 cm^{-1} and between 400 and 500 cm^{-1}, containing the Se_3P-PSe_3 and the P-Se valence vibrations, respectively.

Table 4.1 : Peak frequencies (in cm^{-1}) of the observed modes in the polarised Raman spectra of $Sn_2P_2Se_6$ in the ferroelectric (F), incommensurate (IC) and paraelectric (P) phases, respectively. The last row gives the total number of observed modes in the spectra.

F		IC		P		F		IC		P	
T=100 K		T=220 K		T=295 K		T=100 K		T=220 K		T=295 K	
(b b)	(b,c)	(b,b)	(b,c)	(b,b)	(b c)	(b,b)	(b,c)	(b,b)	(b,c)	(b,b)	(b,c)
A'	A''	A_g	B_g	A_g	B_g	A'	A''	A_g	B_g	A_g	B_g
		12	12	16	16	115	116	115	115	114	114
38	38		34		35		119				
39	43					126	126	124			
	48						141		138		
53	53	53	53	52	52	151	151	148	150	147	148
58	58		59		59	158	158	155	155	152	
62	62	63		62			168		163		162
70	70					220	220	219	219	217	217
72	73					355		351		349	
75	74						448	446	446	444	444
80	79					452	453				
85	85		83	85		454		455	455	454	453
89	88	87	87		88	463	463	460	459		457
93	93		92			467	467				
95	95					485					479
108	110	107	107			487	487	484	485	482	482
Total observed modes						26	28	15	18	12	14

4.3.1 COMPARISON OF $\mathrm{SN_2P_2SE_6}$ TO $\mathrm{SN_2P_2S_6}$

The frequencies of the P-P and P-S vibrational modes can be compared to the corresponding frequencies as measured in $Sn_2P_2S_6$ crystals.[8] The S_3P-PS_3 vibration in $Sn_2P_2S_6$ is found at 381 cm^{-1}. Scaling this frequency with the square root of the mass ratio $\sqrt{M_{PS_3}/M_{PSe_3}}$ yields 262 cm^{-1}. This value overestimates the measured frequency (220 cm^{-1}) in $Sn_2P_2Se_6$ by 19 %. This difference originates from a difference in P-P bond strength of the anions in the two compounds mainly due to the different ion radii of the S and Se ions. From the difference between the mass scaled and observed frequencies one can estimate the P-P bond strength ratio λ_{Se}/λ_S to be ≈ 0.70.

In a similar manner one can compare the P-Se and P-S valence vibrations found around 470 and 575 cm^{-1}, respectively. Scaling the latter frequency with the square root of the effective masses $\mu_{PS_3,PSe_3} = 3M_P M_{S,Se}/(M_P + 3M_{S,Se})$ one finds 531 cm^{-1}. Again a too high value resulting from the difference in bond strengths. The ratio between the bond strengths is estimated to be $\lambda'_{Se}/\lambda'_S \approx 0.78$, in good agreement with the ratio 0.82 found by Drowart *et al.*[9] in dissociation experiments.

4.3.2 SYMMETRY ASPECTS

The selection rules for inelastic light scattering are determined from a symmetry analysis of the vibrational properties of $Sn_2P_2Se_6$. For the paraelectric and ferroelectric phase this is done using a conventional factor group analysis.[10] In the incommensurate phase this method is no longer appropriate. Instead, the convenient superspace approach outlined by Janssen[11] and Currat and Janssen[12] is used to determine the selection rules. Although in principle one should consider all modes with wavevector $\mathbf{k} = l\mathbf{q}$ ($l \in \mathbf{Z}$) only vibrational modes with $\mathbf{k} = 0, \pm\mathbf{q}$ are taken into account. This is justified by the absence of higher order satellites in the X-ray diffraction pattern.[2] The results of the symmetry analysis in the three phases are listed in Tab. 4.2, where $n_{int.}$, n_{trans}^{opt}, n_{rot}^{opt}, and n_{tot} correspond to the number of internal vibrational motions of the $(PSe_3)^{2-}$ anions, external optical translational modes, external optical rotational modes, and the total number of vibrational modes of a given symmetry, respectively. The relatively low symmetry of $Sn_2P_2Se_6$ in all phases leads to a nearly equal number of active modes in the various symmetries. The selection rules found for the paraelectric and ferroelectric phases are in good agreement with the results obtained by Vysochanskii *et al.*[8] for the isostructural $Sn_2P_2S_6$ compound.

Table 4.2 : The number of vibrational modes at $\mathbf{k}=0$ *in the different phases of* $Sn_2P_2Se_6$. *The last column gives the activity of the modes in Raman and IR experiments. For the incommensurate phase only modes with* $\mathbf{k}=0$ *and* $\pm\mathbf{q}$ *are taken into account.*

Paraelectric phase ($P2_1/c$)

irrep.	$n_{int.}$	n_{trans}^{opt}	n_{rot}^{opt}	n_{tot}	activity
A_g	6	6	3	15	(a,a),(b,b),(c,c),(a,c)
B_g	6	6	3	15	(a,b),(b,c)
A_u	6	5	3	14	b
B_u	6	4	3	13	a, c

Incommensurate phase ($P2_1/c$, $\mathbf{q}\approx0.85\mathbf{a}^* + 0.75\mathbf{c}^*$, l=0,±1)

irrep.	$n_{int.}$	n_{trans}^{opt}	n_{rot}^{opt}	n_{tot}	activity
A_g	12	12	6	30	(a,a),(b,b),(c,c),(a,c)
B_g	12	12	6	30	(a,b),(b,c)
A_u	12	11	6	29	b
B_u	12	10	6	28	a, c

Ferroelectric phase (P_c)

irrep.	$n_{int.}$	n_{trans}^{opt}	n_{rot}^{opt}	n_{tot}	activity
A'	12	10	6	28	a,c;(a,a),(b,b),(c,c),(a,c)
A''	12	11	6	29	b;(a,b),(b,c)

Clearly, the spectra reveal most of the predicted modes in the paraelectric and ferroelectric phases. In the incommensurate phase more modes are observed than predicted from the selection rules for the average structure (the paraelectric phase), due to the activity of

$\mathbf{k} = \pm l\mathbf{q}$ ($l \neq 0$) modes. Nevertheless, only a few additional modes are found; the total number of observed modes is much smaller than what one expects from the symmetry analysis in the incommensurate phase (see Tab. 4.2). One can therefore conclude that the incommensurability has only a small influence on the dynamical properties of $Sn_2P_2Se_6$, which is a strong indication that the amplitude of the modulation is rather small.

The internal vibrations of the $(PSe_3)^{2-}$ anions (C_{3v} symmetry) can be classified as

$$\Gamma^{C_{3v}}_{PSe_3^{2-}} = 2A_1 + 2E \quad .$$

The selection rules predict in the commensurate phases a splitting of the P-Se valence vibrations (A_1+E) into six components per scattering geometry, two originating from the A_1, and four from the doubly degenerate E mode. The multiplets found around 470 cm^{-1} indeed show 4-6 modes in each geometry. The relatively large splitting of these modes indicates a rather strong distortion of the $(PSe_3)^{2-}$ pyramids in the crystal. A similar relative splitting of these modes is found in each crystal phase indicating a nearly equal distortion in all phases, this in contrast to the situation in $Sn_2P_2S_6$ crystals[8]

The two $(P_2Se_6)^{4-}$ units per primitive cell. lead to two P-P vibrations at $\mathbf{k} = 0$ which correspond to in-phase (A' or A_g symmetry) and out-of-phase (A'' or B_g) vibrations of the two P-P bonds, respectively. One can expect that the out-of-phase vibration has a smaller second order polarisability than the in-phase vibration. This is indeed observed in the difference of the intensities of the P-P peak in the A' (A_g) and A'' (B_g) spectra.

4.4 LOW ENERGY SCATTERING

Slivka *et al.*[3] have measured the temperature dependence of the soft mode at 32 cm^{-1} in $Sn_2P_2S_6$ associated with the ferroelectric phase transition, revealing a strong coupling of this mode with a Raman active lattice mode at 40 cm^{-1}. In addition, they proposed a coupling of the soft mode to the observed "central peak" in their spectra. Fig. 4.2a) shows the low frequency $c(a,a)\bar{c}$ Raman spectrum of $Sn_2P_2Se_6$ at various temperatures. Also in this case low frequency scattering reminiscent of a central peak is observed, with an intensity increasing with temperature to a maximum at or slightly above the ferroelectric-incommensurate phase transition. At temperatures far above the incommensurate-paraelectric phase transition the quasi-elastic scattering has strongly decreased. In the incommensurate phase a new mode appears in the spectrum at 12 cm^{-1}. This modes hardens with temperature and at room temperature it is found at 16 cm^{-1}. It seems that this mode is the soft mode of the ferroelectric phase transition, although more experiments on its temperature dependence are needed to make any definite conclusions. The temperature dependence of the frequencies plotted in Fig. 4.2b shows a softening of three of the modes at 38, 53 and 61 cm^{-1}. In particular the frequencies of the modes at 38

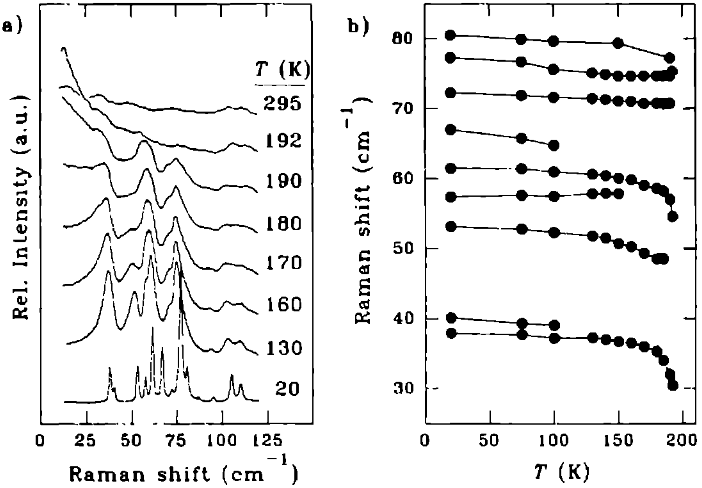

Figure 4.2 : a) Temperature dependence of the low frequency part of the (**a**,**a**) *Raman spectrum of* $Sn_2P_2Se_6$ *in the ferroelectric phase. The intensities are relative to the integrated intensity of the P-P vibration at 220* cm^{-1}.
b) Temperature dependence of the peak frequency of the low frequency energy in the (**a**,**a**) *spectrum of* $Sn_2P_2Se_6$ *in the ferroelectric phase.*

and 53 cm^{-1} decrease strongly upon approaching the phase transition at $T = 293$ K. None of these modes show the usual $\omega \approx (T_0 - T)^\gamma$ behaviour of an uncoupled soft mode near the phase transition. The temperature dependence of the frequencies and intensities give no direct evidence for phonon-phonon interactions, however. Instead a deformation of the lineshape is observed for the modes at 38 and 53 cm^{-1}. The form of the lineshape distortion strongly indicates a coherent coupling of these phonons to a continuum of excitations in the crystal, *i.e.* a Fano type of coupling.[7] The origin of the continuum of states, *i.e.* of the observed quasi-elastic scattering and lineshape distortions is at present unknown. A good candidate for these states, however, is the continuum arising from the dynamics of the local dipole moments in the ferroelectric phase of $Sn_2P_2Se_6$. Another possibility is that the low energy scattering is due to the electronic excitations in this semiconducting material. The spectral intensity of such a coupled system can be described as[7, 13]

$$I(\epsilon) \propto \frac{\epsilon + q}{(1 + \epsilon^2)} , \tag{4.1}$$

with $\epsilon = 2(\omega - \omega_0)/\Gamma$, ω_0 the perturbed phonon frequency, and q the so-called Fano parameter which is in first order inversely proportional to the interaction strength (V) and the density of continuum states (ρ). The linewidth Γ is proportional to ρV^2.

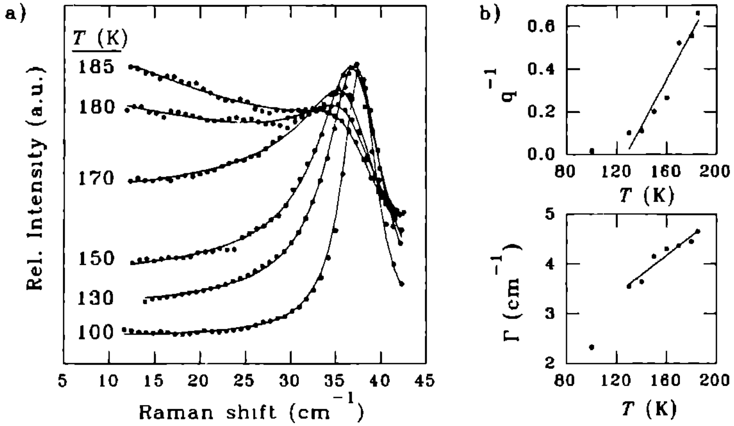

Figure 4.3 : a)Fit of the fano profile (Eq. 4.1) superimposed on a linear underground to the 38 cm^{-1} Raman peak at various temperatures in the ferroelectric phase.
b) The resulting parameters q^{-1} (upper part) and Γ (lower part) of the fits shown in a) as a function of the temperature. The solid lines are a guide to the eye.

Fig. 4.3a) shows the results of a fit of Eq. 4.1 to the experimental lineshape of the 38 cm^{-1} mode for several temperatures in the ferroelectric phase. In these fits a linear underground is assumed to account for the incoherent part of the continuum scattering. A good fit is obtained for all temperatures in the range 20-185 K. Only very close to the phase transition the fit breaks down, mainly due to the weak phonon part in the spectra. The perturbed phonon frequency is found to be $\omega_0 = 37.5\pm0.2$cm^{-1} for all curves. The resulting fit parameters q^{-1} and Γ are shown in Fig. 4.3b). Above 130 K, up to close to the lock-in phase transition both q^{-1} and Γ increase approximately linear with temperature. This indicates that the interaction strength V does not vary strongly with temperature, and that the temperature dependence of both q^{-1} and Γ is caused by an increasing density of continuum states towards the phase transition. As is shown in Fig. 4.4, this increasing density of states is also reflected in the temperature dependence of the relative Raman intensity at 14 cm^{-1}, away from the phonon resonance. Again the temperature dependence is well approximated by a linear behaviour for $130 \text{ K} < T < 190$ K.

4.5 CONCLUSIONS

The number of modes observed in the polarised Raman spectra recorded in the ferroelectric and paraelectric phases are in good agreement with the selection rules. In the incommen-

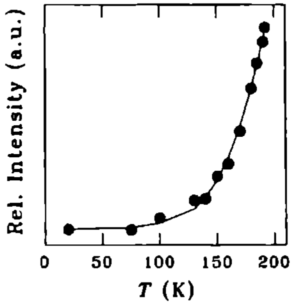

Figure 4.4 : Temperature dependence of the relative Raman intensity at 14 cm^{-1}. The intensity is relative to the integrated intensity of the P-P vibration at 220 cm^{-1}.

surate phase, however, the number of observed phonon modes is far less than the number of active modes predicted by the selection rules, despite the fact that only modes with $\mathbf{k} = 0, \pm\mathbf{q}$ have been taken into account.

At low frequencies a strong "central peak" is observed in the ferroelectric phase, which reaches a maximum intensity at or above the lock-in phase transition. The coupling of this low energy scattering to the phonons leads to a Fano type of distortion of the phonon peak. The temperature dependence of the linewidth and Fano parameter in the ferroelectric phase indicates an increasing density of continuum states upon approaching the lock-in phase transition. While the precise origin of the low energy scattering remains unknown at present, the fluctuations causing it are strongly related to the ferroelectric-incommensurate phase transition. It may very well be that the fluctuations are indeed due to the dynamics of the domain walls in the ferroelectric phase which remain as discommensurations or solitons in the incommensurate phase, consistent with the persistence of the quasi-elastic scattering in the incommensurate phase.

ACKNOWLEDGEMENTS We are grateful to M.I. Gurzan for providing the crystals. One of us (M.M.M.) would like to express his thanks to the staff of the Research institute of Materials of the University of Nijmegen for their hospitality and assistance, and the Dutch and former Soviet Union governments for financial support through a cultural exchange program. Part of this work was financially supported by the Dutch Foundation for Fundamental Research of Matter (FOM).

REFERENCES

1 Yu. M. Vysochanskii, M.M. Maior, V.M. Rizak, V. Yu. Slivka, and M.M. Khoma, Sov. Phys. JETP **68**, 782 (1989).

2 T.K. Barsamian, S.S.Khasanov, V. Sh. Shekhtman, Yu. M. Vysochanskii, and V. Yu. Slivka, Ferroelectrics **67**, 47 (1986).

3 V. Yu. Slivka, Yu. M. Vysochanskii, M.I. Gurzan, and D.V. Chepur, Sov. Phys. Solid State **20**, 2042 (1978).

4 G. Harbeke, E.F. Steigemeier, and R.K. Wehner, Sol. St. Comm. **8**, 1765 (1970).

5 F. Scott, Rev. Mod. Phys, **46**, 83 (1974).

6 R.A. Cowley and G.J. Coombs, J. Phys. C: Solid State Physics **6**, 143 (1973).

7 U. Fano, Phys. Rev. **124**, 1866 (1961).

8 Yu. M. Vysochanskii, V. Yu. Slivka, Yu. V. Voroshilov, M.I. Gurzan, and D.V. Chepur, Sov. Phys. Solid State **21**, 123 (1979).

9 J. Drowart, C.E. Myers, R. Szwarc, E. van der Ausera-Mahieu, and O.M. Uy, High Temp. Sci. **5**, 482 (1973).

10 See for instance G. Turrel, *Infrared and Raman Spectra of Crystals*, (Academic Press, London, 1972).

11 T. Janssen, J. Phys. C: Solid State Physics **12**, 5381 (1979).

12 R. Currat and T. Janssen, Solid State Physics **41**, 201 (1987).

13 M.V. Klein, in *"Light Scattering in Solids I"*, Vol. 8 of Topics in Applied Physics, edited by M. Cardona, (Springer Verlag, Berlin 1983), p169.

A NEW DIELECTRIC MATERIAL FOR LOW TEMPERATURE THERMOMETRY IN HIGH MAGNETIC FIELDS[1]

M.M. Maior[a,b], P.H.M. van Loosdrecht[b], P.J.E.M. van der Linden[b],
S.B. Molnar[a], Yu.M. Vysochanskii[a], M.I. Gurzan[a], and H. van Kempen[b]

[a] *Institute of Physics and Chemistry of Solid State, Uzhgorod State University, 29400 Uzhgorod, Ukraine.*
[b] *Research Institute of Materials and High Field Magnet Laboratory, University of Nijmegen, Toernooiveld, NL-6525 ED Nijmegen, The Netherlands.*

ABSTRACT.

Dielectric experiments on the incommensurate solid solution $(Pb_{0.45}Sn_{0.55})_2P_2Se_6$ for $T = 1.2$ K – 200 K reveal a strong temperature dependence of the real part of the dielectric constant for $T < 45$ K. The relative dielectric sensitivity $d\ln(\epsilon')/dT \approx 2 - 8\ \mathrm{K}^{-1}$ is found to be 2 – 3 times higher in comparison to widely used glass-ceramic temperature sensors. Moreover, the dielectric constant has a very good time stability and is insensitive to magnetic fields up to 20 T ($dT/dB < 10^{-4}$ K/T). These characteristics make this material a very promising candidate for applications in capacitive temperature sensors for low temperature thermometry in high magnetic fields.

---

[1] Submitted to *Applied Physics Letters*.

5.1 INTRODUCTION

Semiconductor sensors provide one of the most sensitive devices used in thermometry. In the presence of a magnetic field, however, their use is strongly limited due to magnetoresistive effects characteristic for semiconductors. Capacitive sensors using dielectric materials with a strong temperature dependence of the dielectric constant are in general less sensitive, but are relatively insensitive to magnetic fields. At present the commercially available glass-ceramic capacitance thermometers are widely used in thermometry in high magnetic fields.[1, 2, 3] In the present paper we report on a study of a new dielectric crystalline material suitable as a medium for low temperature thermometry in high magnetic fields.

At room temperature $Sn_2P_2Se_6$ has a paraelectric phase. Upon lowering the temperature two phase transitions occur to an incommensurate (IC) ($T_i = 220$ K) and a ferroelectric ($T_l = 193$ K) phase, respectively. It was recently shown that upon substituting tin atoms in the cation sublattice of $Sn_2P_2Se_6$ by isovalent lead atoms the temperature region of the incommensurate (IC) phase in these materials becomes more extended and simultaneously shifts towards lower temperatures.[4] For $y > 0.4$ the ferroelectric phase of $(Pb_ySn_{1-y})_2P_2Se_6$ has vanished and the IC phase is stable down to 0 K. The dielectric properties of the solid solutions with $y > 0.4$ deviate substantially from those of pure $Sn_2P_2Se_6$. The sudden drop in the dielectric constant, characteristic for the IC-ferroelectric phase transition disappears for $y > 0.4$ (see Fig. 5.1).

5.2 EXPERIMENTAL

Based on the character of the temperature dependence of the dielectric constant in various representatives of the $(Pb_ySn_{1-y})_2P_2Se_6$ solid solution[5] (see Fig. 5.1) the $y = 0.45$ compound is chosen as the most suitable candidate for further studies. The data shown in Fig. 5.1 for $y = 0.2$, 0.4, 0.5, 0.55, and 0.6 are obtained from sublimation grown crystals. This method provides high quality crystals but yield only small sized crystals, typically a few mm^3, which limits their practical applicability. In order to obtain larger samples, the $y = 0.45$ crystals are grown using the Bridgeman technique. The growth method has been described elsewhere.[6] The Bridgeman grown crystals are generally of somewhat less quality compared to sublimation grown crystals, as is for instance reflected in the lower absolute values of the dielectric constant (see Fig. 5.1).

For the experiments platelets perpendicular to the (100) direction are cut (5×5×1.5 mm^3) from a $(Pb_{0.45}Sn_{0.55})_2P_2Se_6$ crystal. Subsequently Al electrodes are evaporated on the surfaces of the platelets.

Dielectric measurements in the temperature region between 4.2 and 200 K were per-

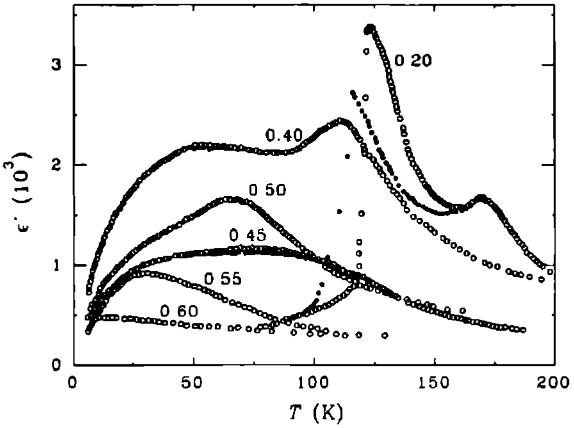

Figure 5.1 : Temperature dependence of the real part of the dielectric function of the $(Pb_ySn_{1-y})_2P_2Se_6$ *solid solutions (open circles: upon heating, filled circles: upon cooling) for y=0.20; 0.40; 0.45; 0.50; 0.55; and 0.60.*

formed in a dynamical flow cryostat in the quasi-static regime with a cooling/heating rate of 0.5 K/min by means of a GENERAL RADIO 1615-A transformer bridge operating at 1 kHz, with a measuring field of 4 V/cm. The sample was mounted inside a copper housing. The temperature is regulated by an OXFORD DTC 2 temperature controller in combination with a thermocouple mounted in the copper housing. The temperature was measured with a calibrated ALLAN-BRADLEY thermoresistor, also mounted in the copper housing. Measurements below 4.2 K have been performed with the copper housing immersed is a pumped liquid He bath cryostat. The temperature was measured using a SMD RuO resistor. For the magnetic field experiments at 1.2 and 4.2 K, the bath cryostat was mounted in a 20 T Bitter magnet at the Nijmegen High Field Magnet Laboratory. In this case, the capacitance of the sample was measured using an ANDEEN HAGERLING 2500A automatic capacitance bridge. A personal computer was used for the data collection.

5.3 RESULTS AND DISCUSSION

The temperature dependence of the dielectric constant of $(Pb_{0.45}Sn_{0.55})_2P_2Se_6$ shows a smeared maximum at 80 K and a plateau-like behaviour with a small thermal hysteresis between 80 and 50 K (see Fig. 5.1). The compounds with $y < 0.45$ exhibit the usual hysteresis which is characteristic for the incommensurate phase. For higher Pb concentrations, where the paraelectric-IC phase transition has shifted below 100 K, the thermal hysteresis in ϵ' is absent. For the $(Pb_{0.45}Sn_{0.56})_2P_2Se_6$ compound, the region below 50 K is of most interest in regard to its possible applicability in temperature sensors. In Fig. 5.2 we have

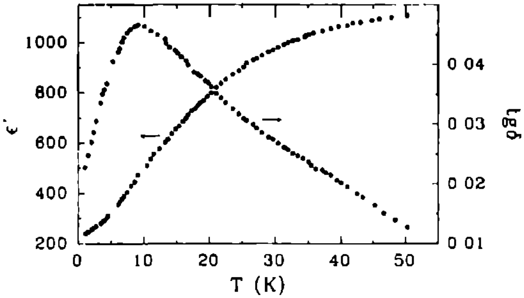

Figure 5.2 : Temperature dependence of ϵ' and tgδ for the $(Pb_{0.45}Sn_{0.55})_2P_2Se_6$ solid solution at E=4 V/cm and f=1 kHz. The arrows indicate the vertical scale for the curves.

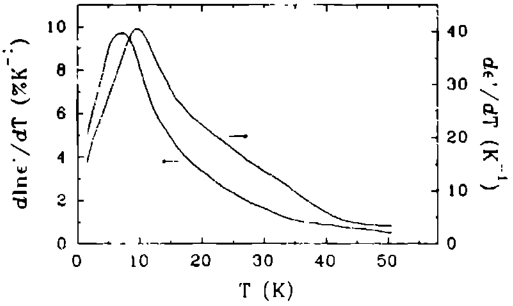

Figure 5.3 : Temperature dependence of $d\epsilon'/dT$ and $d\ln\epsilon'/dT$ for the $(Pb_{0.46}Sn_{0.55})_2$-P_2Se_6 solid solution as calculated from Fig. 5.2. The arrows indicate the vertical scale for the curves.

plotted the dielectric constant and the loss tangent tgδ for $(Pb_{0.45}Sn_{0.55})_2P_2Se_6$ for temperatures below 50 K. The loss tangent shows a peak near 10 K. The dielectric constant exhibits a frequency dispersion of about 0.04 % kHz^{-1} in the 1 – 20 kHz region. Measurements of the time stability of the capacitance and the dielectric loss at 4.2 K showed only very small variations, which could be attributed to pressure variations in the He bath cryostat. The temperature dependence of the absolute $(d\epsilon'/dT)$ and relative $(d\ln(\epsilon')/dT)$

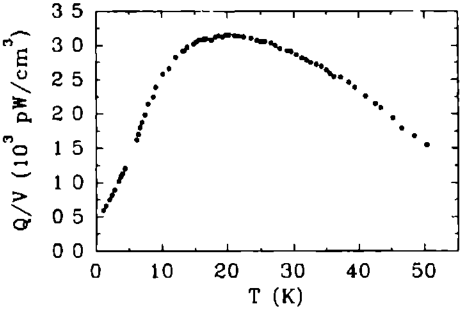

Figure 5.4 : Specific self-heating for the $(\mathrm{Pb}_{0.45}\mathrm{Sn}_{0.55})_2P_2Se_6$ *solid solution calculated from Eq. 5.1.*

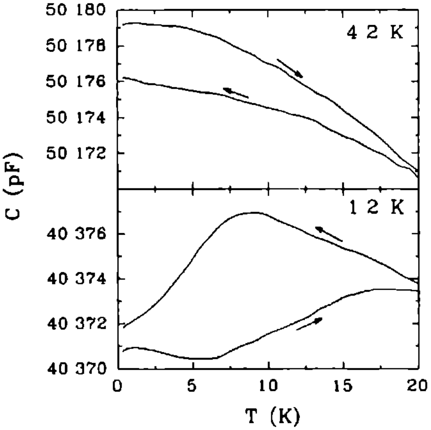

Figure 5.5 : Effect of the magnetic field on the capacitance of an $(\mathrm{Pb}_{0.45}\mathrm{Sn}_{0.55})_2P_2$*-*$Se_6$ *sample at 4.2 K and 1.2 K at a magnetic field sweep rate of 1 T/min.*

sensitivities of the material as a temperature sensor derived from Fig. 5.2 are plotted in Fig. 5.3. The absolute and relative sensitivities reach their maxima at 10 K and 7 K, respectively. An important parameter in thermometry, especially at low temperatures, is the amount of heat produced by the used sensor. For capacitance sensors, this heat is produced by dissipation due to dielectric losses. The specific self-heating in dielectrics is defined as[7]

$$\frac{Q}{V} = \pi f \; \epsilon_0 \epsilon' \; \mathrm{tg}\delta \; E^2 \quad , \tag{5.1}$$

where V is the sample volume of the dielectric subjected to an time varying electric field E with a frequency f. The real part of the dielectric function is denoted by ϵ', and tgδ is the dissipation factor. The calculated temperature dependence of the specific self-heating in $(\mathrm{Pb}_{0.45}\mathrm{Sn}_{0.55})_2\mathrm{P}_2\mathrm{Se}_6$ (f = 1 kHz, E = 4 V/cm) is shown in Fig 5.4. It is worth noting that the self-heating decreases as a function of temperature below 20 K, *i.e.* in the temperature region where a low dissipation is of vital importance. Similar to glass-ceramic thermometers, the self-heating is very small and lies in the pW/cm^3 range. The maximum in the self-heating corresponds to 40 fW dissipation in the used samples.

Fig. 5.5 shows the magnetic field dependence of the capacitance of $(\mathrm{Pb}_{0.45}\mathrm{Sn}_{0.55})_2\mathrm{P}_2\mathrm{Se}_6$ for T = 1.2 K and 4.2 K. The measurements plotted here are recorded at a magnetic field sweep rate of 1 T/min. In general it was found that the amplitude of the hysteresis observed in Fig. 5.5 increases for increasing sweep rates. It is conceivable that part of this hysteresis and its sweep rate dependence is due to local temperature variations in the bath cryostat, caused by for instance eddy currents in in the copper heat shields. Similar effects have been observed in dielectric measurements on glass-ceramic materials.[1] The fact that the capacitance does not restore to its initial value is caused by pressure drifts giving rise to a drift in the overall bath temperature. This drift is also observed in the absence of a magnetic field.

5.4 CONCLUSIONS

In comparing the results on the dielectric parameters of $(\mathrm{Pb}_{0.45}\mathrm{Sn}_{0.55})_2\mathrm{P}_2\mathrm{Se}_6$ reported here to those of the widely used glass-ceramic thermometers we find that $(\mathrm{Pb}_{0.45}\mathrm{Sn}_{0.55})_2\mathrm{P}_2\mathrm{Se}_6$ has a significantly higher absolute (2 − 3 times) and relative (6 − 7 times) thermal sensitivity. In particular, we find for the relative sensitivity $d\ln C/dT = 8.5$ % K^{-1}, whereas for the glass-ceramic materials a value of $d\ln C/dT = 1.3$ % K^{-1} has been reported.[2] At 1.2 K the relative sensitivity is about 5% K^{-1}. Hence, one can expect that even in the sub-Kelvin regime the sensitivity is still appreciable. This regime is currently under investigation.

The first experiments on the time stability in 30 minutes, as well as on the reproducibility upon thermal cycling show variations in the capacitance corresponding to temperature fluctuations of approximately 5 mK. This value gives an upper bound for the variations, and is determined by the experimental conditions. Further experiments are needed to obtain more accurate data.

The magnetic field dependence of the capacitance corresponds to a field sensitivity of at most 0.1 mK/T for $B < 20$ T. It should be noted, however, that a major part of the field dependence of $(Pb_{0.45}Sn_{0.55})_2P_2Se_6$ is caused by the experimental conditions, and does not relate to the field dependence of the dielectric parameters.

In respect to the above conclusions, it seems that the $(Pb_{0.45}Sn_{0.55})_2P_2Se_6$ solid solution provides a most suitable candidate for applications in low temperature thermometry in high magnetic fields.

ACKNOWLEDGEMENTS We are grateful to V. Yu. Slivka for helpful discussions. One of us (M.M.M.) would like to express his thanks to the staff of the Research institute of Materials of the University of Nijmegen for their hospitality and assistance, and the Dutch and former Soviet Union governments for financial support through a cultural exchange program. Part of this work was financially supported by the Dutch Foundation for Fundamental Research of Matter (FOM).

REFERENCES

1 W.N. Lawless, Rev. Sci. Instrum. **42**, 561 (1971).

2 L.G. Rubin and W.N. Lawless, Rev. Sci. Instrum. **42**, 571 (1971).

3 W.N. Lawless, Rev. Sci. Instrum. **46**, 525 (1975).

4 Yu.M. Vysochansky, M.I. Gurzan, M.M. Maior, C.F. Motrja C.F., S.I. Perechinskii, M.V. Potorij, L.A. Salo, M.M. Khoma, V.Yu. Slivka, and Vorosilov Yu.V., Sov. Phys. Solid State **27**, 529 (1985).

5 M.M. Maior *et al.*, to be published.

6 M.I. Gurzan, *PhD thesis*, Uzhgorod State University, Uzhgorod, (1983).

7 H. Frolich, *Theory of Dielectrics*, chapter 1 (Oxford, England, 1957).

PART II

FULLERENES

INTRODUCTION

For a long time graphite and diamond were considered to be the only existing pure forms of carbon in nature. This changed in 1985 with the discovery by H.W. Kroto and R.E. Smalley, and coworkers[1] of two-dimensional closed network molecules, formed by joined hexagons and pentagons with a carbon atom at each of their corners. A new class of materials was found: *the fullerenes*. In a way the fullerenes present, by virtue of their closed structure, the purest form of carbon; there are no chemically terminated end-planes like the faces on graphite and diamond crystals in these molecules. The name of the new class reflects the similarity these molecules have with the geodetic domes designed by the American architect and inventor R. Buckminster Fuller, which he had already patented in 1954.[2] This resemblance is in particular true for the prototype fullerene C_{60}, appropriately dubbed Buckminsterfullerene. The soccerball shaped C_{60} molecule, with its 60 *equivalent* atoms is the simplest representative of the fullerenes. Like all other fullerenes it conforms to the closed network polygon rule formulated by Euler[3], from which one can derive that there are exactly 12 pentagons in a fullerene structure. The high icosahedral symmetry of Buckminsterfullerene, making all its atoms equivalent, is beautifully demonstrated in the appearance of a *single* peak in the ^{13}C-NMR spectrum of C_{60}.[4] This high symmetry has a strong impact on the physical properties of C_{60}. It causes up to fivefold degeneracies of the electronic and vibrational levels, strongly decreases the number of non-zero matrix elements for inelastic (optical) scattering processes, and is responsible for the high degree of orientational disorder in the solid state at ambient temperatures. The high symmetry of Buckminsterfullerene is not a general property of the fullerene family. The next most abundant one, C_{70}, already has a lower D_{5h} symmetry in which one can distinguish five different groups of equivalent atoms. With the lowering of symmetry the experimental and theoretical complexity of the fullerenes increases. This is reflected for instance in the existence of several stable isomeric structures for the higher fullerenes, the difference in the number of observed solid state structures, and in the increasing complexity of the inelastic optical spectra which probe their vibrational properties.

The present part of this thesis is concerned with the vibrational properties of crystalline C_{60} and C_{70}, as well as with the interaction of the vibrational excitations with the electronic system. It is found that the orientational order-disorder transition in solid Buckminsterfullerene induces several changes of the vibrational properties of C_{60}. Compared to molecular C_{60} many more modes are observed in the vibrational Raman spectra of solid C_{60}, induced by the lower symmetry (chapter 6, 7). The new lines, broadenings, lineshifts and changing intensities observed at and below the first order phase transition in C_{60} can be understood in terms of orientational ordering, rotation-vibration couplings, Davydov splittings, and changes in the electronic structure (chapter 6-8).

In the presence of a sufficiently intense 514.5 nm radiation field it is found that an appreciable number of the molecules in solid C_{60} are excited into a long lived ($\tau \approx 0.4$ ms) triplet state. The vibrational properties of triplet-state C_{60} fullerene are found to be substantially different from those of the ground state. The observed irradiance dependence of the vibrational Raman spectrum is explained in terms of a simplified model for the electronic structure of C_{60}(chapter 8).

The last chapter of this part of the thesis is concerned with the vibrational properties of single-crystal C_{70}. The internal vibrational modes observed in the Raman spectra of solid C_{70} are found to be in good agreement with the solid state structure and the corresponding selection rules. The low frequency part of the Raman spectrum reveals at least 10 Raman active lattice modes, in agreement with the selection rules. The frequencies of these modes compare very well with theoretical calculations of the vibrational modes of solid C_{70} taking only a van der Waals interaction into account (chapter 9).

REFERENCES

1 H.W. Kroto, J.R. Heath, S.C. O'Brien, R.F. Curl, and R.E. Smalley, Nature **318** 162 (1985).

2 R. Buckminster Fuller, *"Inventions - The Patented Works of Buckminster Fuller"*, (St. Martins, New York 1983).

3 L. Euler, *"Elementa doctrinae Solidorum"* (1758).

4 R. Taylor, J.P. Hare, A.K. Abdul-Sada, and H.W. Kroto, J. Chem. Soc.: Chemical Communications, 1423 (1990); R.D. Johnson, G. Meijer and D.S. Bethune, J. Am. Chem. Soc. **112**, 8983 (1990).

CHAPTER 6

THE ROTATIONAL ORDERING TRANSITION IN SINGLE-CRYSTAL C_{60} STUDIED BY RAMAN SPECTROSCOPY[1]

P.H.M. van Loosdrecht, P.J.M. van Bentum, and G. Meijer.

Research Institute of Materials, University of Nijmegen, Toernooiveld,
NL-6525 ED Nijmegen, The Netherlands.

ABSTRACT.

Raman spectroscopic data are presented on the rotational ordering FCC → SC transition in single-crystal C_{60}. Splittings and activation of new modes reveal the influence of the cubic structure, and are in agreement with the crystal symmetry in both phases. The temperature dependence of the spectra is consistent with a sharp first order phase transition near 252 K. A simple model is proposed for the explanation of the temperature dependence of the spectra, involving a large vibrational-rotational coupling in the FCC phase, and essentially no rotational disorder in the SC phase.

---

[1] Previously published in *Physical Review Letters* **68**, 1176 (1992).

6.1 INTRODUCTION

Since the discovery of a new form of carbon, dubbed fullerenes, in 1985 by Kroto *et al.*[1], and the recent development of an efficient method to produce these fullerenes by Krätschmer *et al.*[2], numerous theoretical and experimental investigations have been reported on these exciting new molecules and their derivatives.[3] The prototype fullerene is the C_{60} molecule which has the geometrical structure of a soccer ball with a carbon atom on each of the 60 equivalent corners. It was recently shown by Fleming *et al.*[4] that the truncated icosahedron shaped C_{60} molecule crystallises into a cubic form. X-ray investigations[5] on the structural properties of solid C_{60} revealed a face centered cubic (FCC) structure at room temperature, with a (weakly) first order phase transition[6] to a simple cubic (SC) structure at a temperature near 250 K. The X-ray results, as well as NMR experiments[7, 8] show that the FCC → SC phase transition is accompanied by a critical slowing down of the rapid rotations of the C_{60} molecules.

The vibrational properties of C_{60} have been studied experimentally by optical spectroscopies[2, 9] and inelastic neutron scattering[10] and theoretically by various dynamical calculations.[11, 12, 13] A detailed understanding of the vibrational and rotational properties of solid C_{60} would improve the understanding not only of the C_{60} solid itself, but also of the properties of related compounds such as the high temperature superconducting alkali metal doped fullerenes. In this Letter we present Raman spectroscopic data on the vibrational properties of single-crystal C_{60}, particularly in relation to the FCC → SC phase transition in this material. The sensitivity of optical scattering processes to the crystal field makes Raman spectroscopy, together with infrared spectroscopy, a powerful means to study the solid state vibrational properties of condensed matter, as well as to detect structural phase transitions.

6.2 EXPERIMENTAL RESULTS

Unpolarised Raman spectra are recorded in a back-scattering geometry, using a DILOR XY multichannel Raman spectrometer (spectral slit width 3.5 cm^{-1}) with an Ar^+-laser (514.5 nm) as excitation source. The experiments are performed on a sublimation grown high purity C_{60} single crystal[14] ($\sim$ 0.1 mm^3). The high quality of the crystals is confirmed by mass spectrometry, NMR and electron diffraction experiments.[15] The thus obtained crystals exhibit natural faces of the {100} and {111} growth forms of the cubic symmetry. The natural faces of the crystal usually show irreproducible Raman intensities when scanned across the surface. Therefore, the crystal is cut along one of the {100} planes, and immediately thereafter mounted on the cold finger of a flow cryostat (temperature stabilisation better than 0.5 K, absolute temperature calibration ± 3 K). Subsequently, the cryostat is evacuated to $P \approx 10^{-6}$ mbar. We find that the crystal structure is easily destroyed by intense laser-heating due to the strong absorption in the green part of the spectrum, resulting in qualitative changes of the measured Raman spectra. In order to avoid this problem the intensity of the excitation laser is decreased to below 150 μW, focussed to a spot of 30 μm. With these precautions the Raman spectra are reproducible for different spot positions on the crystal, and do not depend on the intensity of the excitation laser.

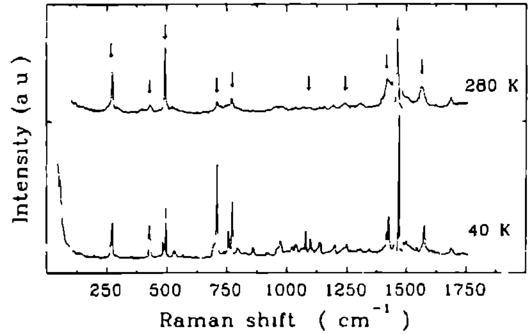

Figure 6.1 : Unpolarised Raman spectra of single-crystal C_{60} in the FCC phase (T = 280 K, upper curve) and in the SC phase (T = 40 K, lower curve). The peaks at ~ 1467 cm^{-1} are scaled down by a factor of 6. The predicted modes for the free molecule are indicated by the arrows.

Two representative Raman spectra are displayed in Fig. 6.1. The upper curve shows the spectrum in the FCC phase (T = 280 K) and the lower curve shows the spectrum for the SC phase (T = 40 K). The 10 modes which are expected purely on the basis of the molecular symmetry are clearly observed in the spectra, though they are generally split up into several lines. Apart from these 10 modes, a number of new modes is observed in both spectra. These splittings and the new activated modes can be understood by considering the crystal symmetry of solid C_{60}. The cubic environment of C_{60} in the crystalline state changes the selection rules for optical scattering processes. In the first place, all 23 modes of gerade symmetry will become Raman active in both the FCC and the SC phase, whereas the ungerade modes remain inactive by virtue of the preservation of the inversion symmetry on the sites of the molecules in the crystal. Secondly, the fourfold (H_g) and fivefold (G_g) degenerate modes of the I_h symmetry split up in the FCC phase, and a further splitting of all modes is expected in the SC phase. A factor group analysis based on the T_h site symmetry yields 37 expected Raman active modes for the FCC phase. For the SC structure which has four molecules per primitive cell and site symmetry S_6, one finds 145 Raman active modes. Because of the resolution of the experiment, thermal broadening and possible (near) degeneracies, one can not expect to observe all these modes however. In the FCC phase the spectra exhibit 29 clear peaks and shoulders, whereas in the low temperature phase we observe 45 modes. The large number of peaks observed in the low temperature phase is consistent with the SC structure.

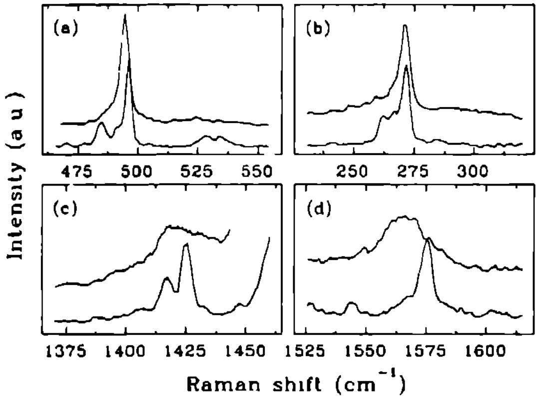

Figure 6.2 : Parts of the unpolarised Raman of single-crystal C_{60} in the FCC phase ($T = 280$ K, upper curves) and in the SC phase ($T = 40$ K, lower curves), showing splittings and broadenings for the (a) 496 cm^{-1} A_g, (b) 273 cm^{-1} H_g, (c) 1425 cm^{-1} H_g, and (d) 1575 cm^{-1} H_g regions of the spectra, respectively.

Some details of the spectra are shown in Fig. 6.2, where the upper curves show parts of the spectra in the FCC phase at $T = 280$ K and the lower curves show the same region for the SC phase at $T = 40$ K. Figure 6.2a shows the splitting of the A_g breathing mode in the SC phase. In the high temperature phase only a single line is expected, which is found at 494 cm^{-1}. In the SC phase, five modes are observed in the displayed region. The strongest peak at 496 cm^{-1} and the shoulder at 493 cm^{-1} can be interpreted as resulting from the $A_g \rightarrow A_g + F_g$ splitting in the SC structure. The strongest mode is the A_g mode, in which the molecules in the primitive cell vibrate in phase, whereas the weaker shoulder at lower frequency can be assigned to the threefold degenerate F_g mode, corresponding to out of phase vibrations of the molecules. The three remaining modes at 485 cm^{-1}, 525 cm^{-1}, and 533 cm^{-1} correspond to gerade modes which are Raman forbidden for the free C_{60} molecule. They are already weakly, though reproducibly, observed in the high temperature spectrum.

Figures 6.2b, c and d show the regions of the 273 cm^{-1}, 1425 cm^{-1} and 1575 cm^{-1} H_g

modes of the molecule, respectively. In the FCC phase, the $H_g \rightarrow E_g+F_g$ splitting is only observable for the 273 cm^{-1} mode, which has a small shoulder on the low frequency side. The two other H_g modes appear as broad peaks in the spectra. In the low temperature SC phase, the splitting of the H_g modes is better resolved. In this case however, one expects 8 Raman active modes per molecular H_g mode according to the $H_g \rightarrow A_g+2E_g+5F_g$ splitting. As explained above, one can not expect to observe all these modes.

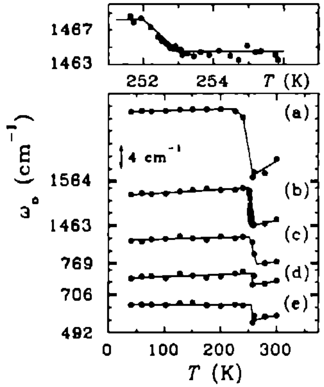

Figure 6.3 : Temperature dependence of the frequency of the Raman active modes at from top to bottom (a) 1575 cm^{-1}, (b) 1467 cm^{-1}, (c) 772 cm^{-1}, (d) 708 cm^{-1}, and (e) 496 cm^{-1}, respectively. The vertical offset for each curve is indicated by the thick tic marks. The inset on the top shows the 1467 cm^{-1} mode near the FCC → SC transition, indicating a discontinuous transition within ~ 1 K. (The solid lines are a guide to the eye.)

Apart from the splittings observed in the spectra, Figs. 1 and 2 also show shifts in frequencies and changes in linewidths of most of the observed modes in spectra recorded for the two phases. In Figs. 3 and 4 the temperature dependence of the frequency ω_0 and the linewidth Γ (HWHM, half width at half the maximum), respectively, of several of the observed modes are plotted. All frequencies and linewidths plotted in these figures have been determined from spectra taken at a well stabilised temperature, except for the frequencies of the 1467 cm^{-1} mode between 250 K and 255 K. The latter frequencies are determined from spectra recorded while scanning the temperature with $dT/dt \approx -0.06$ K/min. The spectra measured in this temperature interval are integrated over 2 minutes. The 1467 cm^{-1} mode clearly shows a step in the frequency at the FCC → SC phase transition, which is found at $T = 252 \pm 3$ K (see Fig. 6.3), which agrees well with the results obtained by other authors.[5, 6] The width of this step-like behaviour of this mode is ~ 1 K,

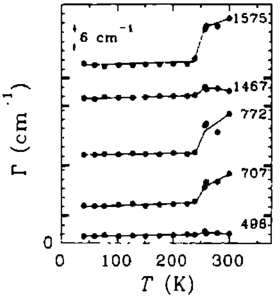

Figure 6.4 : Temperature dependence of the linewidths of the observed Raman active modes at from top to bottom 1575 cm^{-1}, 1467 cm^{-1}, 772 cm^{-1}, 708 cm^{-1} and 496 cm^{-1}, respectively. The vertical offset is indicated for each curve by the thick tic marks. (The solid lines are a guide to the eye.)

as shown explicitly in the top part of Fig. 6.3. This discontinuous behaviour indicates a first order character for the phase transition, in agreement with DSC measurements[6] and the discontinuous volume change of about 2.5 % found by Heiney *et al.*[5]. For the natural growth faces of the crystal we find a more gradual transition, probably due to surface disorder and/or oxygen adsorption.

For all the modes, a discontinuous behaviour is observed in the temperature dependence of the frequency and linewidth. In general a hardening of the modes of the order of 2 – 11 cm^{-1} is observed at the FCC → SC phase transition. These hardenings are consistent with the decrease of volume in the SC phase, relative to the FCC phase.

The linewidth of some of the observed peaks plotted in Fig. 6.4 shows a discontinuous decrease at the phase transition. Especially for the 707 cm^{-1}, 772 cm^{-1} and the 1575 cm^{-1} modes, a quite dramatic change by a factor of 3 – 4 is observed. We anticipate that the large linewidths in the FCC phase result from a coupling of these phonons with the rotational motions of the molecules in the FCC phase, effectively decreasing the lifetimes of the phonons, and hence increasing the linewidths of the observed peaks. After prolonged exposure to air or to high laser power, the FCC → SC transition becomes less pronounced and appears to shift to lower temperatures. For a clean cleaved surface we find no Raman evidence for a second transition at temperatures below 252 K down to 20 K.

6.3 DISCUSSION

To explain the observed behaviour we propose the following simple model. First, at temperatures far above the FCC → SC transition we expect the molecules to rotate freely. The inter-molecular interactions in the solid give rise to a coupling of the vibrational modes with the quasi-continuum of the rotational excitations, leading to a finite lifetime of these modes. This coupling will be strongest for the modes where neighbouring C atoms vibrate out-of-phase. The coupling to the more symmetric A_g modes is expected to be much smaller, as is indeed the case. Near the transition the rotational motions become strongly hindered, and the molecules now rotate in a hopping-like manner. The hindrance of the rotational motions leads to an increase of the matrix elements representing the rotational-vibrational coupling, but simultaneously result in a decrease of the density of available rotational states. Therefore we expect to observe a decreased linewidth for those modes which show already a strong coupling at temperatures far above the phase transition, and an increase for those modes which do not exhibit this coupling at higher temperatures. This behaviour is indeed observed in Fig. 6.4. In the SC phase the rotational disorder is essentially frozen out. This decreases the linewidth, and only a weak temperature dependence is expected. For the understanding of the temperature dependence of the frequency of the various modes we consider the main effect to be the volume change near the phase transition. At high temperatures the molecules can be treated as nearly free, held together only by the weak van der Waals forces between the, by virtue of the rotational motions, approximately spherical molecules. The softening of the modes on approaching the transition is not completely understood, but is probably connected to the decrease of the rotational motions. In this regime where the rotations are of a hopping nature one may expect a decrease of the inter-molecular potential, provided that the volume does not change dramatically upon approaching the phase transition. At the FCC → SC phase transition the modes harden due to the increased interaction potential between neighbouring molecules. After the transition no structural changes occur, and the frequency of the modes will be nearly constant in the SC phase.

Apart from the phonons related to the intra-molecular vibrations of C_{60} which were considered above, the crystal also possesses collective lattice modes, in which the molecules move as a whole. These vibrations can be divided into two classes, one in which the molecules translate, the translational lattice modes, and another class in which the molecules rotate, the librational lattice modes. The first class is of ungerade symmetry for the cubic structure, hence one expects these modes to be only infrared active. The librational modes are of gerade symmetry, and thus are expected to be Raman active (one in the FCC phase and five in the SC phase). Figure 6.5 shows the low frequency part of the Raman spectrum at $T = 150$ K (upper curve). Clearly this curve shows some structure, which is possibly related to the lattice modes of solid C_{60}. After subtraction of a Lorentzian center peak (Fig. 6.5, lower curve), the structure appears more clearly as three distinct peaks centered at 56 cm^{-1}, 81 cm^{-1}, and 109 cm^{-1}, respectively. These peaks could be due to the librational lattice modes, although one would expect these phonons to have a lower

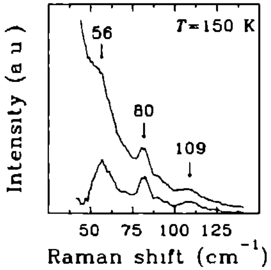

Figure 6.5 : Part of the unpolarised Raman spectrum at T = 150 K (upper curve) clearly showing collective lattice modes in the low frequency region. The lower curve shows the same trace after subtraction of a Lorentzian center peak, revealing three peaks at respectively 56 cm^{-1}, 80 cm^{-1} and 109 cm^{-1}.

frequency. Therefore the precise assignment of these modes remains unclear.

6.4 CONCLUSIONS

In summary, we have presented the first detailed temperature dependent Raman study of a high purity single-crystal C_{60}. The results show the effects of the FCC and SC crystal structures, both by the appearance of modes corresponding to vibrations which are symmetry forbidden for the molecule, as well as by the observation of a splitting of most of the modes. At the phase transition a discontinuous behaviour is observed in the vibrational properties of solid C_{60}, with a width of approximately 1 K. The results are explained in terms of a simple model for the crystal. Together with the X-ray[5], NMR[7, 8] and DSC[6] results, our results indicate a first order FCC → SC phase transition, in which the rotations of the molecules slows down critically. At variance with the interpretation of the NMR results, we find no rotational disorder in the SC phase. For an understanding of the NMR results, possibly the collective rotational motions in the SC phase have to be taken into account. The Raman spectra reveal three peaks at low frequency, corresponding to collective modes of the crystal. The precise nature of these modes has not yet been revealed.

ACKNOWLEDGEMENTS We gratefully acknowledge the financial support of the Dutch Foundation for Fundamental Research of matter (FOM).

REFERENCES

1 H.W. Kroto, J.R. Heath, S.C. O'Brien, R.F. Curl, and R.E. Smalley, Nature **318**, 162 (1985).

2 W. Krätschmer, L.D. Lamb, K. Fostiropoulos, and D.R. Huffman, Nature **347** 354 (1991).

3 R.E. Smalley, *"The almost (but never quite) complete Buckminsterfullerene bibliography"*, available upon request ("Buckybib", Dept. of Chemistry, Rice University, PO Box 1892, Houston, Texas 77251, USA).

4 R.M. Fleming, T. Siegrist, P.M. March, B. Hessen, A.R. Kortan, D.W. Murphy, R.C. Haddon, R. Tycko, G. Dabbagh, A.M. Mujsce, M.L. Kaplan, and S.M. Zahurak, Mat. Res. Soc. Proc. **206**, 691 (1991).

5 P.A. Heiney, J.E. Fisher, A.R. McGhie, W.J. Romanow, A.M. Denenstein, J.P. McCauley Jr., A.B. Smith III, and D.E. Cox, Phys. Rev. Lett. **66**, 2911 (1991). R. Sachidanandam and A.B. Harris, Phys. Rev. Lett. **67**, 1467 (1991).

6 A. Dworkin, H. Szwarc, S. Leach, J.P. Hare, T.J. Dennis, H.W. Kroto, R. Taylor, and D.R.M. Walton, C.R. Acad. Sci. (paris) series II **9**, 979 (1991). G. Kriza, J.-C. Ameline, D. Jerome, A. Dworkin, H. Szwarc, C. Fabre, D. Schutz, A. Rassat and P. Bernier, J. Phys. France I (paris) **1**, 1361 (1991).

7 R.D. Johnson, C.S. Yannoni, H.C. Dorn, J.R. Salem and D.S. Bethune, Science **255**, 1235 (1991).

8 R. Tycko, G. Dabbagh, R.M. Fleming, R.C. Haddom, A.V. Makhija, and S.M. Zahurak, Phys. Rev. Lett. **67**, 1886 (1991).

9 D.S. Bethune, G. Meijer, W.C. Tang, H.J. Rosen, W.G. Golden, H. Seki, C.A. Brown, and M.S. de Vries, Chem. Phys. Lett. **179**, 181 (1990).

10 R.L. Cappetelletti, J.D.R. Copley, W.A. Kamitakahara, F. Li, J.S. Lannin, and D. Ramage, Phys. Rev. Lett. **66**, 3261 (1991).

11 Z. Slanina, J. Rudiński, and E. Ōsawa, J. Mol. Struct. **202**, 169 (1989). and references therein.

12 F. Negri, G. Orlandi, and F. Zerbetto, Chem. Phys. Lett. **144**, 31 (1988).

13 A. Cheng and M.L. Klein, J. Phys. Chem. **95**, 6750 (1991).

14 M.A. Verheijen, G. Meijer, E. Raas, and P. Bennema, Chem. Phys. Lett. **191** 219 (1992).

15 G. van Tendeloo, C. van Heurck, J. van Landuyt, S. Amelinckx, M.A. Verheijen, P.H.M. van Loosdrecht, and G. Meijer, J. Phys. Chem. **96**, 7424 (1992).

6.5 COMMENT AND REPLY TO THIS CHAPTER

VOLUME 69, NUMBER 7 PHYSICAL REVIEW LETTERS 17 AUGUST 1992

Comment on "Rotational Ordering Transition in Single-Crystal C_{60} Studied by Raman Spectroscopy"

In a recent Letter van Loosdrecht, van Bentum and Meijer [1] presented a detailed temperature-dependent Raman study of a C_{60} single crystal. They reported a discontinuous change in frequency and linewidth of the C_{60} Raman lines at the fcc to sc phase transition [2] near 252 K. The strongest change they observed is for the H_g vibration at 1564 cm^{-1} (high T, fcc phase) jumping in frequency to 1575 cm^{-1} (low T, sc phase) within a very narrow temperature interval. The increase in frequency is accompanied by a drastic steplike decrease (≈ 8 cm^{-1}) in linewidth. The authors of [1] attributed the hardening of the 1564-cm^{-1} mode to the volume change [2] near the phase transition implying that a value of 1575 cm^{-1} is characteristic for this mode in the sc phase.

We argue here that instead this behavior is most likely due to a combined effect of nearly overlapping peaks from C_{70} impurities and a drastic change in relative intensities between C_{60} and C_{70} Raman peaks at the phase transition. It is important to clarify this issue because of the implications for the vibrational modes in doped C_{60} [3].

In Fig. 1 we present Raman spectra of a C_{60}, C_{70}, and a mixed C_{60} and C_{70} sample ($\approx 10:1$) in the range of the H_g vibration of C_{60} near 1575 cm^{-1}. The measurements were performed using similar conditions as in [1]. Before recording the spectra all samples had been exposed to air. Except for curve (*b*), the shape of the Raman features in the spectra suggests a superposition of lines. For a C_{60} single crystal (*a*) the Raman feature is centered at 1573 cm^{-1} in agreement with the value of 1575 ± 2 cm^{-1} for air-exposed films [4] and powder [5]. Note the line at 1564 cm^{-1} in the spectrum of the C_{70} film (*b*) which has the largest absolute intensity in the entire spectrum. Evidently the room-temperature Raman feature of the C_{60}/C_{70} film (*c*) is composed of two lines centered at 1565 (C_{70}) and 1575 cm^{-1} (C_{60}). At 12 K (*d*), there is an obvious redistribution in relative intensity, with the C_{60} component having increased dramatically. It thus appears that the jump in frequency reported in [1] is actually due to an increase in intensity of the 1575-cm^{-1} C_{60} peak with respect to the C_{70} line at 1564 cm^{-1}.

The frequency of the 1575-cm^{-1} H_g C_{60} vibration is not characteristic of only the sc phase. The same frequency was also measured at room temperature for air-exposed films [4] which are in the fcc phase [2], as well as for powders and C_{60}/CS_2 solutions [5]. Furthermore, we observed similar relative intensity changes for the peaks at 771 cm^{-1} (C_{60})/768 cm^{-1} (C_{70}) and 709 cm^{-1} (C_{60})/706 cm^{-1} (C_{70}); these peaks were also interpreted as having a discontinuous change in frequency at the phase transition [1]. Independent evidence for C_{70} impurities in the spectra of [1] comes from the features at ≈ 262 cm^{-1} and ≈ 1450 cm^{-1} in their Figs. 2(b) and 2(c) which are characteristic of C_{70} only [4, 5].

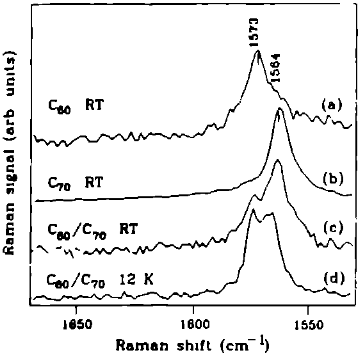

FIG. 1. Unpolarized Raman spectra. (*a*) C_{60} single crystal at room temperature (RT). (*b*) C_{70} film at RT. (*c*) C_{60}/C_{70} film at RT. (*d*) C_{60}/C_{70} film at 12 K.

We thus suggest that at room temperature, vacuum-kept C_{60} crystals containing a small amount of C_{70} show a broad Raman feature at ≈ 1564 cm^{-1} because of the relatively intense C_{70} peak and the broad (due to rotation) peak of C_{60}. In the low temperature, ordered sc phase the free rotation of the C_{60} molecules is hindered, like in air-exposed samples. This leads to an increase in C_{60} peak intensity and to the apparent, drastic frequency shifts and linewidth changes reported in [1].

V. G. H. is an Alexander von Humboldt Fellow.

V. G. Hadjiev and C. Thomsen
Max-Planck-Institut für Festkörperforschung
Heisenbergstrasse 1, D-7000 Stuttgart 80
Federal Republic of Germany

Received 16 April 1992
PACS numbers: 63.20.Hp, 78.30.Hv, 81.30.Hd

[1] P. H. M. van Loosdrecht, P. J. M. van Bentum, and G. Meijer, Phys. Rev. Lett. 68, 1176 (1992).
[2] P. A. Heiney *et al.*, Phys. Rev. Lett. 66, 2911 (1991).
[3] M. G. Mitch, S. J. Chase, and J. S. Lannin, Phys. Rev. Lett. 68, 883 (1992).
[4] D. Bethune *et al.*, Chem. Phys. Lett. 179, 181 (1991).
[5] B. Chase, N. Herron, and E. Holler, J. Phys. Chem. (to be published).

REPLY TO COMMENT ON "ROTATIONAL ORDERING TRANSITION IN SINGLE-CRYSTAL C_{60} STUDIED BY RAMAN SPECTROSCOPY"[2]

P.H.M. van Loosdrecht, P.J.M. van Bentum, and G. Meijer
Research Institute of Materials, University of Nijmegen, Toernooiveld,
NL-6525 ED Nijmegen, The Netherlands.

Hadjiev and Thomsen express a legitimate concern about the possible effects of impurities on the Raman spectra of fullerenes. It is well known that remains from solvents, oxygen or the presence of C_{70} can drastically change the vibrational properties of solid C_{60}. More specifically, in the presence of these impurities the rotational ordering transition extends over a much larger temperature range. In our experiments we tried to avoid pollution as much as possible. First, mass spectroscopic analysis of the chromatographically purified starting material indicate a C_{70} content less than 0.5 %. The multiple sublimation growth technique[1] in vacuum provides a further purification. Second, morphological study, X-ray diffraction, electron diffraction and HREM crystal analysis all indicate a nearly perfect crystal quality and no sign of C_{70}. Third, to exclude possible surface pollution from the growth method the crystals were cleaved to expose a clean fresh surface. To prevent surface deterioration, the crystals are mounted in an optical cryostat which is immediately evacuated. Fourth, some crystals were checked by mass spectroscopic analysis which showed no detectable traces of C_{70}. Finally, the Raman spectra themselves were checked for indications of C_{70}. In the low temperature phase a total of 49 modes was observed, some of which are close to the known C_{70} modes. However no features were observed near 1183 and 1228 cm^{-1} (see the inset in Fig. 6.6), showing the absence of C_{70}. (Hadjiev and Thomsen refer to a peak near 1450 cm^{-1}, which was in fact a spike in our raw data.)

In Fig. 1, we have shown the spectra of the highest H_g mode in the $2a_0$-FCC phase (lower curve, 40 K) and the FCC phase (upper curve, 260 K). A comparison with curve c) and d) in Fig. 1 by Hadjiev and Thomsen clearly shows that the peak shift and broadening observed in our spectra can not be explained by the presence of a small amount of C_{70} impurities. Note that the displacement of the 1566 cm^{-1} mode to 1575 cm^{-1} in the results of Hadjiev and Thomsen is a well known effect of air-exposed C_{60}.[2, 3]

It remains surprising that such a large frequency shift is observed for this mode. Even though a quite large volume change is associated with the rotational ordering transition, it is not not very likely that the intermolecular interactions alone can account for this effect. We propose that in addition, the very strong electronic resonance conditions for 514 nm excitation change. Even very low irradiances of the order of 5 W/cm^2 can lead to an electronic excitation into the metastable triplet state and a corresponding softening of

---

[2] Previously published in *Physical Review Letters* **69**, 1147 (1992).

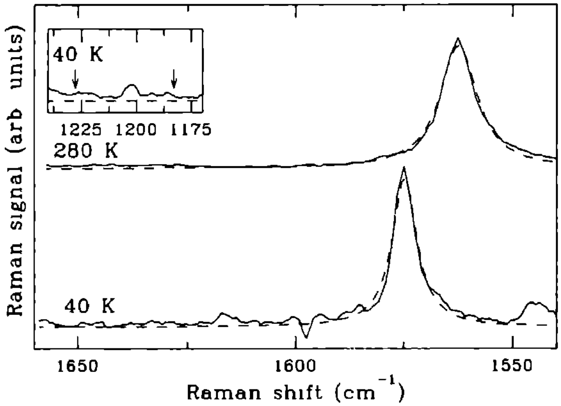

Figure 6.6 : Unpolarised Raman spectra of the highest H_g mode in single crystal C_{60} at $T = 40$ K (lower curve) and $T = 260$ K (upper curve). The dashed lines are fits of a single Lorentzian curve. The inset shows the absence of the 1183 cm^{-1} and 1228 cm^{-1} C_{70} modes (indicated by arrows) in the $T = 40$ K C_{60} Raman spectrum.

the phonon in the high temperature phase.[3] The presence of oxygen blocks the rotational motion and simultaneously quenches the triplet state[4], thus preventing the anomalous softening.

REFERENCES

1 M.A. Verheijen, H. Meekes, G. Meijer, E. Raas, and P. Bennema, Chem. Phys. Lett. **191**, 339 (1992).

2 S.J. Duclos, R.C. Haddon, S.H. Glarum, A.F. Hebard, and K.B. Lyons, Sol. St. Comm. **80**, 481 (1991).

3 P.H.M. van Loosdrecht, P.J.M. van Bentum, and G. Meijer, submitted to Chem. Phys. Lett., and chapter 8 of this thesis.

4 J.W. Arbogast, A.P. Darmanyan, C.S. Foote, Y. Rubin, F.N. Diederich, M.M. Alvarez, S.J. Anz, and R.L. Whetten, J. Phys. Chem. **95**, 11 (1991).

CHAPTER 7

RAMAN SCATTERING IN SINGLE-CRYSTAL C_{60}[1]

P.H.M. van Loosdrecht[a], P.J.M. van Bentum[a,b], M.A. Verheijen[a],
and G. Meijer[a].

[a] *Research Institute of Materials, University of Nijmegen, Toernooiveld,
6525 ED Nijmegen, The Netherlands.*
[b] *IBM Thomas J. Watson Research Center,
Yorktown Heights, NY 10598, U.S.A.*

ABSTRACT.

Raman spectra (using 514 nm and 740 nm excitation) of high purity single-crystal C_{60} are presented for the high and low temperature phases, showing activity of all "gerade" modes. Within the experimental accuracy, the spectra are found to be consistent with the selection rules for Raman scattering in both the high temperature FCC and low temperature $2a_0$-FCC phases of solid C_{60}. A complete assignment of the observed peaks is proposed.

---

[1] Previously published in *Chemical Physics Letters* **198**, 587 (1992).

7.1 INTRODUCTION

The discovery of Buckminsterfullerene[1] (C_{60}), and in particular the development of a method[2] to produce macroscopic quantities of the fullerenes, has launched an enormous research effort to characterise and understand the chemical and physical properties of this exciting new form of carbon as well as of its derivatives.[3] Recently, the solid state properties of the fullerenes have gained much interest, partly induced by the discovery of "high temperature" superconductivity in alkali-intercalated C_{60} [4] and by the unusual dynamics of the nearly spherical C_{60} molecules in the crystal lattice.[5, 6, 7] Crystalline C_{60} is a molecular solid with only weak inter-molecular forces. Despite the weak lattice interactions the presence of the crystal field has a distinct influence on the properties of solid C_{60}. A clear example of this is the phase transition at $T \sim 255$ K, involving a critical decrease of the quasi-free rotational motions. Other manifestations of solid state effects are for instance found in changes of the resonant enhancements of inelastic light scattering processes[8] and the presence of several species of delocalised excitons[9] in solid C_{60}.

Raman spectroscopy has proved to be a convenient method to study the solid state effects on the dynamical properties of C_{60} and related compounds. It has been shown recently that the reduction of the high I_h symmetry of the free molecule in the crystal lattice leads to splittings of molecular degenerate vibrational modes and to activation of modes which are Raman inactive for the free molecule. Also a coupling of the vibrational modes to the rotational excitations of C_{60}, and to the electronic excitations in alkali-intercalated C_{60} have been reported.[10, 11]

The present paper presents a detailed Raman spectroscopic study of the solid state vibrational properties of single-crystal C_{60} in the high temperature FCC and the low temperature $2a_0$-FCC phases.[12] A full assignment of the observed peaks is proposed, deduced from the selection rules and a comparison of the data presented here to other experimental data[2, 13] and to the theoretical results of Negri *et al.*.[14]

7.2 SELECTION RULES

The high symmetry (I_h) of the C_{60} molecule has a large influence on its vibrational properties. Although C_{60} has 174 internal degrees of freedom the icosahedral symmetry reduces this large number to only 46 distinct vibrational modes, the group theoretical classification of which is given by $\Gamma^{mol}_{C_{60}} = 2A_g + 3F_{1g} + 4F_{2g} + 6G_g + 8H_g + A_u + 4F_{1u} + 5F_{2u} + 6G_u + 7H_u$. Experimentally, the number of observable modes is further reduced by selection rules. The strongest reduction occurs for infrared scattering, where only the 4 F_{1u} modes are active. For Raman scattering, one expects the 2 A_g and 8 H_g modes to be active. The most complete picture can be obtained from inelastic neutron scattering, which has no selection rules at all. These differences in selection rules are very useful in the classification of the vibrational modes of the C_{60} molecule.[15]

The vibrational modes and selection rules described above apply only to the free molecule. In the solid state the crystal field influences the vibrational properties as well as the selection rules. A distinction can be made between internal and external modes: the internal modes correspond to the molecular modes of vibration whereas the external modes are the translational and librational vibrations of the molecules as a whole. Because of the rather weak van der Waals bonding between the molecules in solid C_{60}, one expects that the frequencies of the internal modes are only slightly influenced, yielding small shifts and splittings of these modes. The crystal field effectively lowers the symmetry of the molecules, and therefore some of the molecular inactive modes will become active in the solid state.

The room temperature structure of solid C_{60} is FCC (T_h^3) with four equivalent molecules per conventional unit cell.[16] This is possible because, due to the nearly complete rotational freedom, the molecules can be considered to be perfect spheres. At $T \sim 255$ K, the rotational motion of the molecules slows down critically and the crystal structure changes due to the faceted icosahedral nature of C_{60}. The low temperature structure of C_{60} is usually considered to be SC (T_h^6), with four orientationally inequivalent molecules per primitive cell.[5] Recently, van Tendeloo *et al.*[12] found evidence for a superstructure below 100 K, pointing to a $2a_0$-FCC crystal structure with space group T_h^4 for the low temperature phase. In this structure the C_{60} molecules are rotated by an angle ϕ around the <111> directions, just as in the SC phase. In contrast to the SC structure, however, two groups of molecules can be distinguished in the $2a_0$-FCC structure, differing in rotation angle ϕ by 60°.[17] The presence of this superstructure has been unambiguously confirmed in triplet state EPR measurements on C_{60} single-crystals.[9] It is likely that the phase transition from the FCC to the $2a_0$-FCC phase occurs in two steps. At the 255 K transition the rotational disorder freezes, leaving the possibility of rotational excitations involving jumps between the almost equivalent orientations of the two groups of molecules.[6, 7] This makes the two groups equivalent, and the structure is therefore simple cubic. At low temperatures[17, 18] these rotational jumps also freeze, leading to the low temperature $2a_0$-FCC structure.

In both the low and high temperature phases the inversion symmetry on the molecular sites is retained, which ensures a persistence of the complementarity of infrared and Raman spectroscopy. The symmetry splittings of the modes in the FCC, $2a_0$-FCC and SC structures can be determined using factor group analysis. For the $2a_0$-FCC and SC phase, this can be accomplished by taking the site symmetry S_6 into account. The results of this exercise are shown in Tab. 7.1, which indicates the correlation between the molecular modes and the solid state modes in the FCC, $2a_0$-FCC and SC phases. The resulting number of modes derived from this Table, as well as the number of external modes are

Table 7.1 : Correlations between gerade modes of C_{60} for the free molecule (I_h) and the molecule in the FCC (T_h^3), $2a_0$-FCC(T_h^4) and SC (T_h^6) structures. The correlations for the ungerade modes are equivalent.

I_h	→	T_h^3	$T_h^4(2a_0)$	T_h^6
A_g	→	A_g	$2A_g + 2F_g$	$A_g + F_g$
F_{1g}	→	F_g	$2A_g + 2E_g + 6F_g$	$A_g + E_g + 3F_g$
F_{2g}	→	F_g	$2A_g + 2E_g + 6F_g$	$A_g + E_g + 3F_g$
G_g	→	$A_g + F_g$	$4A_g + 2E_g + 8F_g$	$2A_g + E_g + 4F_g$
H_g	→	$E_g + F_g$	$2A_g + 4E_g + 10F_g$	$A_g + 2E_g + 5F_g$

Table 7.2 : The number of internal (n_i) and external (n_e) vibrational modes in the FCC (T_h^3), $2a_0$-FCC(T_h^4) and SC (T_h^6) structures of solid C_{60}. The external modes have been labeled r,t and a for optical rotational, optical translational and acoustic, respectively. The first column gives the irreducible representation of the T_h point symmetry group of the cubic structures. The second column gives the activity in infrared (IR) and Raman ($\|R$ and $\perp R$ for the scattered light respectively parallel and perpendicular to the excitation light) experiments. The total number of modes is given in the last row, with in parenthesis the total number of Raman active modes.

		T_h^3		$T_h^4(2a_0)$		T_h^6	
T_h	act.	n_i	n_e	n_i	n_e	n_i	n_e
A_g	$\|R$	8	-	58	2^r	29	1^r
E_g	$\|R$	8	-	58	2^r	29	1^r
F_g	$\perp R$	21	1^r	174	6^r	87	3^r
A_u	-	7	-	60	2^t	30	1^t
E_u	-	7	-	58	2^t	29	1^t
F_u	IR	22	1^a	186	$5^t,1^a$	93	$2^t,1^a$
n_{total}		73(37)	2(1)	594(290)	20(10)	297(145)	10(5)

shown in Tab. 7.2 together with their activity in Raman and infrared spectroscopy. A detailed discussion of the group theoretical aspects of the vibrational properties in the FCC and SC phase has been given by Dresselhaus *et al.*.[19] Instead of just the 10 Raman active molecular modes, all gerade modes are expected to be active in solid C_{60} and one expects to observe 23 groups of modes in Raman spectra. Since in the high temperature phase the molecules rotate almost freely and are held together by the relatively weak van der Waals interaction, the electronic structure of the C_{60} molecules hardly changes as compared to the free molecule and the splittings are expected to be relatively small. In the same vein, the additional modes induced by the symmetry reduction are expected to be weak. In the low temperature phase a perturbation of the electronic structure of the C_{60} molecules can be expected since the electrostatic interaction between the electron rich and electron poor parts of the molecules is no longer negligible.[20] The numerical differences in the selection rules for Raman scattering in the $2a_0$-FCC and SC structures can theoretically be used to investigate whether or not the SC structure exists as an intermediate phase between the $2a_0$-FCC and FCC phases. Because the expected frequency differences due to the superstructure are, however, very small it seems doubtful that these differences can be observed experimentally. It is more likely that the distinction between the SC and the $2a_0$-FCC phase is observable in the number of IR active external translational, or Raman active external rotational modes.

7.3 RAMAN SPECTRA OF SINGLE-CRYSTAL C_{60}

The production of the high purity C_{60} single-crystals used in this study has been described in detail elsewhere.[21] The vapour growth method used ensures a high crystal quality, as well as a further purification of the chromatographically purified starting material. The absence of impurities such as residual solvents, oxygen or other fullerenes is extremely important because they strongly influence the structural and dynamical properties of solid C_{60}. The crystal quality, already indicated by the morphology revealing only {100} and {111} faces, has been checked on crystals obtained from the same growth batch. X-ray diffraction revealed a FCC structure at room temperature with no indications for any other phase.[22] High resolution electron microscopy[23] confirmed the pure FCC phase and also revealed some structural defects, common to this kind of cubic structures.

The crystals used in the experiments are mounted in a flow cryostat (temperature stabilisation better than 0.1 K, absolute temperature ± 2 K), which was evacuated to $5 \cdot 10^{-6}$ mbar immediately after (within a few minutes) they are either removed from their vacuum kept quartz growth tubes, or cleaved in air. This procedure prevents the degradation of the samples that occurs when the crystals are kept in air and ensures a clean surface. This is of vital importance since the presence of oxygen degrades the samples, leading to changes in the electronic and vibrational properties.[24] Raman experiments have been performed in a backscattering geometry using a DILOR multichannel spectrometer (spectral slit width 3.5 cm^{-1} at 514 nm, and 1.5 cm^{-1} at 740 nm), with either an argon ion laser (514 nm, $d \approx 30\mu\text{m}$ spot) as excitation source, or a Ti:sapphire-laser (740 nm). C_{60} is easily excited into a triplet state under the influence of 514 nm radiation. Since the interest of the present work is the ground state vibrational properties of C_{60}, the irradiance has been kept below 5 W/cm^2. It has been shown[24] that at least in the low temperature phase the population of the triplet states is negligible at these irradiances.

Fig. 7.1 shows the unpolarised Raman spectra of C_{60} as recorded in the high (280 K, spectrum (a)) and the low temperature phase (40 K, spectrum (b)) under 514 nm excitation. A large number of internal modes is observed in both phases (49 in the low

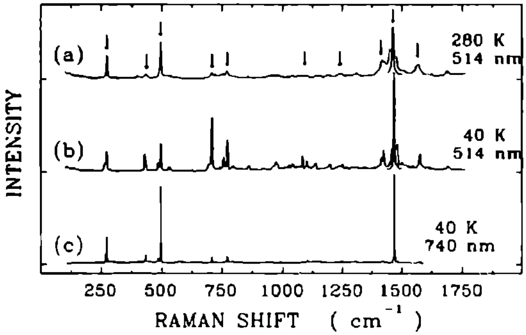

Figure 7.1 : Unpolarised Raman spectra of single-crystal C_{60} for (a) T=280 K, λ_{laser}=514 nm, (b) T=40 K, λ_{laser}=514 nm, and (c) T=40 K, λ_{laser}=740 nm. The modes which are Raman active for the free molecule are denoted by an arrow in spectrum (a). The strong out-of-phase ring mode at ~ 1468 cm^{-1} has been scaled down by a factor of 5 in spectra (a) and (b). The 740 nm spectrum (c) has been corrected for the detector response and a blank excitation source spectrum has been subtracted.

temperature phase and 21 in the high temperature phase). Polarised Raman experiments at 100 K yielded an intensity ratio $I_{\perp}/I_{\parallel}$ of 0.3 – 0.9 for most of the peaks, and ~ 0.02 for the two A_g modes. These modes correspond to an in-phase (496 cm^{-1}) and out-of-phase (1468 cm^{-1}) dilatory vibration of the hexagonal and pentagonal rings of the molecule. The spectra have been fitted to Lorentzian shaped peaks, which gave a satisfactory result. The fitted mode frequencies (ω_0), full width at half maximum (γ) and relative intensities (I) are tabulated for both phases in the first 6 columns of Tab. 7.3. Also shown in Fig. 7.1 is the low temperature (40 K) spectrum of C_{60} recorded using 740 nm, 150 W/cm^2 excitation (spectrum (c)). This spectrum has been corrected for the wavelength dependence of the detector response, and a blank excitation source spectrum has been subtracted. The peak

*Table 7.3 : Vibrational modes of C_{60}. In the first six columns the frequency ω_0, linewidth γ and relative intensity I of the observed Raman modes are given for respectively the FCC (280 K) and the $2a_0$-FCC (40 K) phase. The column labeled IN/IR/CS_2 lists the frequencies observed by inelastic neutron scattering at 25 K[13], room temperature infrared spectroscopy[2] (marked with *), and by Raman spectroscopy for C_{60} dissolved in CS_2 at room temperature (this work, marked with †). In the last column the tentative assignments of the modes are given. The column labeled Ref. 14 gives the calculated vibrational frequencies of Negri et al..*

280 K (fcc)			40 K ($2a_0$ fcc)			IN/IR/CS_2	Ref 14	assignment
ω_c (cm^{-1})	γ (cm^{-1})	I (a.u.)	ω_c (cm^{-1})	γ (cm^{-1})	I (a.u.)	ω_s (cm^{-1})	ω_0 (cm^{-1})	
			57					Lattice
			80			80		
			108			102		
						137		
						264		
			262	4	1.2	264[1]	258	H_g
			266	5	2.0			
272	4	9.4	272	3	4.4	271		
						344	358	G_u
						355	531	H_u
						404	350	F_{2u}
						404	403	G_u or H_u
			428	4	4.4	425[1]	440	H_g
432	11	2.4	433	4	1.8	432		
			485	4	2.2	488	476	G_g
			492	4	1.1	491[1]	513	A_g
494	5	8.3	496	3	5.1	488		
						526 527*	544	F_{1u}
526	21	1.7	527	5	0.7		597	F_{1g}
			533	16	3.4	536		
						563 577*	637	F_{u}
			567	8	1.1		614	G_g
			579	6	0.4	576		
			600	7	0.4		637	F_{2g}
						673	690	F_{2u}
			696	14	5.7		691	H_g
708	12	2.7	709	4	14.2	715		
724	7	0.4	738	16	2.5			
759	70	10.4	757	6	5.0		770	G_g
			764	8	0.1			
772	8	1.6	772	4	8.3	765	801	H_g
			796	14	3.9			
						813	999	F_{u}
			860	9	2.7	840	834	F_{g}
						890	1212	F_{2u}
			914	3	0.3		890	F_{2g}
			922	7	0.9			
962	45	8.1	959	8	1.5			
			972	13	6.7	971		
			1022	8	2.0	971	975	F_{1g}
1036	16	0.7	1038	12	4.1	1044		
1080	24	4.2	1079	4	3.3	1100[1]	1154	H_g
			1099	7	3.7	1089		
			1110	4	0.4			
			1126	15	2.6	1122	1158	G_g
1154	22	1.7	1138	8	3.7			
						1183*	1241	F_{1u}
1193	28	1.4	1300	7	2.1	1247[1]	1265	H_g
1243	46	2.9	1244	20	1.2	1217		
			1252	4	0.6			
1307	37	2.3	1345	11	1.5	1327	1389	F_{1g}
						1428*	1437	F_{1u}
1422	25	15.2	1406	8	0.1	1426	1465	H_g
			1417	5	2.6			
			1425	5	5.9			
1463	8	100	1468	4	100	1448 1468[1]	1442	A_g
1478	6	1.7	1480	7	6.6		1450	G_g
			1499	12	4.4			
1506	16	1.1	1514	14	3.3		1470	F_{2g}
			1528	10	1.5	1520		
			1544	6	1.3	1571[1]	1644	H_g
1566	20	10.5	1566	16	2.4	1563		
			1575	6	5.4			
						1603		F_{2u}
1687	13	2.6	1687	3	0.6	1702	1585	G_g
			1694	9	1.4			

Table 7.4 : Peak frequencies ω_0, linewidth γ and relative peak intensities I of the Raman active modes in C_{60} for 740 nm excitation. Only the clearest modes are given.

ω_0 (cm^{-1})	γ (cm^{-1})	I (a.u.)	ω_0 (cm^{-1})	γ (cm^{-1})	I (a.u.)
266	1.5	11	1079	2	1
272	1.5	30	1100	2	3
274	2	7	1244	2	2
429	4	3	1251	3	2
434	1.5	10	1425	2	2
484	3.5	4	1468	2	100
496	1	84	1481	3	2
708	2	7	1576	3	4
773	2	8			

frequencies, linewidths and relative peak intensities are listed in Tab. 7.4. It should be noted that the penetration depth for 514 nm radiation in C_{60} is approximately 3μm. For 740 nm, the penetration depth is orders of magnitude larger. The 150 W/cm^2 used for the 740 nm spectrum can therefore be considered as a low irradiance excitation. The 740 nm and 514 nm spectra show comparable absolute intensities, despite the higher irradiance and the larger penetration depth for 740 nm excitation. This evidently reflects the resonance effects in the 514 nm spectra.

7.4 INTERPRETATION OF THE SPECTRA

The 514 nm spectra depicted in Fig. 7.1 (spectra (a),(b)) clearly show Raman activity in crystalline C_{60} of modes which are inactive for the free molecule. Moreover, a large number of splittings can be observed, especially in the low temperature spectrum. Details of the spectra, revealing these splittings have been published previously.[10] Both results are consistent with the selection rules derived in section I. In particular, all gerade molecular modes are observed in the low temperature spectrum. Also the 740 nm spectrum (Fig. 7.1 spectrum (c) and Tab. 7.4) shows some new lines and splittings, although less prominent than in the 514 nm spectra. Except for one mode at 274 cm^{-1}, all peaks observed in the 740 nm spectra are also found in the spectra recorded using 514 nm excitation. The presence of this mode in the 740 nm spectrum is probably caused by the improved spectral resolution (1.5 cm^{-1}) of this spectrum.

There are two possible causes for the difference in the number of observed peaks in the 514 nm and 740 nm spectra. In the first place weak peaks are difficult to detect in the red part of the spectrum because of the reduced detector efficiency, and also due to the presence of broad spectral features of the Ti:sapphire-laser. Secondly, resonance effects play an important role in the 514 nm spectrum.[25] Modes which are only weakly active using 740 nm excitation are strongly enhanced in the 514 nm spectrum. Even non resonant first order inactive modes can become active near the resonance, although normally these modes are only observed very close to the actual resonance. It is assumed that all observed peaks in the 514 nm spectrum, listed in Tab. 7.3, result from resonance enhanced first order Raman processes. The relative intensities of the Raman bands presented in Fig. 7.1(a),(b) are also strongly influenced by the (pre)resonant enhancement of electronic nature. This is evident from a comparison of these spectra to the spectrum presented in Fig. 7.1(c), and to the FT-Raman spectra obtained by Chase and Fagan[26] recorded using 1.064 μm excitation. The non-resonant data show comparable intensities for the two A_g modes and the H_g squashing mode, whereas near the resonance the out-of-phase ring mode is found to be a factor of five stronger. Moreover, the two H_g modes at 1100 and 1250 cm^{-1}, which have a pronounced presence in the 1.064 μm spectra[26], are of very low intensity in the spectra of Fig. 7.1(a),(b).

Polarised 514 nm Raman experiments at $T = 100$ K show that the A_g modes are weakly active in the perpendicular scattering geometry. This is consistent with the $2a_0$-FCC structure for the low temperature phase. In the FCC phase, the A_g modes are also found to be active in the perpendicular scattering geometry, indicating a violation of the selection rules in this case. This may be induced by defect structures in the FCC phase. There are several differences between the spectra of the low and high temperature phases (Fig. 7.1(a) and (b)). The low temperature spectra reveal newly activated modes and splittings of modes already active at high temperatures, reflecting the reduced symmetry in the $2a_0$-FCC phase. In general the frequencies of the modes in the low temperature phase are shifted towards higher frequencies, accompanied by a decrease of the linewidths. Also changes in the intensities have been observed. The absolute intensities are generally found to be a factor of 3 – 4 stronger in the $2a_0$-FCC phase compared to those in the FCC phase. In addition to this, some of the relative intensities are drastically changed in the low temperature phase, for instance the H_g modes in the 700 – 800 cm^{-1} region double in relative intensity compared to the FCC phase. The above described differences are partly due to the critical decrease of the rotational freedom in the low temperature phase[10], partly to the changes in the electronic structure[20], *i.e.* in the resonance effects in the $2a_0$-FCC phase, and partly to the presence of triplet state excited C_{60}^{*} in the FCC phase. The softening associated with the presence of C_{60}^{*}[24] is illustrated in Fig. 7.2, which shows the irradiance dependence of the frequency of the out-of-phase ring mode. For low irradiances (< 10 W/cm^2) this mode softens reversibly, *i.e.* if the power density is decreased, the mode hardens again. For irradiances exceeding 10 W/cm^2 the spectra change irreversibly, indicating a "photo-transformation"[27] of C_{60}. The character of this

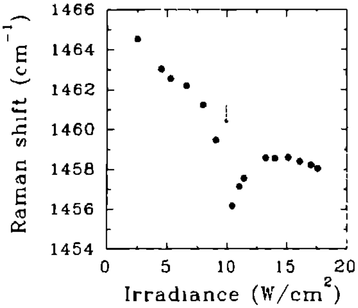

Figure 7.2 : Irradiance dependence of the frequency of the out-of-phase mode in single-crystal C_{60} at T=293 K, recorded using 514 nm excitation. The arrow indicates a "photo-transformation" of C_{60}.

transformation is still unclear, but, in view of the relatively large frequency shift, is seems likely that it involves a molecular transformation rather than structural changes of the crystal lattice. Extrapolating from Fig. 7.2, the ground state frequency of the out-of-phase mode is estimated to be 1466 cm^{-1}, consistent with the 300 K results obtained with 740 nm excitation (not shown here).

Apart from the Raman data of this work, Tab. 7.3 shows the infrared data of Krätschmer *et al.*[2], and the neutron scattering data of Coulombeau *et al.*[13], as well as the frequencies obtained from Raman spectra (514 nm) of C_{60} dissolved in CS_2. By combining the data of the different experimental methods, and the theoretical results obtained by Negri *et al.*[14] (see Tab. 7.3), one can come to an assignment of the observed peaks to the various symmetry modes of the free C_{60} molecule. This is done in the last column of Tab. 7.3. It is clear from the Table that all gerade modes are indeed observed in the Raman spectra. The frequencies of the observed experimental modes agree very well with the results of Ref. 14, who performed their calculations at a time when no experimental data were available. Recently, Negri *et al.*[15] showed that their results compare very well to other experimental data not discussed here, including Raman[28], inelastic neutron scattering[29], and high resolution energy loss spectroscopy[30] results. A further improvement and extension of the assignment to the symmetry modes can be expected when low temperature infrared data on single-crystal C_{60} become available, data that can reveal most of the ungerade modes (see Tabs. 7.1 and 7.2).

In the low frequency part of the FCC spectra, a broadening of the Rayleigh wing is observed, which extends to ~ 150 cm^{-1}. Part of the intensity here can be explained by the, to some extent, disordered surface of C_{60}, which induces diffuse scattering of the incident laser beam. However, one should consider that the rotational excitations of C_{60} are also a source of low frequency scattering, and may be responsible for part of the intensity in this region. At low temperatures, the broadening of the Rayleigh wing is found to be strongly reduced. Furthermore, often some additional structure is observed at 56 cm^{-1}, 80 cm^{-1}, and 108 cm^{-1}. This structure is not observed in all spectra and the presence depends on the spot position on the crystal. Therefore, it seems feasible that it is induced by the presence of impurities or by defects in the crystal structure. This is in line with the observed violation of the selection rules for the A_g modes. Distinct low frequency peaks have also been observed in inelastic neutron scattering experiments[13], confirming that they originate from external motions of C_{60}. In Raman scattering only the external rotational modes are expected to be active. The relatively high frequencies, however, indicate that these peaks can not be of rotational origin and it is more likely that the structure results from activated translational modes. Using the inter-molecular potential derived by Girifalco[31], the frequencies of the external vibrational modes, which are proportional to $\sqrt{M^{-1}\partial^2 V(\mathbf{r})/\partial\mathbf{r}^2}$, can be estimated to lie in the range of 25 – 85 cm^{-1}. Since the Girifalco potential neglects the contribution of the electrostatic interaction[20], this estimate can be considered to give a lower boundary for the translational modes. Coulombeau *et al.*[13] explained the discrepancy between theoretical predictions[32] and their neutron scattering results by assuming a rather strong temperature dependence of these modes. The low frequency features reported here do not show a strong temperature dependence. Far-infrared experiments might give some more insight in the low frequency vibrational properties of C_{60}.

7.5 CONCLUSION

The vibrational properties of solid C_{60} in the low and high temperature phase have been studied using low irradiance, 514 nm Raman spectroscopy. The wavelength used has the advantage that resonance enhancements reveal Raman active modes which can not be observed in non-resonant Raman spectroscopy. It has been shown that, within the experimental accuracy, the spectra of the different crystal phases are in agreement with the selection rules as derived in section II, and a full symmetry assignment of the observed peaks has been proposed. Spectra recorded using 740 nm excitation show that the differences in the Raman spectra recorded at 514 nm for the high and low temperature phase are partly due to the rotational ordering, to changes in the resonance Raman cross sections, and to the presence of triplet state excited C_{60}^{*} in the FCC phase.

ACKNOWLEDGEMENTS This work was financially supported by the Dutch Foundation for Fundamental Research of Matter (FOM).

REFERENCES

1 H.W. Kroto, J.R. Heath, S.C. O'Brien, R.F. Curl, and R.E. Smalley, Nature **318**, 162 (1985).

2 W. Krätschmer, L.D. Lamb, K. Fostiropoulos, and D.R. Huffman, Nature **347**, 354 (1991).

3 R.E. Smalley, *"The almost (but never quite) complete buckminsterfullerene bibliography"*, available upon request ("buckybib", Dept. of Chemistry, Rice University, P.O. Box 1892, Houston, Texas 77251, U.S.A.).

4 A.F. Hebard, M.J. Rosseinsky, R.C. Haddon, D.W. Murphy, S.H. Glarum, T.T.M. Palstra, A.P. Ramirez and A.R. Kortan, Nature **350**, 600 (1991).

5 P.A. Heiney, J.E. Fisher, A.R. McGhie, W.J. Romanow, A.M. Denenstein, J.P. McCauley Jr., A.B. Smith III, and D.E. Cox, Phys. Rev. Lett. **66**, 2911 (1991); R. Sachidanandam and A.B. Harris, Phys. Rev. Lett. **67**, 1467 (1991).

6 R. Tycko, G. Dabbagh, R.M. Fleming, R.C. Haddom, A.V. Makhija, and S.M. Zahurak, Phys. Rev. Lett. **67**, 1886 (1991).

7 R.D. Johnson, C.S. Yannoni, H.C. Dorn, J.R. Salem and D.S. Bethune, Science **255**, 1235 (1991).

8 K. Sinha, J. Menéndez, R.C. Hanson, G.B. Adams, J.B. Page, O.F. Sankey, L.D. Lamb, and D.R. Huffman, Chem. Phys. Lett. **186**, 287 (1991).

9 E.J.J. Groenen, O.G. Poluektov, M. Matsushita, J. Schmidt, J.H. van der Waals, and G. Meijer, Chem. Phys. Lett. **197**, 314 (1992).

10 P.H.M. van Loosdrecht, P.J.M. van Bentum, and G. Meijer, Phys. Rev. Lett. **68**, 1176 (1992), and chapter 6 of this thesis.

11 S.J. Duclos, R.C. Haddon, S. Glarum, A.F. Hebbard, and K.B. Lyons, Science **254**, 1625 (1991).

12 G. van Tendeloo, S. Amelinckx, M.A. Verheijen, P.H.M. van Loosdrecht, and G. Meijer, Phys. Rev. Lett. **96**, 7424 (1992).

13 C. Coulombeau, H. Jobic, P. Bernier, C. Fabre, D. Schütz, and A. Rassat, C.R. Acad. Sci. II **313**, 1387 (1991).

14 F. Negri, G. Orlandi, and F. Zerbetto, Chem. Phys. Lett. **144**, 31 (1988).

15 F. Negri, G. Orlandi, and F. Zerbetto, Chem. Phys. Lett. **190**, 174 (1992).

16 R.M. Fleming, A.P. Ramirez, M.J. Rosseinsky, D.W. Murphy, R.C. Haddon, S.M. Zahurak, and A.V. Makhija, Nature **352**, 787 (1991).

17 W.I.F. David, R.N. Ibberson, T.J.S. Dennis, J.P. Hare, and K. Prassides, Europhys. Lett. **18**, 219 (1992).

18 X.D. Shi, A.R. Kortan, J.M. Williams, A.M. Kini, B.M. Savall, and P.M. Chaikin, Phys. Rev. Lett. **68**, 827 (1992).

19 G. Dresselhaus, M.S. Dresselhaus, and P.C. Eklund, Phys. Rev. B **45**, 6923 (1992).

20 M. Sprik, A. Cheng, and M.L. Klein, J. Phys. Chem. **96**, 2027 (1992).

21 M.A. Verheijen, H. Meekes, G. Meijer, E. Raas, and P. Bennema, Chem. Phys. Lett. **191**, 219 (1992).

22 J. de Boer, University of Groningen (1992), unpublished.

23 G. van Tendeloo, C. van Heurck, J. van Landuyt, S. Amelinckx, M.A. Verheijen, P.H.M. van Loosdrecht, and G. Meijer, J. Phys. Chem. **96**, 7424 (1992).

24 P.H.M. van Loosdrecht, P.J.M. van Bentum, G. Meijer, submitted to Chem. Phys. Lett., and chapter 8 of this thesis.

25 M. Matus, H. Kuzmany, and W. Krätschmer, Sol. St. Comm. **80**, 839 (1991).

26 B. Chase and P.J. Fagan, J. Am. Soc. **114**, 2252 (1992).

27 P. Zhou, A.M. Rao, K-A. Wang, J.D. Roberson, C. Eloi, M.S. Meier, S.L. Ren, X.X. Bi, and P.C. Eklund, Appl. Phys. Lett. **60**, 287 (1992).

28 D.S. Bethune, G. Meijer, W.C. Tang, H.J. Rosen, W.G. Golden, H. Seki, C.A. Brown, and M.S. de Vries, Chem. Phys. Lett. **179**, 181 (1991).

29 K. Prassides, T.J.S. Dennis, J.P. Hare, J. Thomkinson, H.W. Kroto, R. Taylor, and D.R.M. Walton, Chem. Phys. Lett. **187**, 455 (1991); R.L. Cappetelletti, J.D.R. Copley, W.A. Kamitakahara, F. Li, J.S. Lannin, and D. Ramage, Phys. Rev. Lett. **66**, 3261 (1991).

30 G. Gensterblum, J.J. Pireaux, P.A. Thiry, R. Caudano, Ph. Lambin, A.A. Lucas, and K. Krätschmer, Phys. Rev. Lett. **67**, 2171 (1991).

31 L.A. Girifalco, J. Phys. Chem. **96**, 858 (1992).

32 A. Cheng and M.L. Klein, J. Phys. Chem. **95**, 6750 (1991).

CHAPTER 8

RAMAN SCATTERING IN TRIPLET STATE EXCITED C_{60}^{*}[1]

P.H.M. van Loosdrecht[a], P.J.M. van Bentum[a,b], and G. Meijer[a].

[a] *Research Institute of Materials, University of Nijmegen, Toernooiveld,*
NL-6525 ED Nijmegen, The Netherlands.
[b]*IBM Thomas J. Watson Research Center,*
Yorktown Heights, NY 10598, U.S.A.

ABSTRACT.

The low temperature Raman spectrum of $2a_0$-FCC single-crystal C_{60} recorded using low irradiance, 514 nm excitation shows only a single peak in the region of the 1468 cm^{-1} out-of-phase ring mode. For higher irradiances a new broad peak appears in the spectrum at a somewhat lower frequency. Simultaneously, an increase of the luminescence is observed. As the irradiance increases the new peak gains intensity and shifts to lower frequencies, whereas the original peak slowly disappears. It is argued that this peak originates from electronically excited C_{60}^{*}. A simple electronic four level model is proposed to explain the observed effects.

---

[1] To be published in *Chemical Physics Letters* (1993).

8.1 INTRODUCTION

Buckminsterfullerene (C_{60}), the related fullerenes and their derivatives have proved to be an exciting new field of research.[1, 2] The development of an efficient method to produce these new forms of carbon in macroscopic quantities[3] made it possible to study not only the molecular, but also the solid state properties of the fullerenes. The high symmetry of the prototype C_{60} makes this molecule one of the most interesting representatives. The I_h symmetry leads for instance to the peculiar rotational dynamics[4] in solid C_{60}. At room temperature the C_{60} molecules have a large degree of rotational freedom, resulting in a cubic closest packing FCC structure. At $T \sim 255$ K the rotational freedom freezes and a first order phase transition[5, 6] to a simple cubic (sc) structure takes place. In this phase the molecules can still rachet between equivalent orientations. Finally, the low temperature structure, in which the racheting has also frozen out, is $2a_0$-FCC.[7, 8]

The relatively small influence of the crystal field, the rotational-vibrational coupling in solid C_{60}[9] and the electron-phonon interaction[10] in superconducting alkali-intercalated C_{60} make the vibrational dynamics of solid C_{60} specially interesting. The vibrational properties of C_{60} have been studied both theoretically[2, 11] and experimentally.[2, 3, 12, 13, 14] Raman spectroscopy has proved to be a convenient method to study the solid state vibrational properties of C_{60} and related compounds.[9, 10] It is well known that for 514 nm radiation, the wavelength used in most Raman experiments, the optical absorption is large due to electronic transitions and correspondingly the phonon modes are resonantly enhanced. In this Letter we report detailed studies of the intensity and position of the A_g modes as a function of the excitation power density. The results indicate that already for relatively low radiation intensities C_{60} is excited to a metastable triplet state, with an associated softening of the dominant A_g modes.

8.2 EXPERIMENTAL RESULTS

The crystals used in the experiments are sublimation grown from high purity C_{60} powder. The high quality of the single-crystals has been checked by mass spectrometry, electron diffraction, electron microscopy and X-ray diffraction. Details of the C_{60} production, the growth procedure and the quality analysis have been published elsewhere.[15] The crystals were removed from their quartz growth tubes, and immediately (within a few minutes) mounted on the cold finger of a flow cryostat (stabilisation ± 0.2 K, calibrated to ± 2 K), which was subsequently evacuated to $P \approx 5 \cdot 10^{-6}$ mbar. In this way the effect of contamination with oxygen can be kept to a minimum. Unpolarised Raman spectra of single-crystal C_{60} have been recorded as a function of the irradiance using a DILOR XY multichannel Raman spectrometer (spectral slit width 1.5 cm^{-1}) in a back-scattering geometry. An

Ar$^+$-laser (514.5 nm, focussed to 30μm on a natural surface of solid C_{60}) has been used as excitation source. The obtained Raman spectra did not differ for different randomly chosen spot positions on the crystal. High irradiances easily cause optical damage to the crystals, therefore a low irradiance (2 W/cm^2, total laser power 15 μW) spectrum has been recorded after each measurement. No detectable changes have been noticed in these low irradiance spectra. Only after exposure to very high irradiances (>500 W/cm^2) the spectra changed irreversibly, indicating optical damage to the crystals.

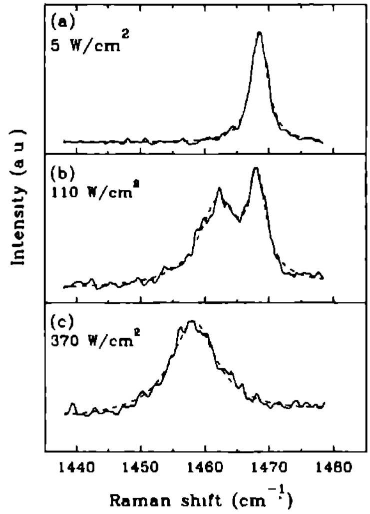

Figure 8.1 : Unpolarised Raman spectra of single-crystal C_{60} at T=40 K showing the region of the A_g out-of-phase ring mode (solid lines). The spectra have been recorded using 514 nm excitation with an irradiance of (a) 5 W/cm^2, (b) 110 W/cm^2 and (c) 370 W/cm^2. The dashed lines are fits of Lorentzian shaped peaks to the data.

Fig. 8.1 shows three typical Raman spectra of the out-of-phase A_g ring mode region recorded at $T = 40$ K using (a) 5 W/cm^2, (b) 110 W/cm^2, and (c) 370 W/cm^2 irradiance respectively (solid lines). The dashed lines in Fig. 8.1 are fits of one (a and c) or two (b) Lorentzian shaped peaks to the data. For low irradiance (spectrum a) we observe the ground state A_g out-of-phase ring mode of the C_{60} molecule, with a center frequency $\omega_0 = 1468$ cm^{-1} and a full width at half the maximum (FWHM) of 3 cm^{-1}. For moderate irradiance (50 W/cm^2 $\leq P \leq$ 300 W/cm^2) a new broad (FWHM = 8 cm^{-1}) peak appears in the spectrum, initially centered at 1465 cm^{-1}Simultaneously, the coexisting original A_g mode, which remains at the same position with approximately the same width loses

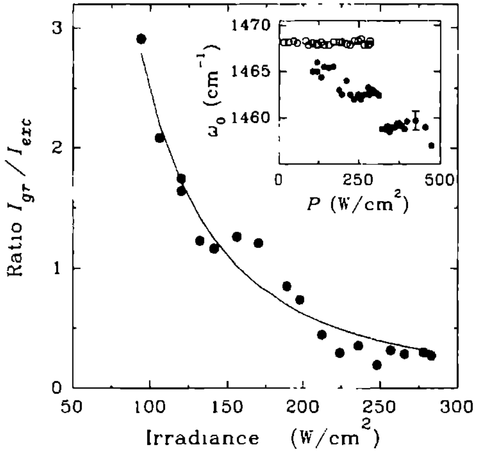

Figure 8.2 : Ratio of the peak intensities of the 1468 cm^{-1} A_g mode (I_{gr}) and the new modes (I_{exc}) as a function of the irradiance at $T=40$ K (dots). The solid line shows a fit of an inverse square irradiance dependence to the data (see text). The inset shows the irradiance dependence of the frequency of the 1468 cm^{-1} peak (open circles) and the additional modes (closed circles).

intensity, *i.e.* spectral intensity is transferred to the new modes. For irradiances exceeding 300 W/cm^2 the original A_g mode has completely vanished and a further broadening and softening is observed. In Fig. 8.2 we have plotted the peak intensity ratio of the ground state mode to the extra modes I_{gr}/I_{exc}, showing a gradual shift of oscillator strength with increasing irradiance. The inset shows the center positions of the modes as a function of the irradiance. It is clear that there is no continuous shift of the phonon modes, but rather a gradual appearance of distinct new modes. At an irradiance of approximately 300 W/cm^2 a quasi-discontinuous transition occurs and only a single broadened peak is observed.

The appearance of the new modes in the spectrum is accompanied by an increase of the "background" intensity. The irradiance dependence of this intensity (taken at 540 nm), which originates from luminescence processes, is plotted in Fig. 8.3 (dots). The overall behaviour is an increase of the luminescence upon increasing irradiance. Superimposed on this behaviour steps in the luminescence can be observed, which coincide with discontinuous changes of the frequency of the additional mode.

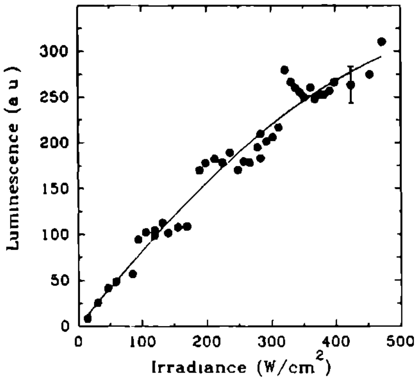

Figure 8.3 : Luminescence signal at 540 nm as a function of the irradiance. The solid line is a fit to $1/(1+\mathcal{R})$ *with* $\mathcal{R} \propto I^2$.

8.3 TRIPLET STATE EXCITATION

The observed changes in the spectra induced by the high irradiance are completely reversible. No changes have been observed in the low irradiance spectra recorded immediately after the recording of the high irradiance spectra. This instantaneous reversibility together with the increasing luminescence and the relatively strong absorption of 514 nm radiation in C_{60} is a strong indication that the new peaks in the spectra are vibrational modes of electronically excited C_{60}^* corresponding to the 1468 cm^{-1} A_g out-of-phase ring mode of the ground state molecule. The lower frequency of the new modes is consistent with this interpretation; being a full shell system, any excited state of C_{60} is an anti-bonding state, and will have weaker intra-molecular forces. In view of this picture, the peak intensity ratio of the normal A_g mode (I_{gr}) to the new mode (I_{exc}) should give a good measure for the ratio of the number of molecules in the ground state to those which are excited.

It should be noted that for low irradiance, when the new mode is not yet observable, the total A_g intensity increases linearly with the irradiance. For higher irradiance, this linear increase changes to a monotonic decrease of the total A_g intensity, which includes the new mode now. This behaviour points to a strong irradiance dependence of the optical penetration depth of the 514 nm radiation field, caused by optically induced electronic transition processes in the excited C_{60} molecules. In addition one may expect a change in the resonance conditions leading to a decrease of the resonant enhancement[17] of the Raman modes. Also differences in the Raman cross section for the ground state and excited molecules may play a minor role here. Clearly, changes of the penetration depth or the cross section do not influence the irradiance dependence of I_{gr}/I_{esc}. Note that none of the above described effects are observed in Raman spectra recorded using 740 nm (1.67 eV) excitation[16], an energy below the S_0-T_0 energy gap[18] for which optical excitations are expected to be of minor importance.

To understand the observed effects in the irradiance dependence of the Raman spectrum we propose the following qualitative model. Consider the simplified energy level diagram for the electronic structure of C_{60} depicted in Fig. 8.4. The left part of the diagram shows the electronic ground state ($|1\rangle$, h_u symmetry), and an excited singlet state ($|2\rangle$, t_{1u} symmetry). Optical transitions between these two states are first order forbidden. The (weak) appearance of this transition in absorption spectra[18, 19] indicates, however, that this transition is vibrationally allowed. The level $|3\rangle$ in the right part of the diagram represents the triplet (t_{1g} or t_{2g} symmetry) level that is populated by inter-system crossing $|2\rangle \rightarrow |3\rangle$, with a rate γ_{23}. The band of levels $|4\rangle$ schematically represents the various electronic states that can be populated with one additional photon, starting from state $|3\rangle$. The arrows in Fig. 8.4 indicate the most important stimulated absorption processes ($\sigma_{ij}I_0$, where σ is the absorption cross section and I_0 the photon flux) and (non)-radiative emission processes (γ_{ij}) between the various levels. Only the relevant processes are shown. The cross section for absorption of 514 nm radiation by ground state C_{60} molecules is[18] $\sigma_{12} \sim 2.5\cdot10^{-18}$ cm^2. After singlet excitation, a very efficient inter-system crossing to the lowest triplet state takes place with $\gamma_{23} = 3\cdot10^{10}$ s^{-1}.[20] Groenen *et al.*have measured the lifetime of the triplet states at $T = 1.2$ K using pulsed EPR experiments in an initially nearly fully triplet state excited single-crystal of C_{60} to be approximately 0.4 ms.[21, 22] This long lifetime leads to the conclusion that there is no efficient path for decay of triplet excited molecules to the ground state. In particular triplet-triplet annihilation seems to be of minor importance in

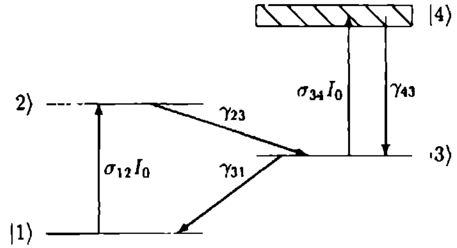

Figure 8.4 : Simplified electronic energy level diagram for C_{60}. The arrows indicate the most important electronic transitions in the presence of a 514 nm radiation field.

solid C_{60}. The absorption cross section in the triplet state is about one order of magnitude larger than σ_{12}.[23]

Of present interest is the ratio $\mathcal{R}$ of the population of the ground state to the total population of the excited levels. Given the model of Fig. 8.4, the steady state populations of the excited levels relative to that of the ground state are $\frac{N_2}{N_1} = \frac{\sigma_{12}}{\gamma_{23}} I_0$; $\frac{N_3}{N_1} = \frac{\sigma_{12}}{\gamma_{31}} I_0$; $\frac{N_4}{N_1} = \frac{\sigma_{12}\sigma_{34}}{\gamma_{31}\gamma_{43}} I_0^2$. Using these relations, the ratio $\mathcal{R}$ is

$$\mathcal{R}(I_0) = (\frac{\sigma_{12}}{\gamma_{31}} I_0 \, [1 + \frac{\gamma_{31}}{\gamma_{23}} + \frac{\sigma_{34}}{\gamma_{43}} I_0])^{-1} \approx (\frac{\sigma_{12}}{\gamma_{31}} I_0 \, [1 + \frac{\sigma_{34}}{\gamma_{43}} I_0])^{-1} \,, \tag{8.1}$$

where the approximation $\gamma_{31}/\gamma_{23} \ll 1$ is used. Note that for low irradiance the ratio of electronically excited molecules is proportional to $\sigma_{12} I_0/\gamma_{31}$. At 40 W/cm^2, $\sigma_{12} I_0/\gamma_{31} \sim 0.1$ and indeed the new line starts to appear for this irradiance. For values lower than 40 W/cm^2 one expects to observe the ground state vibrations in Raman spectroscopy, while for substantially higher irradiance the spectrum of electronically excited C_{60}^{*} is observed.

8.4 DISCUSSION AND CONCLUSION

Now consider the Raman intensity ratio of Fig. 8.2 again. The data in this figure can be satisfactorily fit to an inverse square irradiance dependence (solid line). This means that as soon as the triplet state $|3\rangle$ is populated, further excitation into the triplet manifold will occur. This is in line with the reported optical limiting properties of C_{60} [24], and with the broad FWHM of the C_{60}^{*} peak in the Raman spectra. The subsequent excitation into the triplet manifold leads to an increasing weakening of the C-C bonds in the molecules. Therefore the new C_{60}^{*} modes in the Raman spectra should appear at successively lower frequencies upon increasing irradiance, as is indeed observed (see inset Fig. 8.2). The luminescence is expected to be proportional to the fraction of molecules that is excited into the triplet manifold. This fraction is equal to $1/(1+\mathcal{R})$. A fit of this relation, using the $\mathcal{R} \propto I^2$ dependence, to the luminescence data of Fig. 8.3 yields also in this case a satisfactory result.

It is known that in the presence of oxygen the triplet state of C_{60} is efficiently quenched and γ_{31} increases by orders of magnitude.[25] So in a way, removing oxygen from the sample (thereby decreasing γ_{31}) has the same effect as increasing the irradiance, as only the ratio $\sigma_{12} I_0/\gamma_{31}$ is important. This led to the erroneous conclusion[26, 27] that the 1468 cm^{-1} mode is oxygen induced, and that the real C_{60} mode has a lower frequency, as it appeared in the spectra of oxygen free samples. It can now be concluded that this lower frequency mode is in fact originating from electronically excited C_{60}^{*}. In *in-situ* experiments[28] with a total absence of oxygen one expects that $\gamma_{31} \ll 2.5 \cdot 10^3$ s^{-1}, leading to an appreciable triplet state population already at very low irradiance.

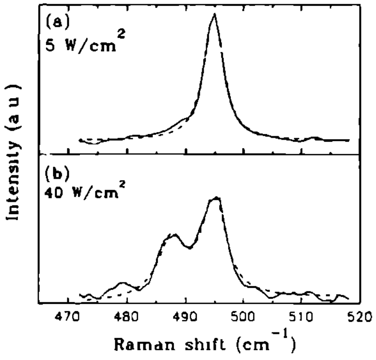

Figure 8.5 : Unpolarised Raman spectra of single-crystal C_{60} at $T=300$ K showing the region of the A_g in-phase ring mode (solid lines). The spectra have been recorded using 514 nm excitation with an irradiance of (a) 5 W/cm^2, (b) 40 W/cm^2. The dashed lines are fits of Lorentzian shaped peaks to the data.

The observed changes in the 1468 cm^{-1} region are not the only effects originating from triplet excited C_{60}^*. For the in-phase A_g mode a similar behaviour has been observed, *i.e.* the appearance of a new mode at a somewhat lower frequency. This is illustrated in Fig. 8.5, where the in-phase A_g mode region recorded at $T = 300$ K is shown for a) 5 W/cm^2 and b) 40 W/cm^2. In the FCC phase, the triplet state excitations become important already at very low irradiances. Apart from the activation of the new modes in the spectra, this results for instance in lineshape changes of the H_g squashing mode (not shown) which point to a Fano[29] type of coupling between this mode and the electronic excitations in C_{60}. The fact that in the FCC phase the triplet state is much easier produced might add to the discontinuous changes of Raman spectra observed at the rotational ordering transition.[9]

In summary, we have presented a Raman study of the vibrational properties of single-crystal C_{60} in the excited state, concentrating on the A_g out-of-phase ring mode. The irradiance dependence of the spectra can be explained in terms of a simple four level model for the electronic structure of C_{60}. For low irradiances only a single peak is observed which is assigned to the A_g mode of ground state C_{60}, rather than to an oxygen induced mode.

ACKNOWLEDGEMENTS We gratefully acknowledge the financial support of the Dutch Foundation for Fundamental Research of Matter (FOM).

REFERENCES

1 H.W. Kroto, J.R. Heath, S.C. O'Brien, R.F. Curl, and R.E. Smalley, Nature **318**, 162 (1985).

2 R.E. Smalley, *"The almost (but never quite) complete buckminsterfullerene bibliography"*, available upon request ("buckybib", Dept. of Chemistry, Rice University, P.O. Box 1892, Houston, Texas 77251, U.S.A.).

3 W. Krätschmer, L.D. Lamb, K. Fostiropoulos, and D.R. Huffman, Nature **347**, 354 (1991).

4 R. Tycko, G. Dabbagh, R.M. Fleming, R.C. Haddom, A.V. Makhija, and S.M. Zahurak, Phys. Rev. Lett. **67**, 1886 (1991); R.D. Johnson, C.S. Yannoni, H.C. Dorn, J.R. Salem and D.S. Bethune, Science **255**, 1235 (1991).

5 A. Dworkin, H. Szwarc, S. Leach, J.P. Hare, T.J. Dennis, H.W. Kroto, R. Taylor, and D.R.M. Walton, C.R. Acad. Sci. II **9**, 979 (1991).

6 P.A. Heiney, J.E. Fisher, A.R. McGhie, W.J. Romanow, A.M. Denenstein, J.P. McCauley Jr., A.B. Smith III, and D.E. Cox, Phys. Rev. Lett. **66**, 2911 (1991); R. Sachidanandam and A.B. Harris, Phys. Rev. Lett. **67**, 1467 (1991).

7 G. van Tendeloo, S. Amelinckx, M.A. Verheijen, P.H.M. van Loosdrecht, and G. Meijer, Phys. Rev. Lett. **69**, 1065 (1992).

8 W.I.F. David, R.N. Ibberson, T.J.S. Dennis, J.P. Hare, and K. Prassides, Europhys. Lett. **18**, 219 (1992).

9 P.H.M. van Loosdrecht, P.J.M. van Bentum, and G. Meijer, Phys. Rev. Lett. **68**, 1176 (1992), and chapter 6 of this thesis.

10 S.J. Duclos, R.C. Haddon, S. Glarum, A.F. Hebbard, and K.B. Lyons, Science **254**, 1625 (1991).

11 F. Negri, G. Orlandi, and F. Zerbetto, Chem. Phys. Lett. **144**, 31 (1988). F. Negri, G. Orlandi, and F. Zerbetto, Chem. Phys. Lett. **190**, 174 (1992).

12 D.S. Bethune, G. Meijer, W.C. Tang, H.J. Rosen, W.G. Golden, H. Seki, C.A. Brown, and M.S. de Vries, Chem. Phys. Lett. **179**, 181 (1991).

13 K. Prassides, T.J.S. Dennis, J.P. Hare, J. Thomkinson, H.W. Kroto, R. Taylor, and D.R.M. Walton, Chem. Phys. Lett. **187**, 455 (1991); R.L. Cappetelletti, J.D.R. Copley, W.A. Kamitakahara, F. Li, J.S. Lannin, and D. Ramage, Phys. Rev. Lett. **66**, 3261 (1991).

14 G. Gensterblum, J.J. Pireaux, P.A. Thiry, R. Caudano, Ph. Lambin, A.A. Lucas, and K. Krätschmer, Phys. Rev. Lett. **67**, 2171 (1991).

15 M.A. Verheijen, H. Meekes, G. Meijer, E. Raas, and P. Bennema, Chem. Phys. Lett. **191**, 219 (1992), and references therein.

16 P.H.M. van Loosdrecht, P.J.M. van Bentum, M.A. verheijen, G. Meijer, Chem. Phys. Lett. **198**, 587 (1992), and chapter 7 of this thesis.

17 M. Matus, H. Kuzmany, and W. Krätschmer, Sol. St. Comm. **80**, 839 (1991).

18 S. Leach, M.Vervloet, A. Desprès, E. Bréheret, J.P. Hare, T.J. Dennis, H.W. Kroto, R. Taylor, and D.R.M. Walton, Chem. Phys. **160**, 451 (1992).

19 H. Ajie, M.M. Alvarez, S.J. Anz, R.D. Beck, F. Diederich, K. Fastiropoulos, D.R. Huffman, W. Krätschmer, Y. Rubin, K.E. Schrivers, D. Sensharma, and R.L. Whetten, J. Phys. Chem. **94**, 8630 (1990).

20 M.R. Wasielewski, M.P. O'Niel, K.R. Lykke, M.J. Pellin, and D.M. Gruen, J. Am. Chem. Soc. **113**, 2774 (1991).

21 E.J.J. Groenen, O.G. Poluektov, M. Matsushita, J. Schmidt, J.H. van der Waals, and G. Meijer, Chem. Phys. Lett. **197**, 314 (1992).

22 E.J.J. Groenen, private communication.

23 T.W. Ebbesen, K. Tanigaki, and S. Kuroshima Chem. Phys. Lett. **181**, 501 (1991).

24 L.W. Tutt and A. Kost, Nature **356**, 225 (1992).

25 J.W. Arbogast, A.P. Darmanyan, C.S. Foote, Y. Rubin, F.N. Diederich, M.M. Alvarez, S.J. Anz, and R.L. Whetten, J. Phys. Chem. **95**, 11 (1991).

26 S.J. Duclos, R.C. Haddon, S.H. Glarum, A.F. Hebard, and K.B. Lyons, Sol. St. Comm. **80**, 481 (1991).

27 K. Sinha, S. Guha, J. Menéndez, D. Wright, and T. Karcher, Phys. Rev. B (in press).

28 P. Zhou, A.M. Rao, K-A. Wang, J.D. Roberson, C. Eloi, M.S. Meier, S.L. Ren, X.X. Bi, and P.C. Eklund, Appl. Phys. Lett. **60**, 287 (1992).

29 U. Fano, Phys. Rev. **124**, 1866 (1961).

CHAPTER 9

LATTICE VIBRATIONS IN CRYSTALLINE C_{70}[1]

P.H.M. van Loosdrecht, M.A. Verheijen, H. Meekes,
P.J.M. van Bentum[a] and G. Meijer.

Research Institute of Materials, University of Nijmegen, Toernooiveld,
NL-6525 ED Nijmegen, The Netherlands.
[a] *Also at IBM Thomas J. Watson Research Center,*
Yorktown Heights, NY 10598, U.S.A.

ABSTRACT.

Raman spectroscopy in single-crystal C_{70} at low temperatures reveals a large number of Raman active intra-molecular modes, consistent with the selection rules and in agreement with theoretical predictions. Librational and vibrational lattice modes are observed in the low frequency region of the spectrum, consistent with the selection rules for monoclinic $C_{70}$with space group $P112_1/m$. We discuss the lattice modes in terms of a simplified model of the crystal potential. Near 280 K we observe a phase transition, which is assigned to the order-disorder transition for the rotational motion around the long molecular axis.

---

[1] To be published in *Physical Review B* (1993).

9.1 INTRODUCTION

The discovery[1] of the carbon cage fullerenes and in particular the development of an efficient method[2] to produce macroscopic quantities of this new form of carbon sparked an intense effort to reveal and understand the physical and chemical properties of these exciting new materials, in both the molecular and in the condensed state.[3] The fullerenes provide a unique form of a molecular solid where the inter-molecular binding is rather weak and the nearly spherical shape of the molecules provides a large degree of rotational freedom. While the structure, electronic properties and crystal dynamics of the more symmetrical prototype C_{60} is reasonably understood, little is known about the crystal potential and the dynamics of solid C_{70}. Only recently one has succeeded to grow C_{70} single crystals of sufficient size and quality to allow a careful crystallographic and optical investigation.

The room temperature crystal structure of solid C_{70} was originally found to be highly defected FCC.[4] Verheijen *et al.*[5] showed this phase to be a true defect phase, and showed the actual room temperature structure to be a deformed hexagonal close packed (DHCP) structure, with rotational freedom around the long molecular axis. The molecular anisotropy of C_{70} gives rise to two rotational ordering transitions in the solid state.[4] Near 270 K the disordered rotations around the long molecular axis freeze out resulting in a monoclinic ($P112_1/m$, $Z = 4$) crystal structure. Slightly above room temperature (around 335 K) the rotations around the short molecular axes become also disordered yielding an ideal HCP phase. At still higher temperature, an irreversible phase transition to a perfect FCC crystal structure occurs.[5]

In this Letter we present the first Raman experiments on both the intra-molecular (internal) and inter-molecular (lattice) modes of single-crystal C_{70} at low temperature. The results are consistent with the proposed monoclinic superstructure of crystalline C_{70} at low temperatures and with the proposed approximation of the crystal potential.[5]

9.2 EXPERIMENTAL

The C_{70} crystals used in this work are grown from the vapour phase by sublimation of high purity C_{70}.[5] Mass spectroscopy of the chromatographically purified starting material as well as of the obtained crystals showed no traces of C_{60} or residual solvents (purity > 99.5 %). No sign of C_{60} is observed in the Raman spectra. X-ray and electron diffraction experiments and high resolution electron microscopy showed that crystals with a HCP morphology are indeed also microscopically HCP ($P6_3/mmc$, $Z = 2$). For the Raman experiments crystals with the HCP growth habit are chosen. To avoid surface contamination, the crystals are cut in air and immediately thereafter mounted in an optical flow cryostat (stabilisation

±0.2 K, absolute error ±2 K) which is subsequently evacuated to $P \approx 10^{-6}$ mbar.

Unpolarised Raman spectra have been recorded with a DILOR XY multichannel Raman spectrometer using either an Ar^{+}-laser (514 nm) or a Ti:sapphire-laser (771 nm) as excitation source. The small penetration depth ($< 1\mu m$) in crystalline C_{70} at 514 nm makes spectra recorded using this wavelength sensitive to surface effects. The much larger penetration depth ($\gg 10\mu m$) at 771 nm make this excitation wavelength better suited to probe the solid state properties of C_{70}. The irradiance is kept below 5 W/cm^2 in order to minimise optically induced changes in the structural and electronic properties of C_{70}.[6]

9.3 RESULTS

Fig. 9.1 shows two unpolarised Raman spectra of solid C_{70} at $T = 23$ K recorded using 771 nm (upper curve) and 514 nm (lower curve) excitation. The spectra are recorded with a spectral slit width of 1.5 cm^{-1} and 3.5 cm^{-1} for 771 nm and 514 nm excitation respectively. The spectral intensity is corrected for the system response (to within 20 %). The increase in background signal above 1000 cm^{-1} in the 771 nm spectrum is caused by weak luminescence originating from electronically excited C_{70}. The position of the phonon modes is independent of the excitation wavelength although the relative intensities vary strongly due to electronic resonance effects and differences in penetration depth. Similar effects have been observed in C_{60}.[7, 8]

The spectrum of C_{70} is rather complex due to the relatively low D_{5h} symmetry of the molecule. The molecular selection rules predict 53 Raman active modes which are classified as $12A_1'+22E_2'+19E_1''$. One can expect Davydov splittings and activation of molecular inactive modes to occur in solid C_{70}, as is the case for C_{60}.[9, 10] The selection rules in monoclinic $C_{70}(Z = 4$, site symmetry $C_s)$ predict 408 Raman active modes, including activation of all 122 (free) molecular modes. The 74 clearest modes observed in the 771 nm spectrum, and given in Tab. 9.1, are assumed to correspond to molecular modes. The C_{70} spectra of Fig. 9.1 show a peak at 1471 cm^{-1}, corresponding to the position of the A_g pentagonal pinch mode of C_{60}.[11] The absence of the C_{60} A_g breathing mode in the spectra (see inset Fig. 9.1) indicates that this mode originates from C_{70}, rather than from the presence of C_{60} impurities. The spectra presented here are consistent with the data reported by Bethune *et al.*[11]. As expected from the selection rules, all reported infrared active modes are observed in the Raman spectrum as well. A fair agreement is found with the theoretical data of Bakowies and Thiel[12], provided their data is scaled with a factor 0.9 as suggested by them. In particular the predicted absence of modes in the 800-1000 cm^{-1} region is experimentally confirmed. Based on the intensities, the underlined modes in Tab. 9.1 are tentatively assigned to the non-degenerate A_1' molecular modes of C_{70}. The root mean square deviation between these modes and the theoretical A_1' prediction is

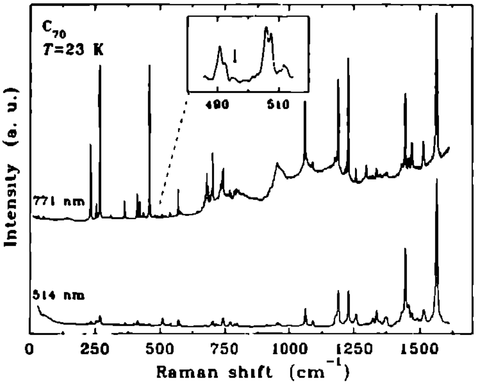

Figure 9.1 : Unpolarised Raman spectrum of crystalline C_{70} at T=23 K using 771 nm (upper curve) and 514 nm (lower curve) excitation. The large number of observed modes reflects the relatively low D_{5h} symmetry of C_{70}. The inset shows the absence of the 496 cm^{-1} A_g breathing mode of C_{60} (indicated by the arrow) in the C_{70} spectra.

31 cm^{-1}.

Although solid state effects are evident in the internal mode region as discussed above, their clearest manifestation is found in the lattice mode region (0-100cm^{-1}). Fig. 9.2a shows two examples (circles) of the low frequency part of the unpolarised 771 nm Raman spectrum recorded at T = 23 K on two different crystals from the same growth batch. Based on morphological considerations we assume that the surface measured in the upper spectrum is the {001} face, while for the lower spectrum it is the {101} face. Several Raman active librational and vibrational phonon modes are observed. Although the relative intensities for the two crystal faces are different, the various modes are found at the same frequencies. It should be noted that the spectra do not depend on the spot position on a certain crystal face, and that only a weak polarisation dependence is found. The latter is in agreement with the monoclinic nature of the low temperature structure of solid C_{70}. The solid curves through the data points in both spectra are fits of Lorentzian lines centered at the frequencies indicated in the figure with a typical FWHM of $\sim$ 2 cm^{-1}, superimposed on a Gaussian background. The latter is due to insufficient suppression of the Rayleigh peak when using the multichannel detector. In single channel measurements the Rayleigh contribution is absent for $\omega > 3$ cm^{-1} and no features are found between 3 and 10 cm^{-1}.

The observation of the 11 lattice modes (indicated in Fig.9.2a) is in agreement with the monoclinic superstructure at low temperatures. The phonon modes for monoclinic

Table 9.1 : Peak frequencies (in cm^{-1}) in the unpolarised 771 nm Raman spectrum of crystalline C_{70} at T=23 K. The relative intensities and full widths at half maximum intensity (in cm^{-1}) for each peak are given next to the frequency values. The underlined frequencies are assigned to the A_1' molecular modes of C_{70}. Only the clearest peaks and shoulders are given.

ω_0 (cm^{-1})	I	Γ (cm^{-1})	ω_0 (cm^{-1})	I	Γ (cm^{-1})	ω_0 (cm^{-1})	I	Γ (cm^{-1})	ω_0 (cm^{-1})	I	Γ (cm^{-1})	ω_0 (cm^{-1})	I	Γ (cm^{-1})
228	4.0	1.3	434	3.6	1.6	677	4.7	1.8	795	4.2	2.8	1311	1.6	2.7
231	44.4	1.4	458	97.8	1.4	680	16.7	2.2	800	1.4	3.0	1322	2.8	4.4
233	35.6	1.4	479	2.0	1.4	683	8.6	34.0	948	2.0	2.0	1335	6.4	2.4
252	4.4	3.0	491	1.3	1.6	685	5.0	1.8	1061	35.1	2.1	1338	5.3	1.9
253	8.3	1.3	506	1.9	1.8	697	3.0	1.3	1069	1.6	2.0	1351	1.4	2.5
$\underline{267}$	100.0	1.4	507	1.4	1.2	$\underline{703}$	30.1	1.2	1089	5.1	5.3	1377	2.0	3.5
303	1.1	2.0	520	1.0	2.4	729	3.4	2.9	1176	5.1	5.8	1432	2.5	2.0
309	2.1	2.6	523	0.6	1.5	733	6.5	2.5	1187	12.9	3.0	$\underline{1447}$	48.5	2.7
335	1.1	1.3	537	3.5	2.2	738	5.3	2.8	$\underline{1189}$	52.1	2.4	1459	8.9	4.1
339	0.7	1.0	$\underline{569}$	16.4	1.3	740	11.9	3.3	1217	4.0	3.1	1471	19.0	4.8
362	11.2	1.4	578	2.4	1.8	$\underline{743}$	14.8	1.7	1223	7.1	1.6	1514	16.5	5.0
408	3.2	1.9	643	1.9	1.6	768	4.2	1.6	1229	73.3	2.2	1557	4.5	1.6
410	14.6	1.4	661	2.1	1.9	774	3.3	1.3	1258	9.0	2.2	$\underline{1565}$	93.1	4.4
418	4.0	1.4	670	3.1	2.6	785	4.0	2.8	1261	1.7	1.5	1568	15.3	1.7
420	10.1	1.3	674	5.8	2.9	790	4.9	2.1	1297	8.4	3.0			

C_{70} are given by $\Gamma^{v}_{ext} = 4A^{v}_{g}+2B^{v}_{g}+2B^{v}_{u}+A^{v}_{u}$ and $\Gamma^{l}_{ext} = 2A^{l}_{g}+4B^{l}_{g}+2B^{l}_{u}+4A^{l}_{u}$, where the superscripts denote vibrational (v) and librational (l) modes. Only the 12 gerade lattice modes are Raman active, and two of the A^{v}_{g} modes are expected to be (nearly) degenerate.

In Fig. 9.2b the low frequency part of the spectrum is shown for temperatures close to the rotational ordering transition. It is clear that the various modes broaden considerably when approaching the phase transition. At room temperature only a weak, broad feature around 23 cm^{-1} survives. In the HCP phase (above 335 K) no lattice modes are observed. In Fig. 9.3 we have plotted the peak frequencies of the various modes as a function of temperature. From the abrupt change near 280 K it is clear that the selection rules for the vibrational/librational lattice modes change dramatically when the rotational motion around the long axis lifts the non-equivalence of neighbouring molecules. Verheijen *et al.*[5] reported the monoclinic C_{70}→DHCP-C_{70} phase transition to occur around 270 K. In the DHCP phase ($\Gamma = A^{l}_{2g}+B^{v}_{2g}+E^{l}_{1g}+E^{v}_{2g}+B^{l}_{2u}+E^{l}_{2u}$) one expects only two doubly degenerate modes; a vibrational mode with motions in the x-y plane, and a librational mode with rotations around the short molecular axes. Both modes will have approximately the same frequency. Hence, the 23 cm^{-1} feature could result from activity of both the E^{v}_{g} and E^{l}_{g} modes of the DHCP phase. The low intensity and broadening are not unexpected in view of the rotational disorder. In addition to the changes above 280 K, a weak change in the temperature dependence of some of the modes is observed near 150 K.

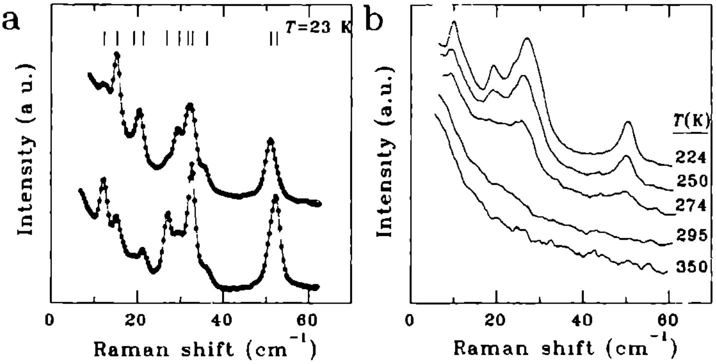

Figure 9.2 :

a *Low frequency part of the unpolarised Raman spectra (T=23 K, dots) recorded using 771 nm excitation showing the lattice modes of crystalline* C_{70} *for two different crystals. Upper curve: {001} face, lower curve: {101} face. The solid lines are fits of Lorentzians to the data, whose resonance frequencies are 12, 15, 19, 21, 27, 30, 32, 33, 36, 51, and 53* cm^{-1}*, as is indicated by the markers.*

b *Unpolarised 771 nm lattice mode spectrum of crystalline* C_{70} *near the rotational phase transition for* $T = 224, 250, 274, 295$ *and 350 K.*

9.4 DISCUSSION

A reasonable estimate of the vibrational frequencies is obtained by calculating the eigenvalues of the dynamical matrix of a simple force constant model for monoclinic C_{70}, including nearest and next nearest neighbour interactions only. A suitable theoretical model for the lattice energy in the DHCP phase, which agrees well with experimental structure results[5] is obtained by considering a Lennard-Jones type of interaction ($\sigma = 3.24$ Å and $\epsilon = 3.68$ meV[5]) between rings of carbon atoms in a C_{70} molecule rotating around its long molecular axis. The unit cell dimensions found by minimising the lattice energy in the DHCP phase are a = b = 9.9 Å, and c = 18.4 Å. The interaction potential thus found for the DHCP phase is used as an approximation for the potential in the monoclinic phase. Additional electrostatic interactions, which are probably needed to correctly describe the low temperature structure are neglected.[13] The force constants needed in the dynamical model are the one between two nearest neighbours in the $z = c/4$ plane for in plane vibrations (γ), and those between the next nearest neighbours in the $z = c/4$ and $z = 3c/4$ planes for in and out-of-plane vibrations (α_s and α_z, respectively). The force constants for the dynamical

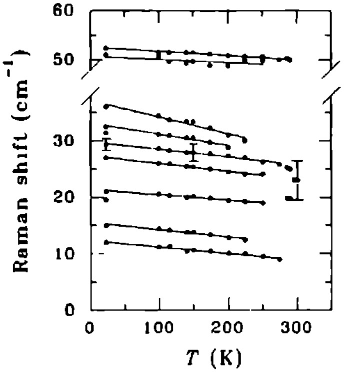

Figure 9.3 : Temperature dependence of the peak frequencies of the observed lattice modes. The solid lines are a guide to the eye. Most prominent is the disappearance of most of the modes above 280 K, indicating the rotational order-disorder phase transition.

model are determined by calculating the second derivative of the crystal potential with respect to the vibrational displacements to give $\alpha_x = 8.4$ kg·s^{-2}, $\alpha_z = 13.8$ Kg·s^{-2}, $\gamma = 20.4$ Kg·s^{-2}. From the eigenvalues of the dynamical matrix we expect four A_g^v modes with polarisabilities in the ab plane at respectively. 29, 32 (doubly degenerate) and 56 cm^{-1} and two B_g^v modes polarised along the c-axis at 33 and 58 cm^{-1}. We indeed find experimentally two groups of modes around 32 cm^{-1} and 52 cm^{-1}. Although the agreement is rather striking, it may be somewhat fortuitous in view of the various approximations and the neglect of electrostatic interactions.

A prediction of the librational frequencies cannot easily be given with sufficient accuracy within this simple model. Cheng and Klein[14] performed a molecular dynamics simulation, using a different Lennard-Jones type of interaction potential ($\sigma = 3.4$ Å and $\epsilon = 2.41$ meV). At low temperatures they find a triclinic crystal structure with a librational density of states characterised by 6 modes in the 5-15 cm^{-1} region. The absolute value of these theoretical predictions is about a factor of two lower than found experimentally. This may partly be due to the specific choice of the potential parameters and partly by the neglect of electrostatic interactions. Tentatively one could assign the two lowest frequency modes to librations involving rotations around the long molecular axis, and a group of four modes in the 18 to 35 cm^{-1} range to those involving rotations about the short axes. A definitive assignment of the various vibrational and librational modes has to await a more detailed calculation of the molecular dynamics.

9.5 CONCLUSION

In summary, the low temperature Raman spectrum of high purity single-crystal C_{70} has been presented revealing a large number of Raman active internal modes, consistent with the selection rules. A reasonable agreement is found with the theoretically predicted frequencies.

The low frequency Raman spectrum reveals 11 lattice modes with only a weak polarisation dependence, consistent with the selection rules for a monoclinic superstructure at low temperature. A simple force constant model for the vibrational lattice modes is found to be in good agreement with the observed spectrum. The frequencies of the librational modes are found to be nearly twice the value of recent theoretical predictions. Combining the data presented here with a full molecular dynamics simulation can lead to a better understanding of the crystal potential, and thus of the crystal structure and phase transitions in C_{70}. The expected monoclinic $C_{70}\rightarrow$DHCP-C_{70} phase transition is observed by the disappearance of most of the lattice modes above $T = 280$ K.

REFERENCES

1 H.W. Kroto, J.R. Heath, S.C. O'Brien, R.F. Curl, and R.E. Smalley, Nature (London) **318**, 16 (1985).

2 W. Krätschmer, L.D. Lamb, K. Fostiropoulos, and D.R. Huffman, Nature **347**, 354 (1990).

3 R.E. Smalley, *"The almost (but never quite) complete buckminsterfullerene bibliography"*, available upon request ("buckybib", Dept. of Chemistry, Rice University, P.O. Box 1892, Houston, Texas 77251, U.S.A.).

4 G.B.M. Vaughan, P.A. Heiney, J.E. Fischer, D.E. Luzzi, D.A. Ridkets-Foot, A.R. McGhie, Y.W. Hui, D.E. Cox, W.J. Romanow, B.H. Allan, N. Coustel, J.P. McCauley Jr., and A.B. Smith III, Science **254**, 1350 (1991).

5 M.A. Verheijen, H. Meekes, G. Meijer, P. Bennema, J.L. de Boer, S. van Smaalen, G. van Tendeloo, S. Amelinckx, S. Muto, and J. van Landuyt, Chem. Phys. **166**, 287 (1992).

6 P.H.M. van Loosdrecht, P.J.M. van Bentum, and G. Meijer, submitted to Chem. Phys. Lett., and chapter 8 of this thesis.

7 M. Matus, H. Kuzmany, and W. Krätschmer, Sol. St. Comm. **80**, 839 (1991).

8 P.H.M. van Loosdrecht, P.J.M. van Bentum, M.A. Verheijen, and G. Meijer, Chem. Phys. Lett. **198**, 587 (1992), and chapter 7 of this thesis.

9 P.H.M. van Loosdrecht, P.J.M. van Bentum, G. Meijer, Phys. Rev. Lett. **68**, 1179 (1992), and chapter 6 of this thesis.

10 L.R. Narasimhan, D.N. Stoneback, A.F. Hebard, R.C. Haddon, and C.K.N. Patel, Phys. Rev. B **46**, 2591 (1992).

11 D.S. Bethune, G. Meijer, W.C. Tang, H.J. Rosen, W.G. Golden, H. Seki, C.A. Brown, and M.S. de Vries, Chem. Phys. Lett. **179**, 181 (1991).

12 D. Bakowies and W. Thiel, Chem. Phys. **151**, 309 (1991).

13 M. Sprik, A. Cheng, and M.L. Klein, J. Phys. Chem. **96**, 2027 (1992).

14 A. Cheng and M.L. Klein, submitted to Phys. Rev. B.

SAMENVATTING

In dit proefschrift worden met behulp van een aantal experimenten de dynamische en electronische eigenschappen van incommensurabel gemoduleerde kristallen en fullereenkristallen bestudeerd. Hierbij is voornamelijk gebruik gemaakt van raman- en infraroodspectroscopie, twee optisch spectroscopische technieken die uitermate geschikt zijn om excitaties in vaste stoffen te bestuderen.

Raman- en infraroodspectroscopie zijn technieken die gebruik maken van de interactie tussen fotonen en excitaties in vaste stoffen, vloeistoffen, gassen of plasma's. Een foton kan onelastisch verstrooid worden aan bijvoorbeeld het kristalrooster, aan de electronen of aan gekoppelde excitaties in het kristal. Als dit volledig onelastisch gebeurt, dat wil zeggen, dat alle energie van het foton geabsorbeerd wordt door de excitatie in het kristal, spreekt men van absorptie. Een dergelijk proces kan plaatsvinden als de energie van het foton gelijk is aan de energie van een van de mogelijke excitaties in het kristal. In het algemeen betekent dit dat de energie van het foton in het infrarode deel van het spectrum ligt. Door nu te kijken bij welke foton-energie absorptie van licht plaatsvindt kan men dus iets leren over het excitatiespectrum van het bestudeerde materiaal. Als de energie van het foton beduidend groter is dan die van de excitaties in het kristal kan het foton slechts een deel van zijn energie verliezen (of winnen) door een verstrooiïngsproces. In dit geval spreekt men van raman- of brillouinverstrooiïng. Dit is een zogenaamd tweede-orde proces met een zeer lage waarschijnlijkheid. Gemiddeld ondergaat slechts één op de honderdmiljoen fotonen zo'n onelastische botsing. Om het toch mogelijk te maken dergelijke processen te bestuderen wordt bij ramanspectroscopie in het algemeen gebruik gemaakt van krachtige lichtbronnen in de vorm van lasers. Uit de frequentieverdeling van het verstrooide licht kan men informatie halen over de energieverdeling van de excitaties in een kristal.

Zowel infrarood- als ramanspectroscopie kijkt dus naar het excitatiespectrum van een kristal. Er is echter een belangrijk verschil in de manier waarop de optische verstrooiïng plaatsvindt. In het eerste geval koppelt het licht direct aan de electrische polarisatie van de excitatie, terwijl in het tweede geval een koppeling plaatsvindt aan de geïnduceerde polarisatie. Dit heeft gevolgen voor het al dan niet mogelijk zijn van het verstrooiïngsproces, hetgeen bepaald wordt door de symmetrie van het kristal. Het blijkt dat in centrosymmetrische kristallen de beide technieken zelfs complementair zijn, dat wil zeggen dat de excitaties die met infraroodspectroscopie bestudeerd kunnen worden niet zichtbaar zijn in ramanspectroscopie en vice versa.

In de klassieke definitie is een kristal een materiaal waarvan de atomen (of molekulen) in de drie-dimensionale ruimte een periodieke structuur vormen. Dat wil zeggen dat de afstanden tussen gelijke atomen of molekulen in één richting steeds hetzelfde zijn, er is dus translatiesymmetrie. In een incommensurabel gemoduleerd kristal is deze karakteristieke periodiciteit afwezig. Desalniettemin komen de fysische eigenschappen van incommensurabele kristallen in veel aspecten overeen met die van de periodieke kristallen. Evenals in periodieke kristallen vertonen Röntgendiffractiepatronen scherpe intensiteitspieken en is de uitwendige vorm van incommensurabel gemoduleerde kristallen regelmatig van karakter. De tegenwoordige definitie van een kristal is dan ook uitgebreid, zodat deze ook de incommensurabele kristallen omvat.

Een incommensurabel gemoduleerd kristal kan beschreven worden als een periodieke variatie van een gegeven, regelmatige, basisstructuur. Een groot deel van de bekende kristalfysica is gebaseerd op de translatiesymmetrie van het kristalrooster. Hoewel incommensurabele kristallen in drie dimensies niet translatiesymmetrisch zijn, is het mogelijk deze kristallen te beschrijven als een translatiesymmetrische structuur, zij het dat hiervoor overgegaan moet worden naar een hogere $(3+d)$ dimensie. De d extra dimensies leggen in deze beschrijving de periodieke variaties vast. Een ander belangrijk concept in de kristalfysica is de symmetrie van het kristalrooster. Evenals in drie-dimensionale structuren kan de symmetrie van een $(3+d)$-dimensionale structuur beschreven worden met een ruimtegroep (een zogenaamde superruimtegroep). De superruimtesymmetrie is zeer nuttig voor het begrijpen van allerlei fysische eigenschappen zoals bijvoorbeeld het röntgen- of electronendiffractie patroon of de onelastische verstrooiïng van licht aan excitaties in een kristal.

In het onderzoek naar incommensurabel gemoduleerde materialen is het gebruik van de superruimtesymmetrie zeer succesvol gebleken zowel in structuurbepalingen als in het beschrijven van andere fysische eigenschappen van incommensurabele kristallen. In dit kader is ook het onderzoek uitgevoerd, dat beschreven wordt in het eerste deel van dit proefschrift. Naast de bestudering van eigenschappen die direct beïnvloed worden door de incommensurabiliteit, en de analyse hiervan in termen van de superruimtesymmetrie, is ook gekeken naar een aantal andere fysische eigenschappen van deze materialen.

De electronische en vibrationele excitaties van het halfmetaal calaveriet ($AuTe_2$) worden bestudeerd in hoofdstuk 1 en 2. De observatie van een groot aantal verstrooiïngsprocessen aan roostervibraties die niet verwacht zouden worden als alleen de gemiddelde structuur van $AuTe_2$ in rekening gebracht wordt, is in goede overeenstemming met de resultaten van een superruimtegroep-analyse. Naast het vibrationele spectrum is ook het electronische spectrum bestudeerd. In dit geval is de invloed van de incommensurabiliteit minder duidelijk. De electronische structuur van een incommensurabel geleidend kristal vertoont een distributie van kleine "gaps", geïnduceerd door de modulatie. Het geobserveerde absorptiespectrum kan echter al goed beschreven worden als een klassiek vrij electron gedrag in combinatie met een interbandbijdrage, zonder deze energiegaps expliciet in rekening te brengen. De resultaten zijn vergeleken met resultaten van andere experimenten en theoretische berekeningen.

In hoofstuk 3 worden experimenten aan het ionogene mengkristal $[N(CH_3)_4]_2ZnCl_{4-x}Br_x$ beschreven. De invloed van de incommensurabiliteit wordt hier overschaduwd door de aanwezigheid van orientationele wanorde in dit kristal. De vibratiefrequenties van de verschillende $[ZnCl_{4-n}Br_n]^{2-}$ (n=0,1,...,4) anionen in dit materiaal kunnen redelijk goed beschreven worden in een eenvoudig veertjesmodel. Het blijkt dat uit spectroscopische metingen vrij eenvoudig een goede schatting voor de mengverhouding x te bepalen is.

De vibrationele eigenschappen van de ferro-electrische halfgeleider $Sn_2P_2Se_6$ worden bestudeerd in hoofdstuk 4. Het complete ramanspectrum is gemeten in alle drie de structurele fasen van dit materiaal. In de buurt van de ferro-electrische naar incommensurabele faseovergang is een sterke centrale component zichtbaar in het spectrum, vermoedelijk veroorzaakt door ramanverstrooiïng ten gevolge van de dynamica van domeinen in de ferroelectrische fase en van solitonen of discommensuraties in de incommensurabele fase. Het blijkt dat deze excitaties sterk koppelen aan de roostervibraties in dit materiaal, hetgeen zich uit in asymmetrische lijnvormen en en in de temperatuursafhankelijkheid van enkele van de waargenomen fononmodes in de ramanspectra.

Tenslotte laat hoofdstuk 5 zien dat incommensurabele materialen niet alleen interessant zijn vanuit een fundamenteel oogpunt gezien, maar ook praktische toepassingen kunnen hebben. De temperatuursafhankelijkheid van de diëlectrische constante van $(Pb_{0.45}Sn_{0.55})_2$-P_2Se_6 maakt dit materiaal uitermate geschikt voor toepassingen in lage-temperatuursensoren. De relatieve ongevoeligheid voor magnetische velden maakt dit materiaal bovendien toepasbaar in hoge magneetvelden.

Het tweede deel van dit proefschrift is gewijd aan een relatief nieuwe klasse van molekulen, de fullerenen. Grafiet en diamant werden tot voor kort beschouwd als de enige stabiele vorm van zuiver koolstof in de natuur. Met de ontdekking van het bestaan van fullerenen in 1985 kwam hier echter verandering in. Fullerenen zijn molekulen die bestaan uit een gesloten twee-dimensionaal netwerk van koolstofatomen. Deze netwerken zijn opgebouwd uit vijf- en zeshoeken, met op ieder hoekpunt een koolstofatoom. De vijfhoeken zijn hierbij nodig om een gesloten netwerk te maken, iets wat Euler al in de achtiende eeuw besefte. De naam van deze klasse van molekulen is ontleend aan de Amerikaanse architect en uitvinder Buckminster Fuller die experimenteerde met geodetische koepels, waarvan er ook enkele gebouwd zijn. Het Aviodome op Schiphol is een van de voorbeelden van zo'n geodetische koepel.

Het kleinste stabiele fullereen is het voetbalvormige C_{60}. Dit molekuul heeft een zeer hoge (icosahedrale) symmetrie, waardoor alle atomen equivalent zijn: Ieder atoom "ziet" precies dezelfde omgeving. Deze hoge symmetrie heeft verstrekkende gevolgen voor een groot aantal fysische eigenschappen. Zo wordt bijvoorbeeld het aantal experimenteel onderscheidbare trillingsmogelijkheden (modes) van het molekuul sterk gereduceerd door de symmetrie. Zonder deze symmetrie zouden er 174 verschillende trillingsmodes zijn. De symmetrie beperkt dit tot slechts 52 onderscheidbare trillingen. Bovendien wordt het aantal mogelijke onelastische lichtverstrooiïngsprocessen sterk beperkt. Van de 52 trillingsmodes zijn er slechts vier actief in infraroodspectroscopie, en slechts tien in ramanspectroscopie.

Het op één na kleinste stabiele fullereen is C_{70}. De structuur van dit min of meer eivormige molekuul kan beschreven worden als twee halve C_{60} molekulen, bijeen gehouden door een band van zeshoeken. C_{70} heeft een veel lagere symmetrie dan C_{60}; er zijn nu vijf groepen van equivalente atomen aan te wijzen. Dit heeft tot gevolg dat het vibratiespectrum van C_{70} aanzienlijk complexer is dan dat van C_{60} wat een nauwkeurige analyse van de vibraties van C_{70} sterk bemoeilijkt.

Sinds de ontdekking van een efficiënte productiemethode voor de fullerenen in 1990 heeft het onderzoek aan deze molekulen een enorme vlucht genomen. Er zijn sindsdien al zo'n duizend artikelen verschenen over de fullerenen en hiervan afgeleide materialen, zoals de supergeleidende alkali-C_{60} verbindingen. Het tweede deel van dit proefschrift is een bijdrage aan dit onderzoek. Het beschrijft enkele experimenten die uitgevoerd zijn om inzicht te krijgen in de fysische eigenschappen van C_{60} en C_{70} in de vaste stof. In het bijzonder is hierbij gekeken naar de vibrationele eigenschappen in relatie tot de kristalstructuur, en hun koppeling met electronische excitaties van de molekulen.

In gecondenseerde vorm zijn de fullerenen molekulaire kristallen met een relatief zwakke (van der Waals) binding tussen de verschillende fullereenmolekulen. De zwakke binding, in combinatie met de bijna ronde vorm van C_{60} en in mindere mate ook van C_{70}, heeft tot gevolg dat de molekulen in C_{60}- en C_{70}-kristallen vrijwel ongehinderd rond kunnen draaien. Dit leidt tot een grote mate van rotationele wanorde in deze kristallen. Bij verlaging van de temperatuur treden een of meerdere fase-overgangen op waardoor de structuren rotationeel geordend worden. Deze fase-overgangen, en in het bijzonder de invloed die deze hebben op de vibrationele eigenschappen, worden bestudeerd in hoofdstuk 6 en 7 voor C_{60}-kristallen en in hoofdstuk 9 voor C_{70}-kristallen.

De symmetrie van een molekuul in een kristal is in het algemeen lager dan die van een vrij molekuul. Dit leidt ertoe dat trillingen, die in een vrij molekuul dezelfde energie hebben, in de vaste stof energetisch kunnen opsplitsen. Daarnaast veranderen ook de selectieregels voor onelastische lichtverstrooiïng, zodat meer modes zichtbaar worden in optische spectra. In kristallijn C_{60} kan men dus beduidend meer dan de 10 raman-actieve molekulaire vibratiemodes verwachten. De experimenten in hoofdstuk 6 en 7 laten inderdaad zien dat een groot aantal trillingsmodes van de C_{60} molekulen actief wordt in de vaste stof, volledig in overeenstemming met de experimenteel bepaalde structuren van kristallijn C_{60} bij verschillende temperaturen. De raman-experimenten aan kristallijn C_{70}, beschreven in hoofdstuk 9, laten eveneens een groot aantal modes zien dat actief wordt ten gevolge van het kristalveld. Daarnaast is het voor C_{70} ook mogelijk gebleken om de laag energetische roostervibraties te bestuderen. Dit zijn vibratiemodes waarbij de molekulen opgevat kunnen worden als vaste lichamen, die onderlinge trillingen ondergaan. Hierbij kan onderscheid gemaakt worden tussen translaties en rotaties van de molekulen, waarbij gebleken is dat de laatste type trillingen de laagste energie hebben. De resultaten zijn in goede overeenstemming met de experimenteel bepaalde structuren in de verschillende kristalfasen, en met dynamische berekeningen voor de lage-temperatuur fase van kristallijn C_{70}.

Bij raman-experimenten aan C_{60} is het gebleken dat het gemeten spectrum zeer gevoelig is voor de intensiteit en de frequentie van het laserlicht dat gebruikt wordt. Bij groen licht (λ=514 nm) van voldoende vermogen verschijnen nieuwe pieken (nieuwe trillingsmodes) in het spectrum. Dit gaat ten koste van de pieken die bij laag vermogen geobserveerd worden. Uit het feit dat dit volledig reversibel gebeurt, dat wil zeggen dat het oorspronkelijke spectrum terugkomt, zodra het laservermogen omlaag gebracht wordt, is af te leiden dat de nieuwe modes geïnduceerd worden door een koppeling van de trillingsmodes aan electronische excitaties van C_{60}. Deze electronische excitatie is vermoedelijk een triplet toestand van het C_{60} molekuul. De resultaten van de experimenten kunnen begrepen worden met behulp van een eenvoudig model voor de electronische structuur van C_{60}.

CURRICULUM VITAE

October 26, 1963	Born at Waalwijk.
1976-1983	Atheneum-B at the Paulus Lyceum, Tilburg.
1983-1988	Physics at the Technical University of Eindhoven. 1986 Three months detachment at the group Environmental Physics of the University of Strathclyde, Glasgow, Great Britain. Subject: Drag properties of coniferous shoots. 1987-1988 One year detachment at the Philips Research Laboratories (PRL) at Eindhoven. Graduate research subject: Transport properties of quantum point contacts.
1988-1992	PhD research at the University of Nijmegen in the groups Theoretical Physics I of Prof.Dr. A.G.M. Janner and Experimental Solid State Physics 2 of Prof.Dr. H. van Kempen. Thesis: *"Dynamical and Electronic Properties of Incommensurate and Fullerene Crystals"*.

LIST OF PUBLICATIONS

1. *"Four terminal magnetoresistance of a two-dimensional electron gas constriction in the ballistic regime."*
   H. van Houten, C.W.J. Beenakker, P.H.M. van Loosdrecht, T.J. Thornton, H. Ahmed, M. Pepper, C.T. Foxon, and J.J. Harris. Phys. Rev. B **37**, 8534 (1988).

2. *"Aharonov-Bohm effect in a singly-connected point contact."*
   P.H.M. van Loosdrecht, C.W.J. Beenakker, H. van Houten, J.G. Williamson, B.J. van Wees, J.E. Mooij, C.T. Foxon, and J.J. Harris. Phys. Rev. B **38**, 10162 (1988).

3. *"Coherent electron focussing with quantum point contacts in a two-dimensional electron gas."*
   H. van Houten, C.W.J. Beenakker, J.G. Williamson, M.E.I. Broekaart, P.H.M. van Loosdrecht, B.J. van Wees, J.E. Mooij, C.T. Foxon, and J.J. Harris. Phys. Rev. B **39**, 8556 (1989).

4. *"On Incommensurate Phases in High T_c Compounds."*
   P.H.M. van Loosdrecht, and A. Janner. In *"Electronic Properties of High T_c Superconductors and Related Compounds."*, Springer Series in Solid-State Sciences, Vol. 99, p29, Eds. H. Kuzmany, M. Mehring, and J. Fink, Springer-Verlag Berlin, Heidelberg 1990.

5. *"Room temperature study of the internal $(ZnCl_{4-x}Br_x)^{2-}$ modes in the solid solution $N((CH_3)_4)_2ZnCl_{4-x}Br_x$."*
   P.H.M. van Loosdrecht. Conference proceedings of SCF19, Eds. G. Schmidt and J. von Cieminski, pp 105-107 (Halle-Wittenberg, Germany 1991).

6. *"A Raman and FIR spectroscopic study of the solid solution $(N(CH_3)_4)_2ZnCl_{4-x}Br_x$."*
   P.H.M. van Loosdrecht, and A. Janner. J. Phys.: Condensed Matter **3**, 8113 (1991).

7. *"Raman study of incommensurately modulated calaverite ($AuTe_2$)."*
   P.H.M. van Loosdrecht, P.J.M. van Bentum, and K. Balzuweit. Ferroelectrics **125**, 517 (1992).

8. *"Rotational ordering transition in single crystal C_{60} studied by Raman spectroscopy."*
   P.H.M. van Loosdrecht, P.J.M. van Bentum, G. Meijer. Phys. Rev. Lett. **68**, 1176 (1992).

9. *"Rotational ordering transition in single crystal C_{60} studied by Raman spectroscopy - Reply."*
   P.H.M. van Loosdrecht, P.J.M. van Bentum, G. Meijer. Phys. Rev. Lett. **69**, 1147 (1992).

10. *"Fascinerende Fullerenen."*
    G. Meijer, M.A. Verheijen, P.H.M. van Loosdrecht. Nederlands Tijdschrift voor Natuurkunde **58**, 75 (1992).

11. *"Phase transitions in C_{60} and the related microstructure, a study by electron diffraction and electron microscopy."*
G. van Tendeloo, C. van Heurck, J. van Landuyt, S. Amelinckx, M A. Verheijen, P.H.M. van Loosdrecht, and G. Meijer. J. Phys. Chem. **96**, 7424 (1992).

12. *"New orientationally ordered low temperature superstructure in high purity C_{60} fullerene."*
G. van Tendeloo, S. Amelinckx, M.A. Verheijen, P.H.M. van Loosdrecht, and G. Meijer Phys. Rev. Lett. **69**, 1065 (1992).

13. *"Raman scattering in single crystal C_{60}."*
P.H.M. van Loosdrecht, P.J.M. van Bentum, M.A. Verheijen, and G. Meijer. Chem. Phys. Lett. **198**, 587 (1992).

14. *"Raman scattering in electronically excited C_{60}^*."*
P.H.M. van Loosdrecht, P.J.M. van Bentum, and G. Meijer. Chem. Phys. Lett. (1993), to be published.

15. *"Lattice vibrations in crystalline C_{70}."*
P.H.M. van Loosdrecht, M.A. Verheijen, H. Meekes, P.J.M. van Bentum, and G. Meijer. Phys. Rev. B (1993), to be published.

16. *"Structure and phase transitions in C_{60} and C_{70} fullerites."*
G. van Tendeloo, S. Muto, S. Amelinckx, M.A. Verheijen, P.H.M. van Loosdrecht, and G. Meijer. Ultramicroscopy (1993), to be published.

17. *"A new dielectric material for low temperature thermometry in high magnetic fields."*
M.M. Maior, P.H.M. van Loosdrecht, P.J.E M. van der Linden, S.B. Molnar, Yu. M Vysochanskii, M.I. Gurzan, and H. van Kempen. Submitted to Appl. Phys. Lett.

18. *"Raman study of the ferroelectric semiconductor $Sn_2P_2Se_6$."*
P.H.M. van Loosdrecht and M M. Maior, Submitted to Phys. Rev. B.

19. *"Structure and lattice dynamics in the ordered phase of solid C_{70}."*
B.J. Nelissen, P.H.M. van Loosdrecht, M.A. Verheijen, A. van der Avoird, and G. Meijer, Submitted to Chem. Phys. Lett.

20. *"Optical properties of incommensurately modulated calaverite."*, P.H.M. van Loosdrecht, A.M. Gerrits, K. Balzuweit, W. König, and P.J.M. van Bentum, Submitted to J. Phys.: Condensed Matter.

21. *"Freezing of the dielectric response in the incommensurately modulated ferroelectric mixed crystal* $(Pb_ySn_{1-y})_2P_2Se_6$.", M.M. Maior, P.H.M. van Loosdrecht, H. van Kempen, S.B. Molnar, Yu.M. Vysochanskii, and V.Yu. Slivka, submitted to J. Phys : Condensed Matter.

INVITED LECTURES.

1. *"Dynamical properties of C_{60} and C_{70}."*
   Conference: Dynamical Properties of Solids XXII, Sept.28 - Oct.1, 1992, Schellerhau, Germany.
2. *"Raman scattering in fullerenes and incommensurate systems."*
   Colloquium at the State University of Uzhgorod, Oct.5, 1992, Uzhgorod, Ukraine.
3. *"Crystal field effects and electronically excited states in C_{60}."*
   Conference: International Winterschool on Electronic Properties of Novel Materials, March 6-13, 1993, Kirchberg, Austria.

STELLINGEN BEHORENDE BIJ HET PROEFSCHRIFT

"Dynamical and Electronic Properties of Incommensurate and Fullerene Crystals".

I

Het niet verplichten van stellingen bij een proefschrift is een verarming van het Nederlandse cultuurgoed.

II

Het ramanspectrum van buckminsterfullereen, dat gemeten wordt met behulp van een 514 nm laser in de afwezigheid van zuurstof, geeft inzicht in de dynamische eigenschappen van triplet C_{60}. Gezien de levensduur verkortende invloed die zuurstof heeft op de triplet toestand van C_{60}, is het aanbevelenswaardig het ramanspectrum van buckminsterfullereen in de grondtoestand te meten in aanwezigheid van zuurstof.

S.J. Duclos, R.C. Haddon, S.H. Glarum, A.F. Hebbard, and K.B. Lyons,
Sol. St. Comm. **60**, 481 (1991).

III

Apparatuur maakt, evenmin als geld, niet gelukkig.

IV

Het decentraliseren van de wachtgeldregeling vormt een zeer effectief middel om de continuïteit van wetenschappelijk onderzoek te ondergraven.

V

Een eenvoudige berekening laat zien dat er vijf raman-actieve libratie modes in FCC-C_{60} zijn, en niet vier, zoals in de literatuur beweerd wordt.

P.H.M. van Loosdrecht, P.J.M. van Bentum en G. Meijer,
Phys. Rev. Lett. **68**, 1176 (1992).

VI

Het is te verwachten dat de afschaffing van de militaire dienstplicht zal leiden tot een afname van het aantal promovendi.

VII

Een objectieve definitie van literatuur is niet te formuleren, daar de toekenning van het predicaat "literair" voor een niet onbelangrijk deel op subjectieve argumenten berust.

VIII

De werking van een koffiezetapparaat blijkt verrassend complex te kunnnen zijn.

IX

De generalisatie van chemische bindingen in een incommensurabel gemoduleerd kristal naar de corresponderende superruimte laat zien dat er slechts een beperkt aantal, in deze beschrijving compacte en dichte, sets van voorkomende bindingen worden gesneden door een kristallografisch hypervlak. Met behulp van dit resultaat is het eenvoudig aan te tonen dat een satellietvlak stabieler kan zijn dan de hoofdvlakken.

X

Gezien de hoge kosten, die verbonden zijn aan het schrijven en beoordelen van wetenschappelijke onderzoeksvoorstellen, in relatie met de beschikbare bedragen, is het aan te bevelen een voorselectie te doen op basis van een samenvatting van de voorgestelde projecten.

XI

Voor het waarnemen van magneto-oscillaties in de vibratiefrequenties van ring- of kooivormige molekulen, zijn magnetische velden in de orde van 10.000 tesla noodzakelijk. Het valt daarom überhaupt niet te verwachten dat deze molekulaire-vibratie magneto-oscillaties in de nabije toekomst waargenomen zullen worden.

F.V. Kusmartsev, Phys. Rev. B 46, 7674 (1992).

XII

Als een numeriek algoritme voor het oplossen van een electrodynamisch probleem resultaten genereert die strijdig zijn met ladingsbehoud, dan is het zoeken naar een alternatieve numerieke methode geen slechte investering.

M.J. Lea, A.O. Stone, P. Fozooni, and J. Frost,
J. Low Temp. Phys. 85, 67 (1991).

Nijmegen, Februari 1993 *Paul van Loosdrecht.*

ISBN: 90-9005863-X